DEVELOPMENT AND MAINTENANCE OF TASTE ORGANS

by

ZHONGHOU WANG

(Under the Direction of Hong-Xiang Liu)

ABSTRACT

Taste buds are the peripheral sensory organs for taste that is important for taking nutrients and avoiding toxins. The development and maintenance of taste organs is one of the central questions in the field of taste biology. In present dissertation, I have explored development of taste organs in following three topics: 1) determining whether taste bud cells are derived from neural crest cells (Chapter 3); 2) as the main focus of the dissertation, exploring roles of EVC2 and Hedgehog signaling in the development of taste papillae and taste buds (Chapter 4); 3) characterizing the expression of SARS-CoV-2 receptor ACE2 in oral epithelium (Chapter 5). Employing lineage tracing, mouse genetic modifications, transcriptomics and other cutting-edge techniques, I found that 1) taste bud cells are not derived from neural crest cells; 2) EVC2 regulates Hedgehog signaling and multiple developmental events of lingual epithelium in mice; 3) SARS-CoV-2 receptor, ACE2, is enriched in a subpopulation of epithelial cells in the basal region of non-gustatory filiform papillae, but not in the taste papillae or taste buds. Studies in present dissertation regarding the development and maintenance of taste buds shed light on understanding of pathogenesis of taste bud degeneration and development of therapeutics for taste bud degeneration in a variety of diseases.

INDEX WORDS: taste buds, cell lineage, Hedgehog signaling, EVC2, ACE2, SARS-CoV-2

# DEVELOPMENT AND MAINTENANCE OF TASTE ORGANS

by

ZHONGHOU WANG

B.S., Huazhong Agricultural University, China, 2015

M.S., University of Georgia, USA, 2017

A Dissertation Submitted to the Graduate Faculty of The University of Georgia in Partial Fulfillment of the Requirements for the Degree

DOCTOR OF PHILOSOPY

ATHENS, GEORGIA

2022

# DEVELOPMENT AND MAINTENANCE OF TASTE ORGANS

by

ZHONGHOU WANG

| | |
|---|---|
| Major Professor: | Hong-Xiang Liu |
| Committee: | Jonathan Eggenschwiler |
| | Woo Kim |
| | Romdhane Rekaya |
| | Franklin West |

Electronic Version Approved:

Ron Walcott
Vice Provost for Graduate Education and Dean of the Graduate School
The University of Georgia
May 2022

# DEDICATION

The dissertation is dedicated to my parents, Mr. Taixiang Wang and Mrs. Ping Jiang. No matter how far I live away from them, they always support and encourage to pursue my goals.

ACKNOWLEDGEMENTS

I would like to give huge thanks to Dr. Hong-Xiang Liu, who has been a great mentor throughout my education program. The dissertation would not have existed without her support and guidance. Huge thanks also go to my committee members, Dr. Jonathan Eggenschwiler, Dr. Woo Kim, Dr. Romdhane Rekaya, and Dr. Franklin West for their guidance and support. I also acknowledge all the colleagues who have been involved in my projects: Dr. Wenxin Yu, Brett Marshall, Dr. Yuta Yoshida, Renita Patel, Dr. Xiaogang Cui, Rebecca Ball, Linlin Yin, Dr. Fuminori Kawabata, Dr. Shoji Tabata, Dr. Wenbiao Chen, Dr. Robert N. Kelsh, Dr. James D. Lauderdale, Dr. Jingqi Zhou, Dr. Romdhane Rekaya, Dr. Kaixiong Ye, Dr. Mohamed Ishan, Dr. Honghao Zhang, Ruchi Shah, Stephanie Nguyen, Dr. Yuji Mishina.

My thanks go to all the Liu lab members who have been involved in discussion and/or providing technical support for my projects: Dr. Guiqian Chen, Prasangi Rajapaksha, Xiushen Wang, Dr. Xiaogang Cui, Shanshan Pu, Nandakumar Venkatesan.

I would like also thank whole RBC group and department of ADS and Dr. Steve Stice and Dr. Francis Fluharty for their leadership in the RBC group and ADS department respectively. I am super grateful for all the academic advices from Dr. Michael J. Azain and Dr. Alexander M Stelzleni. Without their dedication, I couldn't have get the best education under the ADS program.

I give thanks to Mary Redmond Hutson (Duke University, Durham, NC) and Richard Schneider (University of California at San Francisco, San Francisco, CA) as consultants for chicken chimera surgery; to Paul Trainor (Stowers Institute for Medical Research), Prasangi

Rajapaksha (University of Kentucky, Lexington, KY), Jason Payne and Robert Beckstead (University of Georgia, Athens, GA) for technical assistance of labeling neural crest cells in chicken model, and The Jackson Laboratory for transgenic mouse lines. I give thanks to The Georgia Advanced Computing Resource Center (GACRC) for providing high performance computing (HPC) resource, Georgia Genomics and Bioinformatics (GGBC) for providing technical assistance for cDNA library preparation, Biomedical Microscopy Core (BMC) for providing confocal microscope and Georgia Electron Microscopy (GEM) for providing electron microscope. I give thanks to Francisca Burnley for English editing of Chapter 3 and Chapter 5.

My thanks also go to all the administration specialists in department of ADS and RBC including but not limited to: Valerie Christopher, Francisca Burnley, Charlene Betourney, Susan Bradley, Christa L Dempsey, Larkin H Sosby.

At last but not the least, I give thanks to funding resources. Studies in this dissertation was supported by the National Institutes of Health, R01DC012308 and R21DC018089 to HXL, the University of Georgia Research Foundation to KY, R01NS090645 to JDL.

TABLE OF CONTENTS

Page

LIST OF TABLES

Page

LIST OF FIGURES

Page

# CHAPTER 1

# INTRODUCTION

Taste buds are the peripheral sensory organs for taste that is important for animals and humans to take nutrients and avoid toxins. How the development and maintenance of taste buds is regulated is one of the central questions in the field of taste biology. This dissertation consists of four sessions regarding the development and maintenance of taste buds: 1) reviewing current understandings of cell lineage and regulation of taste bud cells (Chapter 2); 2) determining whether taste bud cells are derived from neural crest cells (Chapter 3); 3) exploring roles of EVC and Hedgehog signaling in the development and maintenance of taste buds (Chapter 4); 4) characterizing the expression of SARS-CoV-2 receptor ACE2 in oral epithelium at different stages (Chapter 5).

In Chapter 2, before the three primary research chapters, I first comprehensively reviewed several essential components, e.g., neural trophic factors, molecular signaling pathways, and transcription factors etc., which are involved in regulating proliferation and differentiation of taste bud progenitors and/or survival of differentiated taste bud cells. These findings will shed light on the pathogenesis of taste bud degeneration and development of therapeutics for treatments of taste bud degeneration in a variety of diseases.

Taste buds are taste sensory organs located primarily on the tongue and inside the oral cavity of all vertebrates. In some fishes and amphibians, particularly species with barbels, taste buds are also found in the skin. A large proportion of taste bud cells are glial-like (type I) and a small subset is neuronal-like (type III). Given that glial cells in the peripheral nervous system are

derived from the neural crest and neurons are from either neural crest or epibranchial placodes, a question has been asked whether taste buds could plausibly be derived either from the neural crest, or from the epibranchial placodes, or from the local epithelium. In Chapter 3, we employed three species of animal models, mouse, chicken and zebra fish, to test the hypothesis that neural crest cells contribute to early taste bud cells. Data from three different models consistently indicates that taste buds are not derived from neural crest cells.

Taste loss caused by taste bud cell degeneration is a severe heath issue. However, there are still no treatments for taste bud cell regeneration, which is largely due to the lack of understanding of mechanisms underpin taste bud development and maintenance. Hedgehog signaling pathway has been reported to play essential roles in multiple events of taste organ development. Mis-regulation of Hedgehog signaling in embryos caused a number of birth defects in humans. Ellis–van Creveld syndrome, which is a Hedgehog signaling-related genetic disorder characterized by short limb dwarfism, polydactyly, abnormal development of fingernails as well as regional loss of taste papillae. The mechanisms of how regional taste papilla loss remain unknown. In Chapter 4, to understand how taste bud development is affected in Ellis–van Creveld syndrome and to further study how EVC2 and Hedgehog signaling regulates taste papilla and taste bud development, *Evc2*$^{-/-}$ mice and Gli1-CreER/RFP mice were employed. Through thorough examination, we found that taste papillae increased in number and size but with normal innervation in *Evc2*$^{-/-}$ tongues. Hedgehog signaling was impaired in tongue epithelial cells specifically in tongue tip region at E12.5. And RNA-seq experiment revealed that extracellular matrix (ECM) genes were dramatically up-regulated in *Evc2*$^{-/-}$ tongue epithelium. Moreover, enlarged and flatten fungiform papillae are observed in E18.5 *Evc2*$^{-/-}$ mice. BCL11B, a transcription factor essential for taste papilla morphogenesis, was missing or down-regulated in

the abnormal fungiform papillae in *Evc2*$^{-/-}$ mice. Together our data revealed that EVC2 regulates Hedgehog signaling and the development of taste organs in a region- and stage-specific manner.

As a result of the COVID-19 pandemic, evidence revealed that SARS-CoV-2 infection caused taste loss at a higher rate than influenza. *ACE2*, the entry receptor of SARS-CoV-2, has been identified in the oral epithelium; however, it is unclear at what developmental stage *ACE2* expression emerges and whether *ACE2* is expressed in taste buds. In Chapter 5, to identify the specific developmental stages when *ACE2* expression emerges, we analyzed RNA-Seq data from embryonic and newborn mouse oral tissue. We found that robust *ACE2* expression was observed in the newborn oral epithelium. In contrast, only extremely low levels, if any, of *ACE2* transcripts in the embryonic stage oral tissue were detected in the embryonic E12.5 and E14.5 oral tissue. Analyses of three public single cell RNA-seq datasets of adult mouse tongue epithelial cells showed that receptors for various viruses were enriched in distinct clusters of tongue epithelial cells. *ACE2* was enriched in a subpopulation of epithelial cells in the basal region of non-gustatory filiform papillae, but not in the taste papillae or taste buds. Expression of *ACE2* was detected in a small proportion of type III taste cells. Our results indicate that when applied across species, non-gustatory papilla epithelial cells are the prime targets for SARS-CoV-2 infection in the tongue, and thus taste loss in COVID-19 patients is likely not caused by a direct infection of SARS-CoV-2 to taste bud cells. Additionally, fetuses at different stages of development may have distinct susceptibility to the disease.

Overall, in present dissertation three important topics regarding development and maintenance of taste buds have been explored: embryonic origin of taste buds, regulation of taste bud development and maintenance, and pathogenesis of taste loss caused by SARS-CoV-2.

Studies in present dissertation shed light on understanding of pathogenesis of taste bud degeneration and development of therapeutics for taste bud degeneration in a variety of diseases.

# CHAPTER 2

# LITERATURE REVIEW: LINEAGE AND REGULATION OF TASTE BUD CELLS[1]

[1] Zhonghou Wang, Hong-Xiang Liu. To be submitted to *Developmental Dynamics.*

## 2.1 Abstract

In adults taste bud progenitors continuously replenish taste buds to maintain their homeostasis. Despite of their importance, the understanding of lineage of taste bud cells and the regulation of taste bud development and maintenance remain incomplete. Lack of understanding of taste bud cell lineage and the taste bud development regulation prevents finding cure for taste bud degeneration caused by various diseases. Recent studies unveiled several essential components, e.g., neural trophic factors, molecular signaling pathways, and transcription factors etc., which can regulate proliferation and differentiation of taste bud progenitors and/or survival of differentiated taste bud cells. In this article, we will comprehensively review these findings that would shed light on pathogenesis of taste bud degeneration and development of therapeutics for taste bud degeneration in a variety of diseases.

## 2.2 Introduction

Taste buds are primarily located at the tongue and soft palate in oral cavity in mammals. In mice, shortly after tongue swellings emerge, taste papilla placodes are specified from tongue epithelium at embryonic (E) day 12.5. Then taste papilla placodes undergo morphogenesis and early taste buds show up at E18.5. More differentiated taste bud cells emerge in taste buds after birth and almost all the taste buds are mature in 4-week-old mice.

The half-life of differentiated taste bud cells is 10 days on average in rodents [1]. To maintain intact taste sensation, dying taste bud cells have to be replaced by new taste bud cells differentiated from surrounding taste bud cell progenitors throughout lifetime. Exploring how taste bud progenitors are regulated is extremely important for understanding taste bud homeostasis and taste bud cell degeneration, and finding therapeutics for promoting taste bud cell regeneration happened in various conditions: aging, head-neck surgeries, chemotherapy,

radiotherapy, viral or bacterial infection, etc. Recently the taste loss found in COVID-19 patients at higher prevalence than other viral infections has impaired life quality of COVID-19 patients and raised huge interests and attention to taste disorders in scientific community [2, 3]. However, there are still no effective therapeutics for taste bud loss yet, due to poor understanding of taste bud cell lineage and regulation.

The taste bud progenitor/stem cells p, e.g., *K14*$^+$ cells, *Gli1*$^+$ cells, referred in many research [4, 5] are likely heterogeneous. Cells of those unknown subtypes or states may play specific roles in taste bud homeostasis and taste bud cell regeneration in normal and abnormal conditions. Moreover, the knowledge of regulatory factors of taste bud homeostasis is too little to translate for treatments of taste disorders. With development and availability of mouse lines for inducible genetic modifications, numerous new advances regarding taste bud homeostasis have been made. Multiple types of regulators, e.g., neural trophic factors, signaling pathways, transcription factors, are well-orchestrated to maintain taste bud homeostasis. This review will focus on recent advances of taste bud cell lineage and regulators. It would provide new insights into understanding taste bud homeostasis and taste bud cell degeneration, and developing therapeutics for taste disorders.

## 2.3 Lineage of taste bud cells

### *2.3.1 Lineage of embryonic taste bud cells*

Taste papilla placode specification, which occurs at E12.5, shortly after tongue swellings emerge. Taste papilla placodes which express Sonic hedgehog (SHH) proteins, are specified from relatively homogeneous tongue epithelium at E11. Lineage-tracing studies using *Shh*-CreER transgenic mouse line revealed that *Shh*-CreER labeled cells, with tamoxifen treatment at E12.5, were detected in early taste buds, but not detected in 4-month-old mice. This suggested

that taste papilla placode cells are early taste bud cell progenitors, but not long-term taste bud cell progenitors [6]. However, before specification of taste papilla placodes (at E11), tongue epithelial cells ($SHH^+$) can give rise to both early taste bud cells and surrounding basal epithelial cells [7]. The latter , i.e., basal epithelial cells, have been demonstrated to be stems cells for taste bud maintenance [5, 8].

In last decade, numerous attempts have also been made to explore additional source of progenitors of taste bud cells beyond tongue epithelium. Neural crest cells, a transient stem cell population in early embryos, have been reported to give rise to a broad spectrum of cell types [9], including tongue mesenchymal cells [10]. The multipotency of neural crest cells and their derived mesenchymal stromal cells make it logical to wonder whether neural crest cells are non-epithelial source of progenitors for taste bud cells. However, studies using two transgenic mouse lines labelling neural crest cells, Wnt1-Cre and Sox10-Cre, showed inconsistent results. In Wnt1-Cre mice, no tongue epithelial cells were labeled [6, 11] while Sox10-Cre labels all three types of differentiated taste bud cells [12]. Recently, employing inducible lineage-tracing mouse line, Sox10-CreER, together with chimera chicken model and transgenic fish lines to trace neural crest cells in three species, it has been found that neural crest cells do not give rise to taste bud cell progenitors [13].

*2.3.2 Lineage of adult taste bud cells*

Adult taste bud cells are constantly renewed by taste bud progenitor/stem cells in the surrounding basal epithelial cells throughout lifetime. Understanding of adult taste bud cell lineage has significant implications on developing therapeutics for taste bud degeneration. Multiple types of cells in distinct compartments have been found to serve as stem/progenitor cells for taste buds.

In a mature taste bud, there are three morphological types of differentiated taste bud cells. All three types of differentiated taste bud cells come from $SHH^+$ post-mitotic progenitors in the basal region of taste buds [14]. And $SHH^+$ post-mitotic progenitors are derived from *Lgr5*-expressing cells [15]and *Lgr6*-expressing cells at posterior tongue and anterior tongue, respectively. *Lgr5*-expressing and *Lgr6*-expressing cells are located in the surrounding of taste buds and actively-replicating taste bud progenitors. *in vitro* studies showed that single *Lgr5*-expressing cells and *Lgr6*-expressing cells can generate taste bud organoids that contain all three types of differentiated taste bud cells. Moreover, *Lgr5/6*-expressing cells and their progeny can no longer be traced one month after tamoxifen treatment using inducible Cre mouse model *in vivo*, suggesting *Lgr5/6*-expressing cells are short-term taste bud progenitors [16].

*Gli1*-expressing cells are located in the basal layer of tongue epithelium (anterior tongue) in taste papillae [4]. *Gli1*-expressing cells and their progeny can be traced over three months in lineage-tracing experiment using *Gli1-CreER* mice, indicating that *Gli1*-expressing cells are long-term progenitors for taste bud cells. In addition to differentiating to taste bud cells, *Gli1*-expressing cells also give rise to non-gustatory cells, suggesting the bipotential of *Gli1*-expressing cells [17]. Another long-term lineage tracing study investigating *Axin2*-expressing cells indicated that *Axin2* marked long-term self-renewing taste bud progenitors [18]. Based on the location, *Gli1*-expressing cells and *Axin2*-expressing cells were at least partially overlapping. As *Axin2* is expressed by multiple types of cells, further characterization is indispensable to identify more specific location or cell types which serve as stem cell niche or stem cells, respectively, for taste buds.

In anterior two thirds of tongue epithelium, non-gustatory papillae, filiform papillae, outnumbered gustatory papillae. $Bmi1^+$ cells, which are the long-lasting stem cells of non-

gustatory cells have been well-characterized. Single *Bmi1*$^{+}$ cells can give rise to the whole filiform papillae *in vivo*, but not fungiform papillae where taste buds reside [19]. However, Over-expressing of SHH in basal tongue epithelial cells between gustatory papillae caused generation of ectopic cell clusters that express taste bud cell markers in basal tongue epithelium, indicating the competency of tongue basal epithelium in filiform papillae to become taste bud cells [20]. However, it remains unclear whether the entire basal epithelium has such plasticity or only a sub-population of basal epithelial cells can differentiate into taste bud cells upon receiving SHH. Collectively, an intriguing question remains: do long-lasting specific progenitors exclusively for taste bud cells exist? If the answer is yes, these cells very likely express *Gli1 and Axin2*, and dissecting cellular heterogeneity of tongue basal epithelial cells will be of significance for a clear understanding the entire adult taste bud lineage.

## 2.4 Regulation of taste bud development and homeostasis

### *2.4.1 Regulation of early taste bud development*

#### *2.4.1.1 Neural input*

Taste bud cells are innerved by gustatory nerves which in turn transduce signals to higher level nervous system. Although gustatory nerves emerge under tongue epithelium prior to taste papilla placode specification, it has been well-documented that innervation is not required for the specification of taste papilla placodes. There are multiple lines of evidences supporting that early taste bud development is in-dependent of innervation. Taste papilla placodes (SHH$^{+}$) can successfully develop in mouse tongue explants *in vitro* [21] and in genetically modified mouse models in which innervation is impaired or lost, e.g. Bdnf$^{-/-}$ mice [6], Neurog1$^{-/-}$/ Neurog2$^{-/-}$ mice [22]. In amphibians, taste bud cells are differentiated normally in the absence of innervation after

the surgery. In this study, the presumptive oropharyngeal region is cut and grafted ectopically to the trunk of a host embryo [23].

Whether innervation is required for early taste bud development is still controversial. Shoba Thirumangalathu et al. reported that taste papilla placode cells can differentiate into taste bud cells in $Bdnf^{-/-}$ mice, in which taste bud innervation is lost [6]. However, recently Di Fan et al. reported that in absence of gustatory nerves caused by deletion of two proneural transcription factors, Neurog1 and Neurog2, development of early taste buds is impaired. And they attributed normal taste bud development in $Bdnf^{-/-}$ mouse models to uncomplete ablation of taste bud innervation [22].

Overall, the existing evidences suggests that $SHH^{+}$ taste papilla placode specification does not require innervation but development of $K8^{+}$ taste bud cells does require proper innervation. Furthermore, little is known about roles of neural factors secreted by lingual nerves during development of early taste buds.

*2.4.1.2 Signaling pathways*

Cell-cell communication is detrimental to embryo development. Signaling pathways plays central roles in cell-cell communication. Multiple signaling pathways have been reported to be involved in early taste papilla and taste bud development in both autocrine and paracrine manners.

*2.4.1.2.1 Wnt/β-catenin signaling*

Wnt/β-catenin signaling plays a key role in taste papilla development. One of the ligands for Wnt/β-catenin signaling, Wnt10b, is expressed in taste papilla placodes during placode specification. Characterized by TOPGAL mice, Wnt/β-catenin signaling activities are present in developing taste papillae. Disrupted Wnt/β-catenin signaling by knocking out β-catenin-

encoding gene, *Ctnnb1,* impaires development of fungiform papillae while over-expression of stabilized β-catenin *in vivo* caused more fungiform papillae in the anterior tongue [24].

For the proper development of taste buds, Wnt/β-catenin signaling needs to be spatiotemporally regulated. Stabilizing β-catenin prior to taste papilla placode specification leads to enhanced Wnt/β-catenin signaling activity, which in turn interrupts taste bud development. In contrast, after taste papilla placode specification stabilizing β-catenin in $SHH^{+}$ placodal cells increase cell population inside individual taste buds and size of fungiform papillae [25].

*2.4.1.2.2 Hedgehog signaling*

Hedgehog signaling is required for proper tongue development. Roles of Hedgehog signaling in tongue development are stage-specific. Treating E12 rat tongue (equals to E10.5 mouse tongue) cultures with cyclopamine *In vitro* prevents tongue growth while treating E14 rat tongue (equals to E12.5 mouse tongue) cultures with cyclopamine *In vitro* does not affect tongue growth [26]. Roles of Hedgehog signaling in tongue formation are also tissue-specific. Knocking-out *Smo*, the coding gene for an essential Hedgehog modulator, by tongue mesenchyme-specific Cre driver *Wnt1*-Cre caused abnormal tongues. In contrast, Knocking-out *Smo* by tongue epithelium-specific Cre driver *Shh*-Cre does not cause obvious defects in tongue development [27].

Hedgehog signaling does not promote taste papilla placode specification. Instead, Hedgehog signaling is able to inhibit this process. Both *in vitro* cultures and *in vivo* studies revealed that blocking hedgehog signaling transduction increased number of fungiform papillae [26, 27]. In tongue cultures treated with cyclopamine ectopic SHH-expressing taste papillae develop in inter-papilla space and intermolar eminence region that is free of taste papillae in

normal mouse tongues [26]. These data indicate that Hedgehog signaling inhibits taste papilla placode specification to different extents in two different regions of tongue epithelium.

*2.4.1.2.3 FGF signaling*

Roles of FGF signaling have been characterized in development of both fungiform papillae in anterior tongue and circumvallate papilla in the posterior tongue, which suggests region-specific roles of FGF signaling in taste papilla development. In the anterior tongue, Fgf10, an ligand of RTK signaling, is expressed in the tongue mesenchyme and *Spry2*, an RTK signaling antagonist, is expressed in the epithelium. Area of fungiform papillae decreased in absence of *Spry2* while area of individual fungiform papilla ($SHH^{+}$) increased in absence of *Fgf10*. The expression of *Sostdc1*, the gene encoding a secreted Wnt inhibitor binding to ECM, is significantly decreased in $Fgf10^{-/-}$ tongues, suggesting FGF signaling can refine range of Wnt signaling post-translationally. [28]

In the posterior tongue, two circumvallate papillae develop in the absence of *Spry2* while no circumvallate developed in absence of *Fgf10*. Regarding the cellular mechanism underlying FGF signaling controlling number of circumvallate, further studies indicate that FGF signaling modulates progenitor field size before circumvallate papilla developed [29].

*2.4.1.3 Transcription factors*

Transcription factors play pivotal roles in cell fate determination [30]. Expression and modification of transcription factors are regulated by intra-cellular autonomous program and/or extra-cellular cues transduced through one or more signaling pathways.

*2.4.1.3.1 SOX2*

SOX2 expression coincides with taste papilla placode specification. Partially loss of *Sox2* in hypomorphic $Sox2^{EGFP/LP}$ mutants did not affect the number or morphology of fungiform

papilla placodes before E14.5. However, after E14.5 tongues with Sox2 mutation showed a gradual reduction of number and size of fungiform papillae. Over-expression of Sox2 in tongue epithelium inhibited development of filiform papillae without altering number of $K8^+$ taste buds. In embryonic tongues, *Sox2* expression is regulated by Wnt/β-catenin signaling. Elevated Wnt/β-catenin signaling activity can enhance *Sox2* expression [31].

*2.4.1.3.2 BCL11B*

BCL11B is broadly expressed in tongue basal epithelium. Deletion of *Bcl11b* causes abnormal morphology of gustatory and non-gustatory papillae. In *Bcl11b*$^{-/-}$ mice, expression of genes encoding hard Keratins, which are essential to maintain the morphogenesis of filiform papillae, are absent or extremely low. However, deletion of *Bcl11b* does not affect differentiation of taste bud cells [32].

*2.4.1.3.3 PAX9*

Roles of PAX9 has been reported in the involvement in circumvallate papilla development. Pax9 is required for development of circumvallate papilla, as well as taste bud development. PAX9 acts upstream to PAX1 and SOX9 to expand the size of progenitor field for circumvallate papilla. In contrast, patterning, morphogenesis and maintenance of taste buds in the anterior tongue do not required PAX9 [33]. However, PAX9 is required for the morphogenesis of filiform papillae in anterior tongue region. Anterior-posterior polarity of filiform papillae is lost in *Pax9* knockout mice [34]

*2.4.2 Regulation of adult taste bud homeostasis*

*2.4.2.1 Neural input*

In adults, neural input is required for taste bud maintenance. Evidences from distinct species indicate loss of taste bud innervation cause taste bud degeneration. Identifying neural trophic factors will elaborate how taste buds are maintained by gustatory nerves and has significant implications in developing therapeutics for taste bud degeneration caused by loss of innervation. Moreover, taste bud cells can secret neural factors to maintain gustatory innervation.

*2.4.2.1.1 Neural dependence of taste bud maintenance*

Innervation by gustatory nerves is indispensable for taste bud maintenance. Taste bud degeneration after lingual nerve cut has been reported in a variety of species, including dogs [35], rats [36], mice [37], hamsters [38], and humans [39]. In mice, taste bud degeneration ipsilateral to the transection are observed 5 days after chorda-lingual nerve cut. The size and number of taste buds are significantly decreased after loss of gustatory nerves. Degeneration of taste buds at different regions is affected to distinct extents. The anterior tongue lost 60 percent of its taste buds at 15 days post nerve cut while the intermediate tongue lost all taste buds at the same time. Moreover, in the contralateral side to the transection of nerves, number of cells per taste bud increased. The reason why this happened remain unclear [37].

*2.4.2.1.2 Neural factors for taste bud maintenance*

The dependence of taste bud maintenance is mediated by neural factors secreted by gustatory nerves. SHH is an essential neural trophic factor for taste bud maintenance [40, 41], despite that SHH is produced by epithelial cells as well. 25% neurons in geniculate ganglion express SHH and those SHH-expressing neurons selectively project to fungiform taste buds, not surrounding regions of lingual epithelium. Taste receptor cells are almost completely lost upon

ablation of expression of *Shh* in gustatory nerves using sensory neuron-specific Cre mouse line *Avil*$^{Cre}$ [40]. Another study using Adeno-associated virus 5 Cre to specifically delete *shh* only in gustatory neurons has little effects on taste bud number, size or innervation density. However, viral deletion of neural *Shh* and epithelial deletion of *shh* using Krt5$^{rtTA}$;tetO$^{Cre}$ lead to much more severe degeneration of taste buds than neuron- or epithelium-only deletion of *Shh* [41]. More literature about Hedgehog signaling will be reviewed in 4.2.2.

R-spondins are another type of neural factors which are essential for circumvallate taste bud maintenance. By mining single cell RNA-seq data of gustatory neurons, *Rspo2* has been found to be expressed in gustatory neurons. Systemical administration of *Rspo1* or *Rspo2* via adenovirus successfully regenerated taste bud cells in glossopharyngeal nerve transection models [42]. R-spondins-coding genes, *Rspo1* and *Rspo2*, are required for generation of differentiated taste bud cells in taste organoids *in vitro*. CAR4$^{+}$ cells or TRPM5$^{+}$ cells are hardly detected in medium in absence of *Rspo2* [42]. R-spondins can amplify Wnt/β-catenin signaling by interacting with negative regulator of Wnt/β-catenin signaling, RNF43/ZNRF3, and positive Wnt/β-catenin signaling LGR4/5/6. Double knockout of RNF43/ZNRF3 in stem cells (KRT5$^{+}$) in adult mouse tongue epithelium cause taste cell hyperplasia in both fungiform papillae and circumvallate papilla [43]

*2.4.2.1.3 The reciprocal relationship between taste buds and innervating nerves*

Maintenance of taste buds and gustatory innervation actually depends on each other. Gustatory innervation is maintained by brain-derived neurotrophic factor (BDNF), which is expressed by taste bud cells. Both global [44] and lingual epithelium-specific deletion [45] of *Bdnf* caused reduction of innervation by half, followed by changes of taste buds in size and number. And loss of *Bdnf* specifically reduced total amount of TrkB$^{+}$ gustatory nerves, but not

TrkB$^-$ nerves. As a consequence, expression of a subunit of ENaC channel required for salt transduction was reduced [46]. Moreover, over-expressing *Bdnf* in taste receptor cells can significantly increase gustatory innervation, number of taste bud cells and size of taste buds [47]. Therefore, BDNF is an essential neurotrophic factor mediating both gustatory innervation and taste bud maintenance.

*2.4.2.2 Signaling pathways*

Cell-cell communication via signaling pathways plays essential roles in taste bud maintenance as well. Cues from taste bud cells, taste bud cell progenitors and gustatory nerves affect gene transcription in taste bud cell progenitors through signaling pathways, which in turn regulate proliferation, differentiation and migration of taste bud progenitors to replenish taste buds.

*2.4.2.2.1 Wnt/β-catenin signaling*

Wnt10a, one of the ligands for Wnt signaling, is extensively expressed in adult tongue epithelium. Correspondingly Wnt/β-catenin signaling activity, represented by *Axin2* expression level, is detected in both differentiated and basal taste bud cells. *Axin2*-expressing cells and/or their progeny are able to be traced for more than 6 months in lineage-tracing studies, suggesting *Axin2* marked self-renewing taste bud stem cells. Loss of taste buds is observed in inducible *Wnt10a* deletion tongue epithelium, which indicates Wnt/β-catenin signaling is required for taste bud maintenance [18]. Mechanistically, proliferation of tongue basal epithelial cells is reduced and all three types of differentiated taste bud cells are affected in *Wnt10a*$^{-/-}$ tongue epithelium [48]. Loss-of-function analysis of β-catenin generated similar results [49]. Moreover, Wnt/β-catenin signaling also regulates cell fate specification of differentiated taste bud cells. Elevated Wnt/β-catenin signaling caused by stabilized β-catenin can increase proliferation at the anterior

tongue but decrease proliferation at the posterior tongue. Elevated Wnt/β-catenin signaling also promote differentiation into taste bud cells ($KRT8^+$ ) in tongue epithelium at expense of non-taste cells ($KRT13^+$ ). And with elevated Wnt/β-catenin signaling, ratio of type I taste bud cells increased more than type II taste bud cells do. Almost all ectopic taste bud cells in mutants with elevated Wnt/β-catenin signaling express type I taste bud cell marker. Collectively, Wnt/β-catenin signaling is a promising target of developing novel therapeutics for treating taste disorders [50].

*2.4.2.2.2 Hedgehog signaling*

Hedgehog signaling is another essential signaling pathway responsible for taste bud maintenance. Hong-Xiang Liu et al. first revealed that Hedgehog-responsive cells (*Gli1*$^+$) are located in taste papillae, but not in non-gustatory filiform papilla cells. These *Gli1*-expressing cells are long-term taste bud cell progenitors, as well as filiform papilla cells that are closed to fungiform papillae [17]. Then loss-of-function analysis of the ligand (SHH) [51, 52] , the membrane receptor (Smoothened) [53], and the transcription factor (GLI2) [54] of hedgehog signaling has been performed using either pharmacological or genetic methods. Collectively, Hedgehog signaling maintains taste bud homeostasis by modulating proliferation taste bud progenitors at specific regions and differentiation of taste bud progenitors, but not taste bud cell survival. One striking feature of the roles of Hedgehog signaling is that cell proliferation is only affected at specific regions in fungiform papillae [55, 56], suggesting the heterogeneity of taste bud progenitor cells. Degeneration of taste buds caused by disrupted Hedgehog signaling is reversible. Once removing the impairment of Hedgehog signaling, partial taste bud cell regeneration occurs, which require neural SHH. Pharmacological activation of hedgehog signaling can accelerate the regeneration and even generates ectopic taste bud cells as well [52].

Gain-of-function analysis of ligand (SHH) of hedgehog signaling has been also performed [20]. Similar results as caused by over-expression of *Shh* in tongue epithelium with impaired Hedgehog signaling, over-expression of *Shh* in normal condition also cause ectopic taste buds in basal tongue epithelium, suggesting the competency of tongue epithelium to differentiate to taste bud cells.

HH-interacting protein (HHIP) is a vertebrate-specific Hedgehog signaling component, which can bind Hedgehog proteins to negatively regulate Hedgehog signaling activities. HHIP expression is restricted to filiform papilla cells. After Hedgehog pathway inhibition, degraded filiform-like fungiform papillae started to express HHIP, which suggests that HHIP could determine the fate of filiform papillae during tongue homeostasis [57]

*2.4.2.2.3 Inflammation-related signaling pathways*

In addition to organogenesis-related signaling pathways, inflammation-related pathways also play essential roles in taste bud maintenance, especially under abnormal and disease conditions. Systemic inflammation caused by lipopolysaccharide (LPS) activats expression of a bunch of cytokines in taste bud cells: TNF-α, IFN-γ, IL-6, IL-12, MCP-1, and IL-1β. Meanwhile LPS inhibits proliferation of taste bud cell progenitors and shortens overall turnover period of taste bud cells [58].

Functions of some specific cytokines have been studied individually. Expression of IFN-γ receptors, including IFNGR1, is detected in differentiated taste bud cells. Exogenous IFNs leads to an increase of apoptosis of differentiated taste bud cells [59]. The role of TNF-α in taste bud homeostasis has been established in chronic inflammation caused by high-fat chow-induced obesity. Fewer taste buds in circumvallate has been observed in obese mice than lean mice. Both higher apoptosis in taste buds and reduced proliferation in taste bud progenitors are detected in

obese mice. Importantly, knocking out TNF-α prevents taste bud loss in obese mice without affecting adipogenesis caused by high-fat chow feeding [60].

*2.4.2.3 Transcription factors*

*2.4.2.3.1 SOX2*

SOX2 is one of best-studied transcription factors that regulates taste bud maintenance. The roles of SOX2 in taste bud homeostasis have been explored in both anterior [61] and posterior tongues [62]. SOX2 expression is activated by Hedgehog signaling pathway. Conditional ablation of *Sox2* in taste bud progenitors dramatically increased taste bud cell apoptosis, suggesting SOX2 expression in surrounding progenitors supports taste bud cell survival indirectly. In the future, the cues controlled by SOX2 and secreted by local progenitors are to be determined. Conditional ablation of *Sox2* also causes expansion of proliferating cells from basal epithelium to suprabasal epithelium. All those cellular defects might directly or indirectly cause taste bud loss.

*2.4.2.3.2 Skn-1a*

Homeodomain protein Skn-1a (Pou2f3) is specifically expressed in type II taste bud cells that are marked by Trpm5 or Plcb2 or Ggust. Knocking out *Skn-1a* almost eliminated all type II taste bud cells but generated more type III taste bud cells. Behavior test matched composition changes of taste buds, which was that perception of sweet, umami or bitter, but not citric acid, is significantly reduced in Skn-1a knockout mice. These data indicates that Skn-1a specifies type II taste bud cell lineage [63].

## 2.5 Perspectives for future studies

In this review, we discussed the recent findings regarding the lineage of taste bud cells and how proliferation and differentiation of taste bud progenitors are regulated in both embryonic

and adult mice. These findings have dramatically enlightened us about how taste bud homeostasis is maintained and shed light on cellular and molecular mechanisms of taste bud cell degeneration. Nevertheless, what we have known about taste bud homeostasis is still little and a lot of new questions arise to be answered.

The first question is whether the exclusive taste bud stem cells exist or not. With rapid development of single cell sequencing techniques and emerging single cell transcriptome data sets, it is promising to identify novel subtypes or intermediate state of taste bud progenitors. And lineage tracing studies of these novel subtypes would identify *bona fide* taste bud stem cells. Moreover, non-coding DNA, which had been considered as "junk genome" for a long time, has been proved to play essential roles in gene regulation and cell fate determination in a number of organs or systems. Studies in the field of taste biology, however, are far behind in this area compared to the field studying other organs. To tackle the new challenges, next-generation sequencing-based techniques, like bulk RNA-seq, single cell RNA-seq, and ChIP-seq will generate data that are promising to facilitate research in gene regulation during taste organ development and maintenance.

## 2.6 References


1. Farbman, A.I., *RENEWAL OF TASTE BUD CELLS IN RAT CIRCUMVALLATE PAPILLAE.* Cell Proliferation, 1980. **13**(4): p. 349-357.

2. Yan, C.H., et al., Association of chemosensory dysfunction and COVID-19 in patients presenting with influenza-like symptoms. International Forum of Allergy & Rhinology, 2020. **10**(7): p. 806-813.

3. Wang, Z., et al., SARS-CoV-2 Receptor ACE2 Is Enriched in a Subpopulation of Mouse Tongue Epithelial Cells in Nongustatory Papillae but Not in Taste Buds or Embryonic Oral Epithelium. ACS Pharmacology & Translational Science, 2020. **3**(4): p. 749-758.

4. Liu, H.X., et al., Multiple Shh signaling centers participate in fungiform papilla and taste bud formation and maintenance. Developmental Biology, 2013. **382**(1): p. 82-97.

5. Okubo, T., C. Clark, and B.L. Hogan, Cell lineage mapping of taste bud cells and keratinocytes in the mouse tongue and soft palate. Stem Cells, 2009. **27**(2): p. 442-50.

6. Thirumangalathu, S., et al., *Fate mapping of mammalian embryonic taste bud progenitors.* Development, 2009. **136**(9): p. 1519-1528.

7. Kramer, N., et al., Early taste buds are from Shh+ epithelial cells of tongue primordium in distinction from mature taste bud cells which arise from surrounding tissue compartments. Biochemical and Biophysical Research Communications, 2019. **515**(1): p. 149-155.

8. Golden, E.J., et al., Onset of taste bud cell renewal starts at birth and coincides with a shift in SHH function. eLife, 2021. **10**: p. e64013.

9. Rothstein, M., D. Bhattacharya, and M. Simoes-Costa, *The molecular basis of neural crest axial identity.* Developmental Biology, 2018. **444**: p. S170-S180.

10. Chai, Y., et al., Fate of the mammalian cranial neural crest during tooth and mandibular morphogenesis. Development, 2000. **127**(8): p. 1671-1679.

11. Liu, H.-X., et al., Neural crest contribution to lingual mesenchyme, epithelium and developing taste papillae and taste buds. Developmental Biology, 2012. **368**(2): p. 294-303.

12. Yu, W., et al., SOX10-Cre-Labeled Cells Under the Tongue Epithelium Serve as Progenitors for Taste Bud Cells That Are Mainly Type III and Keratin 8-Low. Stem Cells and Development, 2020. **29**(10): p. 638-647.

13. Yu, W., et al., Taste buds are not derived from neural crest in mouse, chicken, and zebrafish. Developmental Biology, 2021. **471**: p. 76-88.

14. Miura, H., et al., Sonic hedgehog-expressing basal cells are general post-mitotic precursors of functional taste receptor cells. Dev Dyn, 2014. **243**(10): p. 1286-97.

15. Yee, K.K., et al., *Lgr5-EGFP marks taste bud stem/progenitor cells in posterior tongue.* Stem cells (Dayton, Ohio), 2013. **31**(5): p. 992-1000.

16. Ren, W., et al., Single Lgr5- or Lgr6-expressing taste stem/progenitor cells generate taste bud cells ex vivo. 2014. **111**(46): p. 16401-16406.

17. Liu, H.X., et al., Multiple Shh signaling centers participate in fungiform papilla and taste bud formation and maintenance. Developmental Biology, 2013. **382**(1): p. 82-97.

18. Xu, M., et al., WNT10A mutation causes ectodermal dysplasia by impairing progenitor cell proliferation and KLF4-mediated differentiation. Nature Communications, 2017. **8**: p. 15397.

19. Tanaka, T., et al., Identification of stem cells that maintain and regenerate lingual keratinized epithelial cells. Nature Cell Biology, 2013. **15**(5): p. 511-518.

20. Castillo, D., et al., Induction of ectopic taste buds by SHH reveals the competency and plasticity of adult lingual epithelium. Development, 2014. **141**(15): p. 2993-3002.

21. Mistretta, C.M., et al., Cyclopamine and jervine in embryonic rat tongue cultures demonstrate a role for Shh signaling in taste papilla development and patterning: fungiform papillae double in number and form in novel locations in dorsal lingual epithelium. Developmental Biology, 2003. **254**(1): p. 1-18.

22. Fan, D., et al., *Taste bud formation depends on taste nerves.* eLife, 2019. **8**: p. e49226.

23. Barlow, L.A., C.B. Chien, and R.G. Northcutt, *Embryonic taste buds develop in the absence of innervation.* Development, 1996. **122**(4): p. 1103-1111.

24. Liu, F., et al., Wnt-beta-catenin signaling initiates taste papilla development. Nat Genet, 2007. **39**(1): p. 106-12.

25. Thirumangalathu, S. and L.A. Barlow, β-Catenin signaling regulates temporally discrete phases of anterior taste bud development. Development, 2015. **142**(24): p. 4309-17.

26. Liu, H.-X., et al., Sonic hedgehog exerts distinct, stage-specific effects on tongue and taste papilla development. Developmental Biology, 2004. **276**(2): p. 280-300.

27. El Shahawy, M., et al., Cell fate specification in the lingual epithelium is controlled by antagonistic activities of Sonic hedgehog and retinoic acid. PLOS Genetics, 2017. **13**(7): p. e1006914.

28. Prochazkova, M., et al., FGF signaling refines Wnt gradients to regulate the patterning of taste papillae. Development, 2017. **144**(12): p. 2212-2221.

29. Petersen, C.I., et al., FGF Signaling Regulates the Number of Posterior Taste Papillae by Controlling Progenitor Field Size. PLOS Genetics, 2011. **7**(6): p. e1002098.

30. Iwafuchi-Doi, M. and K.S. Zaret, *Cell fate control by pioneer transcription factors.* Development, 2016. **143**(11): p. 1833-1837.

31. Okubo, T., L.H. Pevny, and B.L. Hogan, *Sox2 is required for development of taste bud sensory cells.* Genes Dev, 2006. **20**(19): p. 2654-9.

32. Nishiguchi, Y., et al., *Bcl11b/Ctip2 is required for development of lingual papillae in mice.* Developmental Biology, 2016. **416**(1): p. 98-110.

33. Kist, R., et al., The Formation of Endoderm-Derived Taste Sensory Organs Requires a Pax9-Dependent Expansion of Embryonic Taste Bud Progenitor Cells. PLOS Genetics, 2014. **10**(10): p. e1004709.

34. Jonker, L., et al., Pax9 is required for filiform papilla development and suppresses skin-specific differentiation of the mammalian tongue epithelium. Mechanisms of Development, 2004. **121**(11): p. 1313-1322.

35. Olmsted, J.M.D., *Effects of cutting the lingual nerve of the dog.* Journal of Comparative Neurology, 1921. **33**(2): p. 149-154.

36. Segerstad, C.H.a., G. Hellekant, and A.I. Farbman, Changes in number and morphology of fungiform taste buds in rat after transection of the chorda tympani or chordalingual nerve. Chemical Senses, 1989. **14**(3): p. 335-348.

37. Guagliardo, N.A. and D.L. Hill, *Fungiform taste bud degeneration in C57BL/6J mice following chorda-lingual nerve transection.* Journal of Comparative Neurology, 2007. **504**(2): p. 206-216.

38. Parks, J.D. and M.C. Whitehead, Scanning electron microscopy of denervated taste buds in hamster: Morphology of fungiform taste pores. The Anatomical Record, 1998. **251**(2): p. 230-241.

39. Zuniga, J.R., N. Chen, and I.J. Miller, Jr, *Effects of chorda-lingual nerve injury and repair on human taste.* Chemical Senses, 1994. **19**(6): p. 657-665.

40. Lu, W.-J., et al., *Neuronal delivery of Hedgehog directs spatial patterning of taste organ regeneration.* Proceedings of the National Academy of Sciences, 2018. **115**(2): p. E200-E209.

41. Castillo-Azofeifa, D., et al., Sonic hedgehog from both nerves and epithelium is a key trophic factor for taste bud maintenance. Development, 2017. **144**(17): p. 3054-3065.

42. Lin, X., et al., *R-spondin substitutes for neuronal input for taste cell regeneration in adult mice.* Proceedings of the National Academy of Sciences, 2021. **118**(2): p. e2001833118.

43. Lu, C., et al., RNF43/ZNRF3 negatively regulates taste tissue homeostasis and positively regulates dorsal lingual epithelial tissue homeostasis. Stem Cell Reports, 2022.

44. Mistretta, C.M., et al., Alterations in size, number, and morphology of gustatory papillae and taste buds in BDNF null mutant mice demonstrate neural dependence of developing taste organs. Journal of Comparative Neurology, 1999. **409**(1): p. 13-24.

45. Meng, L., et al., Taste Bud-Derived BDNF Is Required to Maintain Normal Amounts of Innervation to Adult Taste Buds. eNeuro, 2015. **2**(6): p. ENEURO.0097-15.2015.

46. Tang, T., J. Rios-Pilier, and R. Krimm, *Taste bud-derived BDNF maintains innervation of a subset of TrkB-expressing gustatory nerve fibers.* Molecular and Cellular Neuroscience, 2017. **82**: p. 195-203.

47. Nosrat, I.V., R.F. Margolskee, and C.A. Nosrat, Targeted Taste Cell-specific Overexpression of Brain-derived Neurotrophic Factor in Adult Taste Buds Elevates Phosphorylated TrkB Protein Levels in Taste Cells, Increases Taste Bud Size, and Promotes Gustatory Innervation*. Journal of Biological Chemistry, 2012. **287**(20): p. 16791-16800.

48. Xu, M., et al., WNT10A mutation causes ectodermal dysplasia by impairing progenitor cell proliferation and KLF4-mediated differentiation. Nature Communications, 2017. **8**: p. 15397.

49. Gaillard, D., et al., β-catenin is required for taste bud cell renewal and behavioral taste perception in adult mice. PLOS Genetics, 2017. **13**(8): p. e1006990.

50. Gaillard, D., et al., β-Catenin Signaling Biases Multipotent Lingual Epithelial Progenitors to Differentiate and Acquire Specific Taste Cell Fates. PLOS Genetics, 2015. **11**(5): p. e1005208.

51. Castillo-Azofeifa, D., et al., Sonic hedgehog from both nerves and epithelium is a key trophic factor for taste bud maintenance. Development, 2017. **144**(17): p. 3054.

52. Lu, W.-J., et al., *Neuronal delivery of Hedgehog directs spatial patterning of taste organ regeneration.* Proceedings of the National Academy of Sciences, 2018. **115**(2): p. E200-E209.

53. Kumari, A., et al., Recovery of taste organs and sensory function after severe loss from Hedgehog/Smoothened inhibition with cancer drug sonidegib. Proceedings of the National Academy of Sciences, 2017. **114**(48): p. E10369-E10378.

54. Ermilov, A.N., et al., Maintenance of Taste Organs Is Strictly Dependent on Epithelial Hedgehog/GLI Signaling. PLOS Genetics, 2016. **12**(11): p. e1006442.

55. Ermilov, A.N., et al., Maintenance of Taste Organs Is Strictly Dependent on Epithelial Hedgehog/GLI Signaling. PLoS Genetics, 2016. **12**(11): p. e1006442.

56. Kumari, A., et al., Recovery of taste organs and sensory function after severe loss from Hedgehog/Smoothened inhibition with cancer drug sonidegib. Proceedings of the National Academy of Sciences, 2017. **114**(48): p. E10369-E10378.

57. Kumari, A., et al., Hedgehog (HH) pathway endogenous antagonist HHIP: unique lingual expression in filiform papillae during homeostasis and ectopic in fungiform papillae during HH signaling inhibition. Developmental Dynamics. **n/a**(n/a).

58. Cohn, Z.J., et al., Lipopolysaccharide-induced inflammation attenuates taste progenitor cell proliferation and shortens the life span of taste bud cells. BMC Neuroscience, 2010. **11**(1): p. 72.

59. Wang, H., et al., *Inflammation Activates the Interferon Signaling Pathways in Taste Bud Cells.* The Journal of Neuroscience, 2007. **27**(40): p. 10703-10713.

60. Kaufman, A., et al., Inflammation arising from obesity reduces taste bud abundance and inhibits renewal. PLOS Biology, 2018. **16**(3): p. e2001959.

61. Castillo-Azofeifa, D., et al., SOX2 regulation by hedgehog signaling controls adult lingual epithelium homeostasis. Development, 2018. **145**(14).

62. Ohmoto, M., et al., SOX2 regulates homeostasis of taste bud cells and lingual epithelial cells in posterior tongue. PLOS ONE, 2020. **15**(10): p. e0240848.

63. Matsumoto, I., et al., *Skn-1a (Pou2f3) specifies taste receptor cell lineage.* Nature Neuroscience, 2011. **14**(6): p. 685-687.

# CHAPTER 3

# TASTE BUDS ARE NOT DERIVED FROM NEURAL CREST IN MOUSE, CHICKEN, AND ZEBRAFISH [1]

[1] Zhonghou Wang*, Wenxin Yu*, Brett Marshall*, Yuta Yoshida, Renita Patel, Xiaogang Cui, Rebecca Ball, Linlin Yin, Fuminori Kawabata, Shoji Tabata, Wenbiao Chen, Robert N. Kelsh, James D. Lauderdale, and Hong-Xiang Liu. 2021. *Developmental Biology*. 471:76-88. Reprinted here with permission of publisher. * Authors contributed equally to this work.

## 3.1 Abstract

Our lineage tracing studies using multiple Cre mouse lines showed a concurrent labeling of abundant taste bud cells and the underlying connective tissue with a neural crest origin, warranting a further examination on the issue of whether there is an neural crest derivation of taste bud cells. In this study, we mapped neural crest cell lineages in three different models, Sox10-iCreER$^{T2}$/tdT mouse, GFP$^{+}$ neural fold transplantation to GFP$^{-}$ chickens, and Sox10-Cre/GFP-RFP zebrafish model. We found that in mice, Sox10-iCreER$^{T2}$ specifically labels neural crest cell lineages with a single dose of tamoxifen at E7.5 and that the labeled cells were widely distributed in the connective tissue of the tongue. No labeled cells were found in taste buds or the surrounding epithelium in the postnatal mice. In the GFP$^{+}$/GFP$^{-}$ chicken chimera model, GFP$^{+}$ cells migrated extensively to the cranial region of chicken embryos ipsilateral to the surgery side but were absent in taste buds in the base of oral cavity and palate. In zebrafish, Sox10-Cre/GFP-RFP faithfully labeled known neural crest-derived tissues but did not label taste buds in lower jaw or the barbel. Our data, together with previous findings in axolotl, indicate that taste buds are not derived from neural crest cells in rodents, birds, amphibians or teleost fish.

Key words: Taste buds, neural crest, progenitors, mouse, chicken, zebrafish.

## 3.2 Introduction

Taste buds are taste sensory organs located on the tongue and inside the oral cavity of all vertebrates. In some fishes and amphibians, particularly species with barbels, taste buds are also found in the skin. A large proportion of taste bud cells are glial-like (type I) [1-6] and a small subset is neuronal-like (type III) [3, 7-11]. Given that glial cells in the peripheral nervous system are derived from the neural crest [12-15] and neurons are from either neural crest [13-18] or epibranchial placodes [15, 19-24], a question has been asked whether taste buds could plausibly

have been derived either from the neural crest, or from the epibranchial placodes, or from the local epithelium [25]. Barlow and Northcutt used grafting experiments between pigmented and non-pigmented axolotl embryos and showed that neither the neural crest nor epibranchial placodes contribute to taste buds, whereas DiI-labeled endoderm formed both taste buds and the surrounding epithelium in the oropharynx, confirming an endoderm-derived local epithelial origin for taste buds in axolotl [25].

Although compelling evidence demonstrates a non-neural crest origin of taste bud cells in axolotl [25], studies in rodents indicate that, in addition to the lingual epithelium [26-31], neural crest may also contribute to taste bud cells [32-34]. This difference between axolotl and rodents suggests that there may be a difference in taste bud development between non-mammals and mammals.

In mice, evidence that taste bud progenitors arise from local epithelium is solid [25-31]. Stone and colleagues identified local epithelium as taste progenitor source using mosaic X-inactivation chimera mouse model [28], which was later reiterated studies that traced the lineage of local epithelium to taste buds using Cre-LoxP transgenic mouse model [29]. However, the question remains whether surrounding epithelium is the "sole" source of taste bud progenitors.

In the past several years, the use of transgenic mouse lines to trace the lineage of cranial neural crest cells has raised new speculations regarding neural crest derivatives, e.g., tooth bud [35] and olfactory [36, 37] epithelial cells. In the tongue organ, neural crest has been found to be the major contributor to the mesenchyme [38] and connective tissue under the epithelium [32-34]. Our recent findings revealed that a significant proportion of taste bud cells are labeled with P0-Cre [33, 34], Dermo1-Cre [33], Sox10-Cre [32] concurrently with the underlying connective tissue cells in the absence of labeling in the surrounding lingual epithelium. In contrast, Wnt1-

Cre-labeled cells are rarely seen in taste buds although labeled cells are extensive in the underlying connective tissue [34]. Therefore, the published data suggest the possibility of a neural crest derivation of taste buds [32-34] but this fundamental issue has not yet settled. Given that none of these models labels all neural crest cells, nor do they label neural crest cells exclusively [39, 40], animal models that specifically and exclusively label neural crest cell lineages and detailed examinations are imperative.

To address the fundamental issues of whether taste bud cells have a derivation from neural crest cells and whether this contribution is species-specific, we performed lineage tracing for neural crest cells in three model species, using Sox10-iCreER$^{T2}$/tdT mice, GFP$^{+}$/GFP$^{-}$ chicken chimeras, and Sox10-Cre/GFP-RFP zebrafish. We found that in these three models neural crest cell lineages were extensively marked but not found in taste buds. Together with previous findings in axolotl [25], the data from these different model species provide support for the idea that taste buds do not have a neural crest derivation.

## 3.3 Materials and methods

### *3.3.1 Animals*

Animal use was approved by The University of Georgia Institutional Animal Care and Use Committee and was in accordance with the National Institutes of Health Guidelines for care and use of animals for research. Three species of animals were used: mouse, chicken and zebrafish.

Mice were maintained and bred in the animal facility of the Animal and Dairy Science department at the University of Georgia at 22℃ under 12-hour day/night cycles. Sox10-iCreER$^{T2}$ (CBA;B6-Tg(Sox10-icre/ER$^{T2}$)388Wdr/J, Stock#027651) [41] and R26-tdTomato (hereafter tdT) Cre reporter mice (B6.Cg-Gt(ROSA)26Sor$^{tm14(CAG-tdTomato)Hze}$/J, Stock#007914) [42] were obtained from The Jackson Laboratory. The hemizygous Sox10-iCreER$^{T2}$ mice and

homozygous tdT reporter breeders were crossed to generate Sox10-iCreER$^{T2}$/tdT mice. No significant difference was found in the distribution pattern of labeled cells between males and females; therefore, males and females were grouped together and used at the examined stages. Cre negative littermates served as controls. FVB/NJ wild type mice (The Jackson Laboratory, Stock#001800) were used to breed in parallel for fostering caesarean born Sox10-iCreER$^{T2}$/tdT pups.

Chicken embryos were produced by incubating fertilized eggs horizontally in the cabinet incubator (Cat#1502 "SPORTSMAN", GQF Manufacturing Company, Inc, Savannah, GA) in the lab room at the University of Georgia. Fertilized Roslin GFP$^{+}$ donor [43] and Roslin GFP$^{-}$ host chicken eggs were purchased from Clemson University.

Zebrafish were housed in the Paul D. Coverdell Building Fish Facility at the University of Georgia at 28.5℃ under 12-hour day/night cycles. Sox10-EGFP zebrafish (TG(-4.9sox10:egfp)$^{ba2}$ and Sox10-Cre zebrafish (TG(-4725sox10:Cre)$^{ba74}$ were obtained from Dr. Robert N. Kelsh, University of Bath, Bath, UK) [44-46]. Hemizygous Sox10-Cre zebrafish (TG(-4725sox10:Cre)$^{ba74}$ were crossed with homozygous GFP-RFP Cre reporter zebrafish (Tg(eab2:[EGFP-T-mCherry]), from Dr. Wenbiao Chen, Vanderbilt University, Nashville, TN) [47] to generate Sox10-Cre/GFP-RFP zebrafish. Timed pairings were allowed for 30 min for synchronized embryo development.

PCR genotyping was performed using the following primers: (1) mouse Cre allele forward 5'-ATT GCT GTC ACT TGG TCG GC-3' and reverse 5'-GGA AAA TGC TTC TGT CCG TTT GC-3' to detect the mouse Cre recombinase allele; (2) zebrafish Cre allele forward 5'-CCA TGT CCA AAT TTA CTG ACC GTA C-3' and reverse 5'-CAT CTT CAG GTT CTG CGG GAA AC-3' to detect the zebrafish Cre recombinase allele; (3) zebrafish EGFP allele forward 5'-

GTT CAT CTG CAC CAC CGG C-3' and reverse 5'-TTG TGC CCC AGG ATG TTG C -3' to detect the zebrafish EGFP reporter allele; (4) iCreER$^{T2}$ allele forward 5'-GAG ACG GAC CAA AGC CAC T-3' and reverse 5'-CTG CAG CCT CCT CCA CTG-3' to detect the mouse iCreER$^{T2}$ recombinase allele; (5) msSRYz_SexDet forward, 5'-TTG TCT AGA GAG CAT GGA GGG CCA TGT CAA-3' and reverse 5'-CCA CTC CTC TGT GAC ACT TTA GCC CTC CGA-3' to determine the sex of mouse embryos; and tdT allele forward, 5'-CTG TTC CTG TAC GGC ATG G-3' and reverse 5'-GGC ATT AAA GCA GCG TAT CC-3' to determine the expression of tdT reporter.

*3.3.2 Tamoxifen treatment of mice and pups fostering*

Timed pregnant mice were used for labeling neural crest cell lineages specifically. Noon of the day of vaginal plug detection in mice was designated embryonic (E) day 0.5. To induce Cre recombination in embryos at E8.0, tamoxifen (Tmx) (Cat No. T5648; Sigma-Aldrich, Inc, St. Louis, MO) was dissolved in corn oil at a concentration of 11.1 mg/mL, and a single dose of 0.1 mL tamoxifen solution was given through oral gavage using 16 G x 38 mm polyurethane feeding tubes (Cat No. FTPU-16-50, Instech Laboratories, Inc, Plymouth Meeting, PA) to the pregnant dams carrying E7.5 embryos (Tmx$^{E7.5}$). Vehicle (Veh) controls were treated with corn oil at the same stage.

Tamoxifen injection in pregnant mice has been reported to cause dystocia. To resolve this problem, caesarean sections were performed to deliver the Sox10-iCreER$^{T2}$/tdT embryos at E18.5. The delivered pups were fostered by a FVB/J nursing dam immediately after caesarean birth.

*3.3.3 $GFP^+$ neural fold transplantation in $GFP^-$ chicken embryos*

At Hamburger Hamilton 9 stage (29-33 hours post-incubation), a window on the eggshell was opened above the embryos. A drop of sterile 0.5% neutral red (Cat No. N2889-100ML, Sigma-Aldrich, Inc, St. Louis, MO) in 0.9% NaCl was used to stain and stage the embryos under a dissection microscope. According to the previous report that an "insertion" instead of "replacement" of neural folds for graft transplantation increased the survival rate while maintaining the normal development of neural crest and neural crest-derived organs [48], a single side of neural fold at the levels of posterior midbrain and anterior hindbrain were dissected from a $GFP^+$ chicken embryo and inserted into the lesion made laterally adjacent to the counterpart of a $GFP^-$ chicken embryo at the same somite stage. After the surgery, embryos were incubated until desired stages ranging from 1 to 19 days post-surgery (DPS).

*3.3.4 Tissue collections*

Mouse embryos at embryonic E8.0-8.5 were collected between 10am and 4pm. The embryos were also staged by counting somite pairs. Embryos at 7~15-somite stages (n=4 for both vehicle- and tamoxifen-treated groups) were selected and used for further analyses. Pregnant dams were euthanized with $CO_2$ followed by cervical dislocation. The uterus was removed and placed in a petri dish containing 0.1 M phosphate buffered saline (PBS) (Cat No. CP4390-48, Denville Scientific, Inc, Metuchen, NJ). Embryos were dissected from the uterus under a stereomicroscope and fixed with 4% paraformaldehyde (PFA) (Cat No. AAJ19943k2, Thermo Fisher HealthCare, Pittsburgh, PA) in 0.1 M PBS at 4℃ for 2 hours. Postnatal mice were harvested at 2 weeks, 4 weeks, and 8 weeks (n=3 for both vehicle- and tamoxifen-treated at each stage). Mice were euthanized with $CO_2$ followed by transcardial perfusion using 10 mL warm 0.1 M PBS, followed by 10 mL warm and 20 mL cold 2% PFA in 0.1 M PBS. Tongues,

soft palates, heads, and dorsal root ganglia were dissected and further fixed in 2% PFA at 4℃ for 2 hours.

$GFP^+/GFP^-$ chicken chimeras with successful transplantation were collected at 1 (n=5), 2 (n=2), 14 (n=2), and 19 (n=5) DPS. Palates and base of oral cavities were dissected from embryos at 14 and 19 DPS. Whole embryos at 1 and 2 DPS and dissected tissues at 14 and 19 DPS were then fixed with 4% PFA in 0.1 M PBS at 4℃ for 2 hours.

Zebrafish eggs were collected after 1 hour pairing and incubated in 28.8℃ egg water until collections at 7- (n=3), 10- (n=3), and 12-somite (n=3) stages and 5.5 (n=3), 15 (n=3), and 30 (n=3) days post fertilization (dpf) and adult (90 days to 2 years) (n=3). Zebrafish were anesthetized with a neutrally-buffered solution of 0.016% Tricaine (Cat No. T0941, TCI AMERICA, Inc, Portland, OR), followed by decapitation and fixation in 4% PFA at 4℃ for 2 hours. For 30-day-old and adult fish, fixed heads were further treated with 0.5 M EDTA (Cat No. RES3002E, Sigma-Aldrich, Inc, St. Louis, MO) for bone softening, with medium change every other day for 2 weeks.

*3.3.5 Immunohistochemistry*

All fixed tissues were cryoprotected in 30% sucrose in 0.1 M PBS for at least 48 hours at 4℃. Tissues were trimmed and dissected, embedded in O.C.T. (Cat No. 23-730-571, Thermo Fisher Scientific, Pittsburgh, PA) and rapidly frozen as such for: (1) Mice: transverse sections of cranial region of E8.5 embryos, sagittal sections of whole tongue of E12.5 embryos, sagittal sections of the left and right halves of the anterior 2/3 of postnatal oral tongue where fungiform papillae are distributed, sagittal sections of both foliate papillae, left and right halves of soft palate, and coronal sections of single circumvallate papilla; (2) Chickens: transverse sections of cranial region of embryos at 1 DPS, sagittal sections of whole embryos at 2 DPS, base of oral

cavities of embryos at 14 and 19 DPS, and palates of embryos at 19 DPS; (3) Zebrafish: horizontal sections of zebrafish embryos, sagittal sections of heads of 5.5- and 15-dpf-old fish, sagittal sections of lower jaws, barbels, and body segments of 30-dpf and adult fish.

Frozen sections were cut at 8 μm in thickness and mounted onto charged slides (Fisher brand™ Superfrost™ Plus Microscope Slides, Cat No. 12-550-15, Thermo Fisher Scientific, Pittsburgh, PA). Non-specific binding was blocked with 10% normal donkey serum (Cat No. SLBW2097, Sigma-Aldrich, Inc, St. Louis, MO) in 0.1 M PBS containing 0.3% Triton X-100 (Cat No. X100-100ML, Sigma-Aldrich, Inc, St. Louis, MO) for 30 min, followed by overnight incubation with primary antibody diluted with 0.1 M PBS containing 0.3% Triton X-100 and 1% normal donkey serum. Primary antibodies used in this study are listed in Table 3.1.

After rinses in 0.1 M PBS (3 times, 10 min each), sections were incubated in Alexa Fluor® 488 (for E-cadherin, GFP), Alexa Fluor® 546 (for dsRed), and/or Alexa Fluor® 647 (for all the other markers)-labeled secondary antibody (1:500, Invitrogen, Eugene, OR) for 1 hour at room temperature. Sections were rinsed and then counterstained with DAPI (200 ng/mL, Cat No. D1306, Thermo Fisher Scientific, Pittsburgh, PA). After rinses with 0.1 M PBS followed by dipping in Milli-Q water (Direct-Q® 3 UV water purification system, Millipore, MA). Sections were air dried and coverslipped with Prolong® diamond antifade mounting medium (Cat No. P36970, Thermo Fisher Scientific, Pittsburgh, PA).

*3.3.6 Photomicroscopy*

Immunoreacted sections on slides were analyzed under a fluorescent light microscope (EVOS FL, Thermo Fisher Scientific, Pittsburgh, PA) and images were taken using a laser scanning confocal microscope (Zeiss LSM 710, Zeiss, Germany). Whole mount tissues were

examined and images taken using a stereomicroscope (SZX116, Olympus, Japan). Images were assembled using Adobe Photoshop with minimal editing.

## 3.4 Results

### *3.4.1 In mice, Sox10-iCreER$^{T2}$ specifically and extensively labels neural crest cell lineages with a single dose of tamoxifen at E7.5 and labeled cells are not found in taste buds*

In mouse embryos, Sox10 expression has been found specifically in neural crest cells during early embryonic stages [49, 50]. To exclusively map the lineages of Sox10$^{+}$ neural crest cells, we utilized a Sox10-iCreER$^{T2}$ mouse model [41] in which iCreER$^{T2}$ is driven by endogenous Sox10 promoter and tamoxifen administration was performed at E7.5 when neural crest cells were about to be generated [51, 52] and express Sox10 [49, 50]. To validate the specificity and recombination efficiency of Sox10-iCreER$^{T2}$ in labeling neural crest cell lineages, Sox10-iCreER$^{T2}$ expression were analyzed in vehicle and tamoxifen-treated mice (n=3 for each group). In transverse sections of E8.5 (12-somite) Sox10-iCreER$^{T2}$ embryos at 1 day after a single-dose vehicle (corn oil) treatment to the pregnant dam at E7.5 (Veh$^{E7.5}$), Cre recombinases were detected exclusively in Sox10$^{+}$ cranial neural crest cells (Figure 3.1A-B), including the cells in the trigeminal neural crest tissue [53] (Figure 3.1A), branchial arch 1 (Figure 3.1A), and optic eminence (Figure 3.1A). Importantly, Cre immunosignals were restricted to the cytoplasm (arrowheads) of the neural crest cells (Figure 3.1B). In the E8.5 (9-somite) Sox10-iCreER$^{T2}$ embryos with tamoxifen treatment to the pregnant dam at E7.5 (Tmx$^{E7.5}$), Cre immunosignals were found within the nuclei (arrows) of Sox10$^{+}$ neural crest cells (Figure 3.1C). In Tmx$^{E7.5}$ E12.5 Sox10-iCreER$^{T2}$/tdT embryos (n=3), tdT signals were obvious in the spatulate tongue (Figure 3.1D$_1$) and extensively distributed in the tongue mesenchyme under the epithelium (Figure 3.1D$_2$). In young adult (8 weeks, n=3) Sox10-iCreER$^{T2}$ mice (Tmx$^{E7.5}$), tdT signals were

found in tissue compartments that are known to arise from neural crest, including the dorsal root ganglia (Figure 3.1E). No tdT signals were found in corresponding Cre-negative control (data not shown). Together, a single dose of tamoxifen treatment to Sox10-iCreER$^{T2}$ dam at E7.5 was sufficient to label neural crest cell lineages specifically and extensively.

To map the lineage of Sox10$^{+}$ neural crest-derived cells in taste buds, the distribution of Sox10-iCreER$^{T2}$/tdT-labeled cells (Tmx$^{E7.5}$) was thoroughly analyzed in the major tissues containing taste buds including the soft palate and all three types of lingual taste papillae, i.e., fungiform, foliate, and circumvallate, in 2-week, 4-week and 8-week-old mice (n=3 for each stage). In serial sections of the soft palate and tongue tissues, Sox10-iCreER$^{T2}$ driven tdT$^{+}$ cells were extensively distributed in the connective tissue (Figure 3.2A-C). In contrast, Sox10-iCreER$^{T2}$/tdT-labeled cells were not observed in taste buds located by the immunosignals of Krt8 in the soft palate (Figure 3.2C), and in all three types of lingual taste papillae, i.e., fungiform (Figure 3.2A-C), foliate (Figure 3.2C), circumvallate (Figure 3.2A-C). Additionally, tdT$^{+}$ cells were not found in the taste bud-surrounding tongue epithelium, including basal epithelial cells that are known as progenitors of taste bud cells [26-31].

*3.4.2 In GFP$^{+}$/GFP$^{-}$ chicken chimera model, GFP$^{+}$ neural crest cell lineages were labeled and sustained in the craniofacial regions, but not found in taste buds*

To map GFP$^{+}$ neural crest cell lineages in craniofacial regions, a GFP$^{+}$/GFP$^{-}$ chimera chicken model was used. One side of neural folds at the posterior midbrain and anterior hindbrain levels was dissected from a transgenic GFP$^{+}$ chicken [43] and then inserted into an incision lateral to the dorsal neural fold of a GFP$^{-}$ chicken at the corresponding level of rostral-caudal axis (Figure 3.3A). At 1 day post-surgery (DPS) (n=5), ventrally migrating streams of GFP$^{+}$ neural crest cells were observed in the transplantation side of the embryos (Figure 3.3B).

To further validate the identity of $GFP^+$ cells, HNK1 [54] was used to label migrating neural crest cells. $GFP^+$ cells were largely, if not all, labeled by HNK1 (Figure 3.3C). Moreover, $GFP^+$ neural crest cells were in the vicinity of ventral side of mesencephalon, which specifically contributes to oral tissues that host taste buds (Figure 3.3C).

To characterize the migration of neural crest lineages, chimeric embryos were collected at various stages. At 2 DPS (n=2), $GFP^+$ cells populated at the ipsilateral side of pharyngeal arch to the neural fold insertion (Figure 3.4A), which would eventually give rise to oral tissues including beaks. At 14 (n=2) and 19 DPS (n=5), GFP signals were detected in multiple craniofacial regions (Figure 3.4A). Of note, the GFP signals were remained restricted to the surgical side, which could be appreciated by a clear boundary in the midline separating $GFP^+$ and $GFP^-$ tissues in the lower (Figure 3.4A) and upper (Figure 3.4A) beaks. Absence of GFP signals on the contralateral side of surgery was consistent in all examined chimeric embryos (Figure 3.4A).

In sagittal sections of surgical side of pharyngeal arch at 2 DPS and the bases of oral cavities at 14 and 19 DPS, $GFP^+$ cells were extensively and exclusively distributed in connective tissues immediately beneath the epithelium marked by EpCAM (Figure 3.4B). To further confirm whether there were $GFP^+$ cells in taste buds or not, thorough examinations were performed in serial sections of $GFP^+$ gustatory tissues in all surviving 19 DPS chimeric embryos (n=5) in which early taste buds have emerged. In the sections immunostained with a specific taste bud cell marker α-Gustducin, only the taste buds that were surrounded by $GFP^+$ connective tissue cells were included for analysis. A total of 40 taste buds from serial sections of $GFP^+$ base of oral cavities and 37 taste buds from serial sections of $GFP^+$ palates were imaged and analyzed. In contrast to the abundant distribution in the underlying connective tissue (Figure 3.5), $GFP^+$

cells were not observed in oral epithelium including taste buds and adjacent salivary glands in either the base of oral cavities (Figure 3.5A) or palates (Figure 3.5B).

*3.4.3 In zebrafish, Sox10$^+$ neural crest cell lineage was not observed in taste buds*

In addition to the use of mice and chickens, we introduced zebrafish, another widely used animal model for neural crest fate mapping [45, 55-60], to trace the lineage of Sox10$^+$ neural crest cells in taste buds. To verify the Sox10 expression in neural crest cells and not in taste buds, Sox10-EGFP zebrafish [45, 46] were used (n=3 for each embryonic stage). In early embryos, EGFP signals emerged in the trunk region at 7-somite stage (Figure 3.6A) and later appeared in cranial regions in 10- and 12-somite embryos (Figure 3.6A). Importantly, those signals were exclusively found in Sox10$^+$ neural crest cells (Figure 3.6B) in transverse sections of cranial region of 12-somite fish. Of note, in fish at 5.5 dpf (n=3), EGFP signals were absent in the taste buds marked by calretinin (Figure 3.6C).

The specific expression of Sox10 in neural crest while being absent in fish taste buds allowed the use of Sox10-Cre fish model [44] to perform lineage tracing of Sox10$^+$ neural crest to taste buds. The use of GFP-RFP [47], in which the ubiquitous and constitutive GFP expression could be effectively switched to RFP upon Cre induced recombination, gave us a sharp contrast of signals for an easy recognition of Cre-labeled cells. Sox10-Cre driven RFP signals could be found in well-known neural crest-derived organs such as gills (Figure 3.6D) [61, 62]. In lower jaw where most taste buds reside in zebrafish, Sox10-Cre driven RFP signals were not found in taste buds at 15 dpf (n=3), 30 dpf (n=3), and adult stages (n=3) (Figure 3.6E). However, RFP expression was readily observed in cells within the connective tissue in all tissues examined (Figure 3.6E). Similar labeling patterns were also found in adult barbels (Figure 3.6E).

## 3.5 Discussion

### *3.5.1 Taste bud cells are not derived from neural crest*

The neural crest is a multipotent cell population derived from the lateral ridges of the neural plate in early vertebrate embryos [63]. By the fusion of neural folds, neural crest cells leave the dorsal part of the neural epithelium, migrate extensively and give rise to a wide variety of differentiated cell types, including neurons and glial cells of the peripheral nervous system and connective tissue of the head [12, 16-18, 64]. For years, the use of transgenic mouse lines has facilitated the fate mapping of cranial neural crest, and findings have led to new speculated neural crest derivatives, e.g., tooth bud [35] and olfactory [36, 37] epithelial cells. Taste buds have been regarded as solely derived from the surrounding epithelium [26-31]. However, recent findings revealed a potential of neural crest derivation of taste buds in mammals [32-34], thereby suggesting a potential difference in how taste buds from in mammals compared to non-mammalian vertebrate.

In the present study we tested the contribution of neural crest lineage to taste buds in mammals, birds, and teleost fish using Sox10-iCreER$^{t2}$/tdT mouse model, GFP$^{+}$/GFP$^{-}$ chicken chimera model, and Sox10-Cre/GFP-RFP zebrafish model. We report that each of these models marks neural crest lineage specifically or/and extensively. Despite careful examination of multiple individuals in each model, we were unable to find any examples where the neural crest has contributed to cells in the taste buds. Our data, in combination with those from axolotl [25], provide solid evidence that taste buds, composed largely of glial-like (type I) and neuronal-like (type III) cells, are not derived from neural crest in mammalian and non-mammalian animals.

Our recent lineage tracing results using Sox10-Cre mice have indicated three candidates of Sox10-expressing taste bud progenitors: neural crest or non- neural crest derived connective

tissue cells in the core of taste papillae, or von Ebner's glands [32]. The absence of Sox10-iCreER$^{T2}$ (Tmx$^{E7.5}$) labeled cells in taste buds and surrounding epithelium rules out neural crest cells as Sox10-expressing progenitors for taste buds. This leaves two candidates for future work required to assess the Sox10-expressing cell types under the lingual epithelium [32], including non- neural crest-derived connective tissue and/or von Ebner's gland [32].

Even though neural crest does not give rise to taste bud cells, the connective tissue cells in tongue are largely derived from neural crest [32-34]. Neural crest-derived mesenchymal cells interact with the overlying epithelium and play essential roles in taste bud and taste papilla development [65-67]. For examples, mesenchymal FGF10 has been reported to control the size of fungiform papillae via modulating epithelial Wnt/β-catenin signals [65]; and mesenchymal Follistatin modulates epithelial BMP7 signaling to control size and spacing of fungiform papillae and inhibits gustatory fate of intermolar eminence [66]. Future studies using high throughput techniques will be beneficial for identifying novel factors from neural crest derivatives that are required for taste bud formation and maintenance.

*3.5.2 Neural crest lineage tracing: limitations of Cre mouse models and ideal using Sox10-iCreER$^{T2}$*

Cre/loxP site-specific recombination system is a noninvasive approach that enables long-term lineage tracing. In the past several years, a number of Cre mouse lines have been generated for neural crest lineage tracing [39]. For many lines, labeling specificity has been a problem because of ectopic expression of the Cre transgene and/or labeling of markers in cells/tissues beyond neural crest. Additionally, the use of non-inducible Cre can lead to labeling of cell lineages from more than one specific cell type. For example, Wnt1-Cre mainly labeled the mesencephalic stream of neural crest [39, 40], which only partially contributes to pharyngeal

arch 1 [38], i.e., the primordium of the tongue. In addition, ectopic Wnt1 expression from Wnt1-Cre transgene impaired midbrain development [68], and subsequently affected overall development of the mouse. P0-Cre mainly labels rhombencephalic stream of neural crest [40], which is a major contributor to pharyngeal arches [38]. However, the expression of P0-Cre was not neural crest lineage-restricted, e.g., P0-Cre labeled cells were also found in notochord [40], and ectoderm-derived non-gustatory lingual epithelium at embryonic stages [34, 69]. Dermo1-Cre has frequently been used to target mesenchymal cell lineages [70-73], however, instead of neural crest-derived cell labeling only, Dermo1-Cre also labeled mesoderm-derived mesenchymal cells, e.g., osteoblasts, chondrocytes [74], perichondrial, and periosteal cells in the trunk and part of the head region [75]. Sox10 is a specific marker for neural crest cells during early embryonic stages [49, 50]. In a previous study using Sox10-Cre to trace the lineage of Sox10-expressing cells in mouse model, Sox10 expression was found in cells beyond neural crest cell lineage, e.g., von Ebner's gland cells under taste papillae [32]. Together, careful attention must be paid when using these Cre mouse models for tracing neural crest cell lineages in order to avoid erroneous conclusions about the labeled cell types [34]. Indeed, inconsistent observations were obtained in our previous mouse studies using Wnt1-Cre [34], P0-Cre [33, 34], Dermo1-Cre [33], and Sox10-Cre [32] driver lines to trace the lineage of neural crest to taste buds, which raises suspicions about the specificity of those models in labeling the neural crest lineage.

To test our findings of potential neural crest origin of taste buds in Sox10-Cre as well as other Cre-driver lines in previous studies, we introduced an inducible Cre model Sox10-iCreER$^{T2}$ [41] to specifically target Sox10-expressing neural crest lineage. CreER$^{T2}$ is a fusion protein of Cre recombinase and mutant form of the human estrogen receptor that blocks the

nuclear translocation of Cre without exposure to tamoxifen [76]. We showed that tamoxifen administration in a given time window when Sox10 expression was exclusive in migrating neural crest cells triggered Cre recombination in neural crest cells, labeling them and their derivatives. We found that a single dose of tamoxifen administration at E7.5 was reliable and sufficient for DNA recombination in neural crest cells, and that well-known neural crest derivatives were extensively labeled. Our data suggest that use of the Sox10-iCreER$^{T2}$ line in this way is ideal for neural crest lineage mapping in mice. This model enables us to generate definitive data to answer whether neural crest gives rise to particular cell types, e.g., taste bud cells.

*3.5.3 GFP$^{+}$ neural fold insertion in chicken embryos is ideal for longitudinally tracking neural crest cell lineages in ovo*

Chickens share the common marker Vimentin with humans in labeling taste bud cells [77], which makes it unique for neural crest lineage mapping in taste buds and facilitates comparison of findings between these two species. The low survival rate of chimeras up to hatch after neural fold transplantation may limit the neural crest lineage mapping in post-hatch birds. However, taste buds in chickens develop well before hatching, which makes it a good model to use in the present study.

Neural fold transplantation in avian embryos is a well-established, but technically challenging, method to trace cell lineages of the neural crest [78-81]. The development of lines of transgenic chickens in which GFP is ubiquitously expressed facilitates assessment of migrating neural crest and their contribution to tissues without staining in GFP$^{+}$/GFP$^{-}$ chimeras [43]. Such a model system allows for longitudinal *in ovo* observations for neural crest cell migration and lineage tracing. Even though assays involving dye labeling and retroviral infection of neural crest cells can facilitate the experimental procedures and increase the post-surgery

survival rate, neural fold transplantation is more advantageous in providing a highly specific method in labeling neural crest cells. Moreover, we compared $GFP^+$ neural fold insertion into the tissue lateral to the neural fold of $GFP^-$ host embryo with neural fold replacement, and found that insertion increased the embryo survival rate and $GFP^+$ cells from inserted neural fold precede the $GFP^-$ host cells and occupy the target tissue extensively.

*3.5.4 Sox10-Cre zebrafish model is useful for labeling cranial neural crest cell lineages*

Zebrafish is an emerging model with advantages of easily accessible and transparent embryos for genetic manipulation and observation of dynamic developmental processes [45, 55-60]. Here we used lines of fish harboring transgenes for Sox10-EGFP or Sox10-Cre to label neural crest cells. Sox10-derived transgenes in zebrafish have been used by a number of investigators to image neural crest cells and neural crest lineages throughout the developing zebrafish embryo [44, 46, 82-84]. As a consequence, the expression characteristics of the two established transgenic lines used in the current study are well known. Both lines are known to drive expression in migratory neural crest cells and their derivatives at all axial levels of the embryo and have been used to study the role of neural crest in the development of a number of tissues, including craniofacial cartilage, pigment cells, and dorsal root ganglia [44, 46, 82-84]. Additionally, both lines are known to drive expression in cells that are not derived from neural crest, such as in the pectoral fin cartilage, otic epithelium, some neurons and oligodendrocytes of the central nervous system, and in some muscle tissues [39, 44, 46, 82]. Several of these non-neural crest derived cells normally express Sox10 [85]. We confirmed that both the Sox10-EGFP and Sox10-Cre lines are expressed extensively in cranial neural crest cells and their lineages in developing and adult zebrafish, including cells that could potentially contribute to taste buds.

The complete absence of Sox10-Cre–labeled cells in all taste buds in juvenile and adult fish demonstrates that the taste buds in zebrafish did not receive a contribution from neural crest.

In the present study, the use of Sox10-Cre/GFP-RFP zebrafish allowed us to map neural crest derivatives in taste buds. Unlike the Sox10-Cre mouse line, Sox10-Cre labeled cells were not found in zebrafish taste buds. One possible explanation for the differential expression of these transgenes in mice and zebrafish is that there are species-specific differences in Sox10 expression outside of the neural crest. Of note, potential distinct ectopic expression of Cre cannot be ignored. Careful attention needs to be paid to validating the behavior of transgenic constructs both within a species and especially when comparing results across species.

## 3.6 References


1. Farbman, A.I., *Electron microscope study of the developing taste bud in rat fungiform papilla.* Developmental biology, 1965. **11**(1): p. 110-135.

2. Pumplin, D.W., C. Yu, and D.V. Smith, *Light and dark cells of rat vallate taste buds are morphologically distinct cell types.* Journal of Comparative Neurology, 1997. **378**(3): p. 389-410.

3. Barlow, L.A. and O.D. Klein, Developing and regenerating a sense of taste, in Current topics in developmental biology. 2015, Elsevier. p. 401-419.

4. Bartel, D.L., et al., Nucleoside triphosphate diphosphohydrolase-2 is the ecto-ATPase of type I cells in taste buds. Journal of Comparative Neurology, 2006. **497**(1): p. 1-12.

5. Miura, H., et al., Sonic hedgehog–expressing basal cells are general post-mitotic precursors of functional taste receptor cells. Developmental Dynamics, 2014. **243**(10): p. 1286-1297.

6. Lawton, D.M., et al., *Localization of the glutamate–aspartate transporter, GLAST, in rat taste buds.* European Journal of Neuroscience, 2000. **12**(9): p. 3163-3171.

7. Huang, T., L. Ma, and R.F. Krimm, Postnatal reduction of BDNF regulates the developmental remodeling of taste bud innervation. Developmental biology, 2015. **405**(2): p. 225-236.

8. Roper, S.D. and N. Chaudhari, *Taste buds: cells, signals and synapses.* Nature Reviews Neuroscience, 2017. **18**(8): p. 485-497.

9. Murray, R., *The ultrastructure of taste buds.* The ultrastructure of sensory organs, 1973: p. 1-81.

10. Murray, R.G., *Cellular relations in mouse circumvallate taste buds.* Microscopy research and technique, 1993. **26**(3): p. 209-224.

11. Murray, R.G., A. Murray, and S. Fujimoto, *Fine structure of gustatory cells in rabbit taste buds.* Journal of ultrastructure research, 1969. **27**(5-6): p. 444-461.

12. Vega-Lopez, G.A., S. Cerrizuela, and M.J. Aybar, *Trunk neural crest cells: formation, migration and beyond.* International Journal of Developmental Biology, 2017. **61**(1-2): p. 5-15.

13. Morrison, S.J., et al., Prospective identification, isolation by flow cytometry, and in vivo self-renewal of multipotent mammalian neural crest stem cells. Cell, 1999. **96**(5): p. 737-749.

14. Douarin, N.L., et al., *Glial cell lineages in the neural crest.* Glia, 1991. **4**(2): p. 175-184.

15. Sommer, L., *Specification of Neural Crest-and Placode-Derived Neurons.* Patterning and Cell Type Specification in the Developing CNS and PNS: Comprehensive Developmental Neuroscience, 2013. **1**: p. 385.

16. Weston, J.A., A radioautographic analysis of the migration and localization of trunk neural crest cells in the chick. Developmental biology, 1963. **6**(3): p. 279-310.

17. Le Douarin, N.M. and M.-A.M. Teillet, Experimental analysis of the migration and differentiation of neuroblasts of the autonomic nervous system and of neurectodermal mesenchymal derivatives, using a biological cell marking technique. Developmental biology, 1974. **41**(1): p. 162-184.

18. Schweizer, G., C. Ayer-Le Lièvre, and N.M. Le Douarin, *Restrictions of developmental capacities in the dorsal root ganglia during the course of development.* Cell differentiation, 1983. **13**(3): p. 191-200.

19. Ladher, R.K., P. O'Neill, and J. Begbie, From shared lineage to distinct functions: the development of the inner ear and epibranchial placodes. Development, 2010. **137**(11): p. 1777-1785.

20. Begbie, J., et al., *Induction of the epibranchial placodes.* Development, 1999. **126**(5): p. 895-902.

21. Webb, J.F. and D.M. Noden, *Ectodermal placodes contributions to the development of the vertebrate head.* American Zoologist, 1993. **33**(4): p. 434-447.

22. Baker, C.V. and M. Bronner-Fraser, *Vertebrate cranial placodes I. Embryonic induction.* Developmental biology, 2001. **232**(1): p. 1-61.

23. Schlosser, G., Evolutionary origins of vertebrate placodes: insights from developmental studies and from comparisons with other deuterostomes. Journal of Experimental Zoology Part B: Molecular and Developmental Evolution, 2005. **304**(4): p. 347-399.

24. Streit, A., Early development of the cranial sensory nervous system: from a common field to individual placodes. Developmental biology, 2004. **276**(1): p. 1-15.

25. Barlow, L.A. and R.G. Northcutt, *Embryonic origin of amphibian taste buds.* Developmental biology, 1995. **169**(1): p. 273-285.

26. Hamamichi, R., M. Asano-Miyoshi, and Y. Emori, *Taste bud contains both short-lived and long-lived cell populations.* Neuroscience, 2006. **141**(4): p. 2129-2138.

27. Nguyen, H.M. and L.A. Barlow, Differential expression of a BMP4 reporter allele in anterior fungiform versus posterior circumvallate taste buds of mice. BMC neuroscience, 2010. **11**(1): p. 129.

28. Stone, L.M., et al., *Taste receptor cells arise from local epithelium, not neurogenic ectoderm.* Proceedings of the National Academy of Sciences, 1995. **92**(6): p. 1916-1920.

29. Okubo, T., C. Clark, and B.L. Hogan, Cell lineage mapping of taste bud cells and keratinocytes in the mouse tongue and soft palate. Stem cells, 2009. **27**(2): p. 442-450.

30. Miura, H. and L.A. Barlow, *Taste bud regeneration and the search for taste progenitor cells.* Archives italiennes de biologie, 2010. **148**(2): p. 107.

31. Hirota, M., et al., Expression of cyclin-dependent kinase inhibitors in taste buds of mouse and hamster. Tissue and Cell, 2001. **33**(1): p. 25-32.

32. Yu, W., et al., SOX10-Cre-Labeled Cells Under the Tongue Epithelium Serve as Progenitors for Taste Bud Cells That Are Mainly Type III and Keratin 8-Low. Stem Cells and Development, 2020.

33. Boggs, K., et al., Contribution of underlying connective tissue cells to taste buds in mouse tongue and soft palate. PloS one, 2016. **11**(1).

34. Liu, H.-X., et al., Neural crest contribution to lingual mesenchyme, epithelium and developing taste papillae and taste buds. Developmental biology, 2012. **368**(2): p. 294-303.

35. Wang, S.-K., Y. Komatsu, and Y. Mishina, *Potential contribution of neural crest cells to dental enamel formation.* Biochemical and biophysical research communications, 2011. **415**(1): p. 114-119.

36. Suzuki, J., et al., Neural crest-derived horizontal basal cells as tissue stem cells in the adult olfactory epithelium. Neuroscience Research, 2013. **75**(2): p. 112-120.

37. Katoh, H., et al., The dual origin of the peripheral olfactory system: placode and neural crest. Molecular brain, 2011. **4**(1): p. 1-16.

38. O'Rahilly, R. and F. Müller, *The development of the neural crest in the human.* Journal of anatomy, 2007. **211**(3): p. 335-351.

39. Debbache, J., V. Parfejevs, and L. Sommer, Cre-driver lines used for genetic fate mapping of neural crest cells in the mouse: An overview. genesis, 2018. **56**(6-7): p. e23105.

40. Chen, G., et al., S pecific and spatial labeling of P0-Cre versus Wnt1-Cre in cranial neural crest in early mouse embryos. genesis, 2017. **55**(6): p. e23034.

41. McKenzie, I.A., et al., *Motor skill learning requires active central myelination.* science, 2014. **346**(6207): p. 318-322.

42. Madisen, L., et al., A robust and high-throughput Cre reporting and characterization system for the whole mouse brain. Nature neuroscience, 2010. **13**(1): p. 133.

43. Chapman, S.C., et al., Ubiquitous GFP expression in transgenic chickens using a lentiviral vector. Development, 2005. **132**(5): p. 935-940.

44. Rodrigues, F.S., et al., A novel transgenic line using the Cre–lox system to allow permanent lineage-labeling of the zebrafish neural crest. Genesis, 2012. **50**(10): p. 750-757.

45. Wada, N., et al., Hedgehog signaling is required for cranial neural crest morphogenesis and chondrogenesis at the midline in the zebrafish skull. Development, 2005. **132**(17): p. 3977-3988.

46. Carney, T.J., et al., A direct role for Sox10 in specification of neural crest-derived sensory neurons. Development, 2006. **133**(23): p. 4619-4630.

47. Boniface, E.J., et al., FlEx-based transgenic reporter lines for visualization of Cre and Flp activity in live zebrafish. genesis, 2009. **47**(7): p. 484-491.

48. Fish, J.L., et al., Multiple developmental mechanisms regulate species-specific jaw size. Development, 2014. **141**(3): p. 674-684.

49. Southard-Smith, E.M., L. Kos, and W.J. Pavan, *Sox10 mutation disrupts neural crest development in Dom Hirschsprung mouse model.* Nature genetics, 1998. **18**(1): p. 60.

50. Kuhlbrodt, K., et al., *Sox10, a novel transcriptional modulator in glial cells.* Journal of Neuroscience, 1998. **18**(1): p. 237-250.

51. Nichols, D.H., Ultrastructure of neural crest formation in the midbrain/rostral hindbrain and preotic hindbrain regions of the mouse embryo. American journal of anatomy, 1987. **179**(2): p. 143-154.

52. Theveneau, E. and R. Mayor, Neural crest delamination and migration: from epithelium-to-mesenchyme transition to collective cell migration. Developmental biology, 2012. **366**(1): p. 34-54.

53. Kaufman, M.H., *Atlas of mouse development*. 1992: Academic press.

54. Giovannone, D., et al., *Chicken trunk neural crest migration visualized with HNK1.* Acta histochemica, 2015. **117**(3): p. 255-266.

55. Raible, D.W., et al., Segregation and early dispersal of neural crest cells in the embryonic zebrafish. Developmental dynamics, 1992. **195**(1): p. 29-42.

56. Schilling, T.F. and C.B. Kimmel, Segment and cell type lineage restrictions during pharyngeal arch development in the zebrafish embryo. Development, 1994. **120**(3): p. 483-494.

57. Kague, E., et al., Skeletogenic fate of zebrafish cranial and trunk neural crest. PloS one, 2012. **7**(11).

58. Raible, D.W. and J.S. Eisen, Restriction of neural crest cell fate in the trunk of the embryonic zebrafish. Development, 1994. **120**(3): p. 495-503.

59. Lee, R.T.H., et al., An exclusively mesodermal origin of fin mesenchyme demonstrates that zebrafish trunk neural crest does not generate ectomesenchyme. Development, 2013. **140**(14): p. 2923-2932.

60. Lee, R.T.H., J.P. Thiery, and T.J. Carney, *Dermal fin rays and scales derive from mesoderm, not neural crest.* Current Biology, 2013. **23**(9): p. R336-R337.

61. Landacre, F., *The fate of the neural crest in the head of the urodeles.* Journal of Comparative Neurology, 1921. **33**(1): p. 1-43.

62. Mongera, A., et al., Genetic lineage labeling in zebrafish uncovers novel neural crest contributions to the head, including gill pillar cells. Development, 2013. **140**(4): p. 916-925.

63. Huang, X. and J.-P. Saint-Jeannet, *Induction of the neural crest and the opportunities of life on the edge.* Developmental biology, 2004. **275**(1): p. 1-11.

64. Johnston, M., Isotretinoin embryopathy in a mouse model: Cranial neural crest involvement. Teratology, 1985. **31**: p. 26A.

65. Prochazkova, M., et al., FGF signaling refines Wnt gradients to regulate the patterning of taste papillae. Development, 2017. **144**(12): p. 2212-2221.

66. Beites, C.L., et al., Follistatin modulates a BMP autoregulatory loop to control the size and patterning of sensory domains in the developing tongue. Development, 2009. **136**(13): p. 2187-2197.

67. Castillo-Azofeifa, D., et al., Sonic hedgehog from both nerves and epithelium is a key trophic factor for taste bud maintenance. Development, 2017. **144**(17): p. 3054-3065.

68. Lewis, A.E., et al., The widely used Wnt1-Cre transgene causes developmental phenotypes by ectopic activation of Wnt signaling. Developmental biology, 2013. **379**(2): p. 229-234.

69. Kawakami, M., et al., Novel migrating mouse neural crest cell assay system utilizing P0-Cre/EGFP fluorescent time-lapse imaging. BMC Developmental Biology, 2011. **11**(1): p. 1-17.

70. Cornett, B., et al., Wntless is required for peripheral lung differentiation and pulmonary vascular development. Developmental biology, 2013. **379**(1): p. 38-52.

71. Geske, M.J., et al., Fgf9 signaling regulates small intestinal elongation and mesenchymal development. Development, 2008. **135**(17): p. 2959-2968.

72. Lin, C., et al., Tissue-specific requirements of β-catenin in external genitalia development. Development, 2008. **135**(16): p. 2815-2825.

73. Yin, Y., et al., An FGF–WNT gene regulatory network controls lung mesenchyme development. Developmental biology, 2008. **319**(2): p. 426-436.

74. Yu, K., et al., Conditional inactivation of FGF receptor 2 reveals an essential role for FGF signaling in the regulation of osteoblast function and bone growth. Development, 2003. **130**(13): p. 3063-3074.

75. Li, L., P. Cserjesi, and E.N. Olson, *Dermo-1: a novel twist-related bHLH protein expressed in the developing dermis.* Developmental biology, 1995. **172**(1): p. 280-292.

76. Hirrlinger, P.G., et al., Temporal control of gene recombination in astrocytes by transgenic expression of the tamoxifen-inducible DNA recombinase variant CreERT2. Glia, 2006. **54**(1): p. 11-20.

77. Witt, M., et al., *Fingerprinting taste buds: intermediate filaments and their implication for taste bud formation.* Philosophical Transactions of the Royal Society of London. Series B: Biological Sciences, 2000. **355**(1401): p. 1233-1237.

78. Le Douarin, N., A biological cell labeling technique and its use in experimental embryology. Developmental biology, 1973. **30**(1): p. 217-222.

79. Douarin, L., Developmental Relationships between the Neural Crest and the Polypeptide-Hormone-Secreting Cells. The Neural Crest. Cambridge, 1982: p. 91-107.

80. Le Lièvre, C.S. and N. Le Douarin, Mesenchymal derivatives of the neural crest: analysis of chimaeric quail and chick embryos. Development, 1975. **34**(1): p. 125-154.

81. Noden, D.M., The role of the neural crest in patterning of avian cranial skeletal, connective, and muscle tissues. Developmental biology, 1983. **96**(1): p. 144-165.

82. Dutton, J.R., et al., An evolutionarily conserved intronic region controls the spatiotemporal expression of the transcription factor Sox10. BMC developmental biology, 2008. **8**(1): p. 105.

83. Kwak, J., et al., Live image profiling of neural crest lineages in zebrafish transgenic lines. Molecules and cells, 2013. **35**(3): p. 255-260.

84. Kague, E., et al., Skeletogenic fate of zebrafish cranial and trunk neural crest. PloS one, 2012. **7**(11): p. e47394.

85. Dutton, K.A., et al., Zebrafish colourless encodes sox10 and specifies non-ectomesenchymal neural crest fates. Development, 2001. **128**(21): p. 4113-4125.

## 3.7 Figures

***Figure 3.1***. *Sufficiency of a single dose of tamoxifen (Tmx) in activating the nuclear translocation of Cre recombinase that triggered DNA recombination to drive tdT expression in neural crest and neural crest-derived tissues.* ***A-B:*** *Low (A) and high (B) -power images of transverse sections of the cranial region of a vehicle (Veh)-treated Sox10-iCreER$^{T2}$ mouse embryo at E8.5 (12-somite). Immunosignals of Cre (green) in the cytoplasm (arrowheads in B) and Sox10 (magenta) in the nuclei were visualized. White dashed lines in A outline the foregut diverticulum with non-specific staining [40]. TN: trigeminal neural crest tissue; BA1: branchial arch 1; OE: optic eminence.* ***C:*** *High-magnification images of the BA1 region in a transverse section of an E8.5 (9-somite) Sox10-iCreER$^{T2}$ mouse embryo with tamoxifen activation of Cre (Tmx$^{E7.5}$). Arrows point to the Cre immunosignals (green) within nuclei.* ***D:*** *Images of whole mount ($D_1$) and sagittal section ($D_2$) of the tongue from a E12.5 Sox10-iCreER$^{T2}$/tdT mouse embryo with tamoxifen activation of Cre (Tmx$^{E7.5}$). Tongue epithelium was immunoreacted with antibody against E-cadherin (green) in $D_2$.* ***E:*** *Bright field ($E_1$) and tdT fluorescent ($E_2$) images of mouse dorsal root ganglia (arrows) of a Sox10-iCreER$^{T2}$/tdT mouse at 8 weeks with tamoxifen activation of Cre (Tmx$^{E7.5}$). Arrows point to the dorsal root ganglia. Scale bars: 50 μm in A and D (single-plane laser scanning confocal); 10 μm in B and C (single-plane laser scanning confocal); 1 mm in E (stereomicroscopy).*

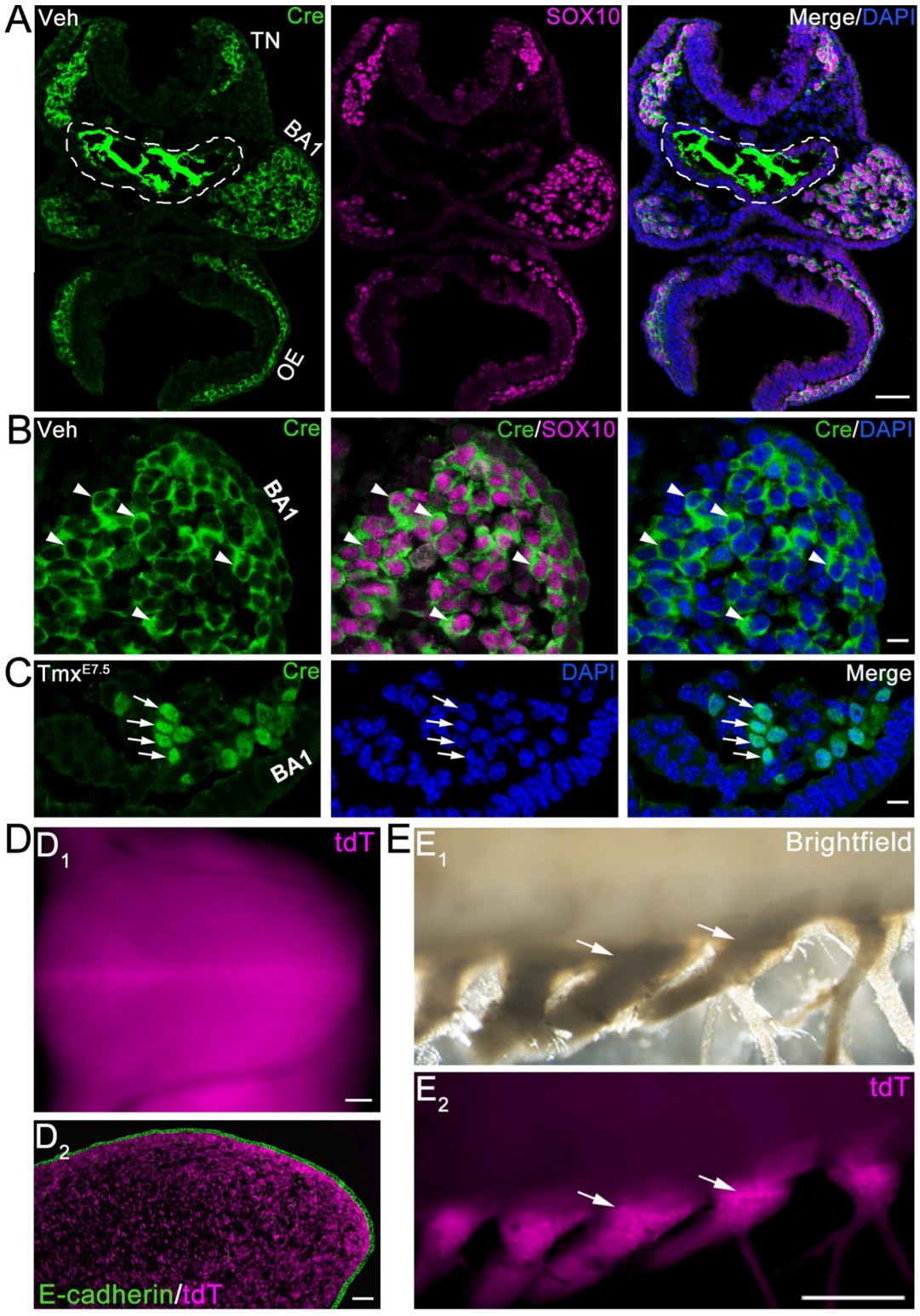
A
Veh
Cre
TN
BA1
OE
SOX10
Merge/DAPI
B
Veh
Cre
BA1
Cre/SOX10
Cre/DAPI
C
Tmx$^{E7.5}$
Cre
BA1
DAPI
Merge
D
D$_1$
tdT
D$_2$
E-cadherin/tdT
E
E$_1$
Brightfield
E$_2$
tdT

***Figure 3.2***. *Single-plane laser scanning confocal photomicrographs to demonstrate the distributions of Sox10-iCreER$^{T2}$/tdT-labeled cells in the tongue and soft palate in postnatal mice (Tmx$^{E7.5}$) at different stages.* ***A-B:*** *Images of a fungiform papilla on a sagittal section ($A_1$, $B_1$) and circumvallate on a coronal section ($A_2$, $B_2$) of tongue at 2 weeks (A) and 4 weeks (B).* ***C:*** *Images of soft palate ($C_1$), fungiform papilla ($C_2$), foliate papilla on a sagittal section ($C_3$), and circumvallate papilla on a coronal section ($C_4$) of tongue tissue at 8 weeks. Taste buds were marked by the immunosignals of Keratin 8 (Krt8, green). White dashed lines demarcate lingual epithelium from the underlying connective tissue. Scale bars: 50 μm for all images.*

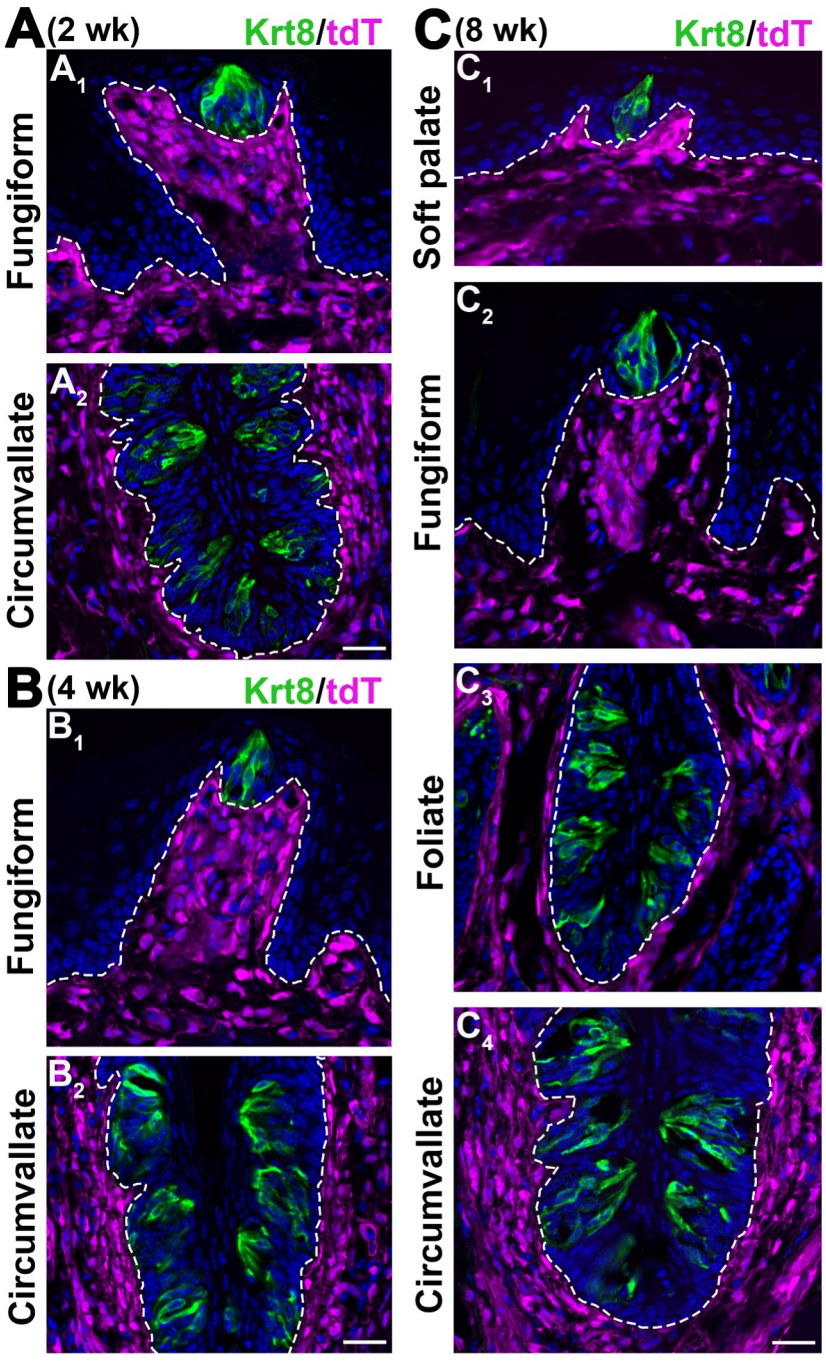
A (2 wk)
Krt8/tdT
A1
Fungiform
A2
Circumvallate
B (4 wk)
Krt8/tdT
B1
Fungiform
B2
Circumvallate
C (8 wk)
Krt8/tdT
C1
Soft palate
C2
Fungiform
C3
Foliate
C4
Circumvallate

***Figure 3.3***. *Migration of $GFP^+$ NC cells ventrally in $GFP^-$ host chicken after the insertion of the $GFP^+$ neural fold.* ***A****: A schematic graph illustrating the insertion of $GFP^+$ neural fold to $GFP^-$ host chicken embryo.* ***B****: Photomicrographs of a $GFP^+/GFP^-$ chicken chimera at 1 DPS. Top: fluorescent image to show GFP signals; Bottom: merged fluorescent and bright-field images.* ***C****: Single-plane laser scanning confocal images of a section ($C_1$) from the position indicated by white line in B and higher power images ($C_2$) from the area indicated by dashed square shown in $C_1$. Sections were immunoreacted for neural crest cell marker HNK1 (magenta). Scale bars: 500 μm in B; 80 μm in $C_1$ and 20 μm in $C_2$.*

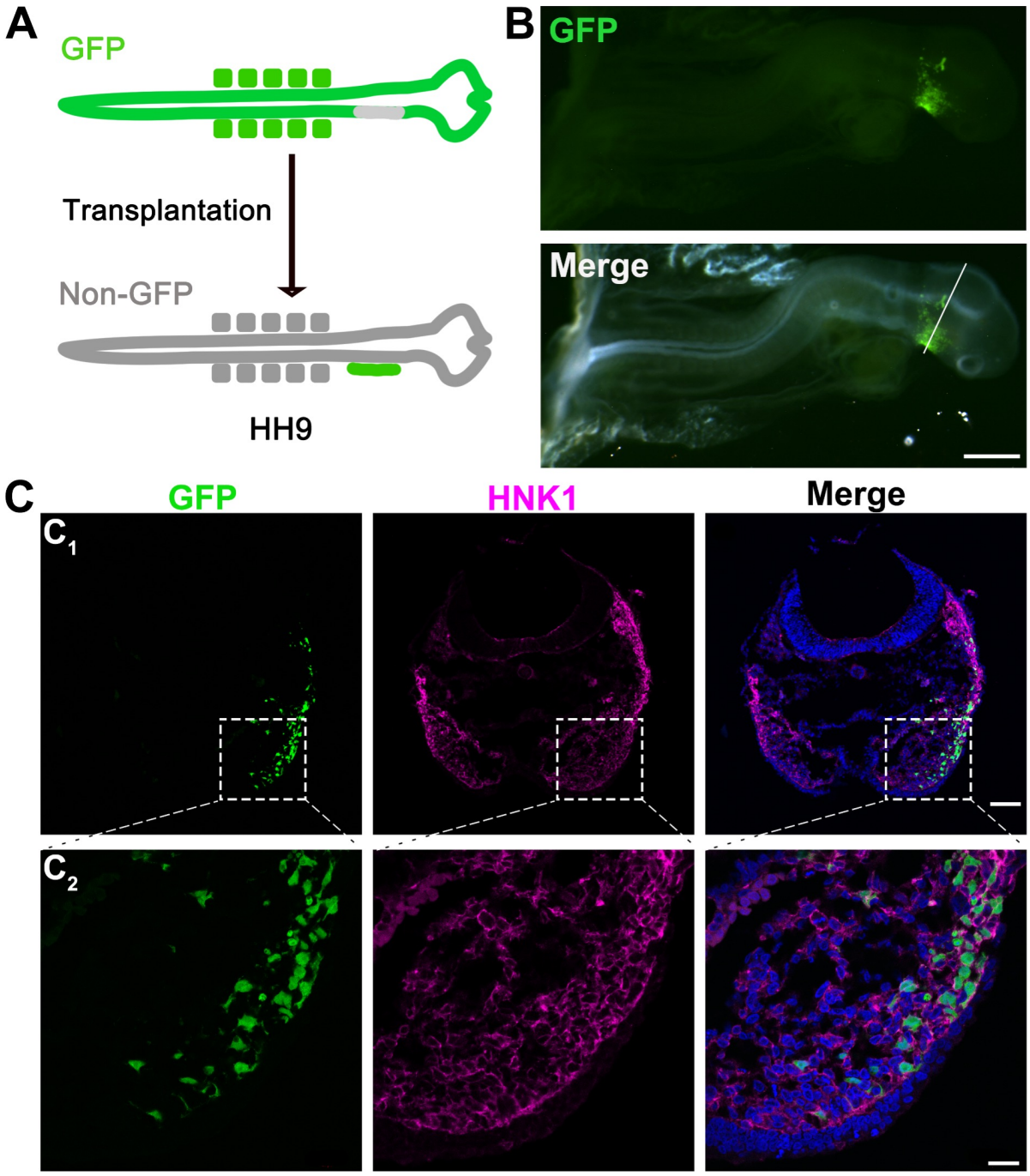
A
GFP
Transplantation
Non-GFP
HH9
B
GFP
Merge
C
GFP
HNK1
Merge
C1
C2

***Figure 3.4***. *Distribution of GFP$^+$ neural fold-derived cells in the craniofacial regions ispilateral to the surgery side.* ***A****: Photomicrographs of a chimeric embryo at 2 DPS, side view of heads and dorsal view of the lower beak (LB) at 14 and 19 DPS, and upper beak (UP) at 19 DPS. Top panel: fluorescent images to show the GFP signals; Bottom panel: merged fluorescent and bright-field images.* ***B****: Single-plane laser scanning confocal images of sagittal sections of pharyngeal arch of chimeric embryo at 2 DPS and base of oral cavities of chimeric embryos at 14 and 19 DPS. Sections were immunoreacted for the epithelial cell marker EpCAM (magenta). White dashed lines demarcate the epithelium from the underlying mesenchyme. Scale bars: 2 mm in A; 20 μm in B.*

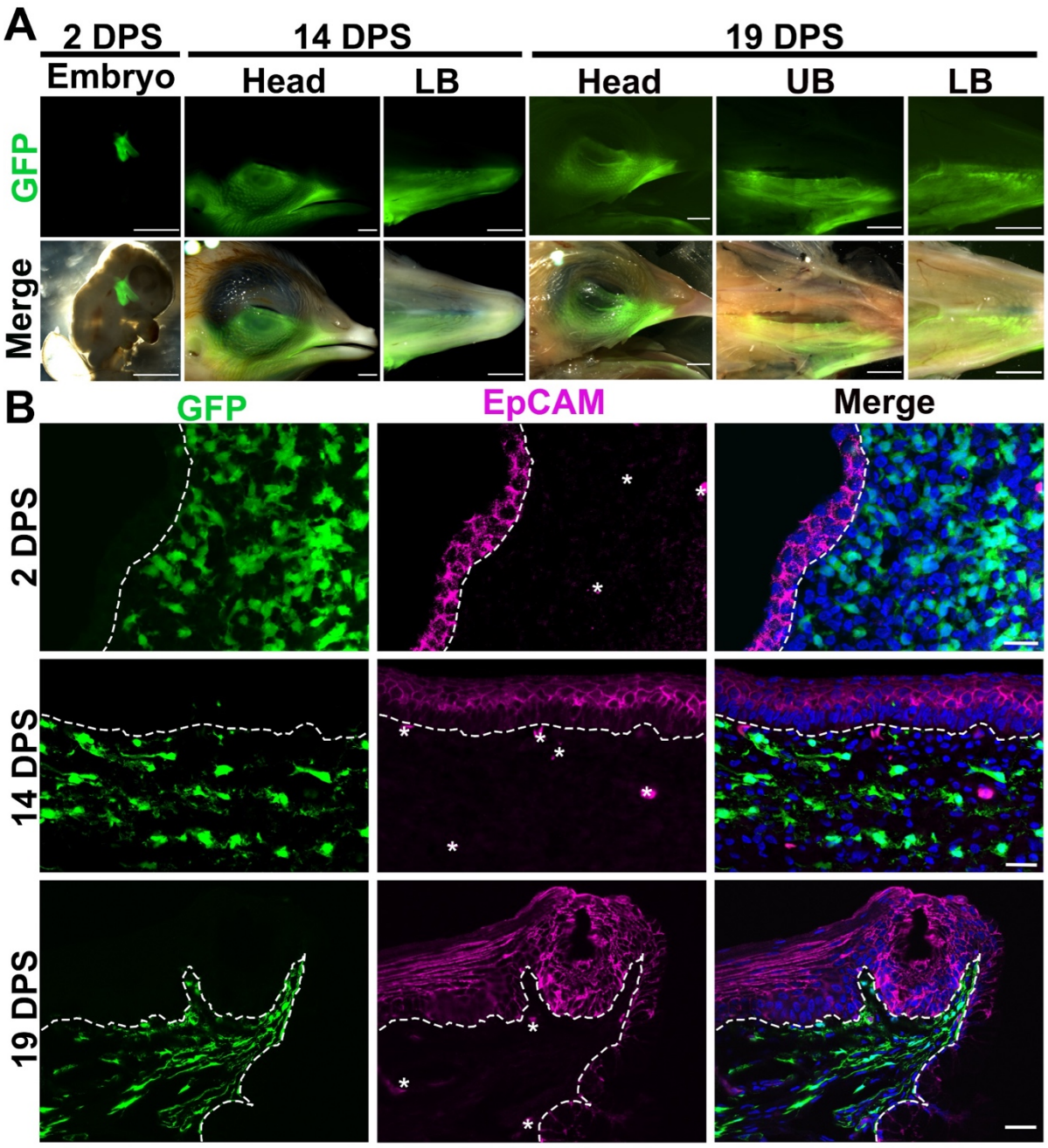
A
2 DPS
14 DPS
19 DPS
Embryo
Head
LB
Head
UB
LB
GFP
Merge
B
GFP
EpCAM
Merge
2 DPS
14 DPS
19 DPS

***Figure 3.5***. *Distribution of GFP$^{+}$ labeled cells in the tissue of oral cavity of chimeric embryos at 19 DPS.* ***A****: Representative images of a sagittal section of the base of oral cavity.* ***B****: Images of a sagittal section of the palate. Sections were immunoreacted for taste bud cell marker α-Gustducin (magenta). White dashed lines encircle taste buds. Autofluorescence in α-Gustducin immunoreacted sections were identified and are marked by asterisks (*). Scales bars: 20 μm for all images (single-plane laser scanning confocal images).*

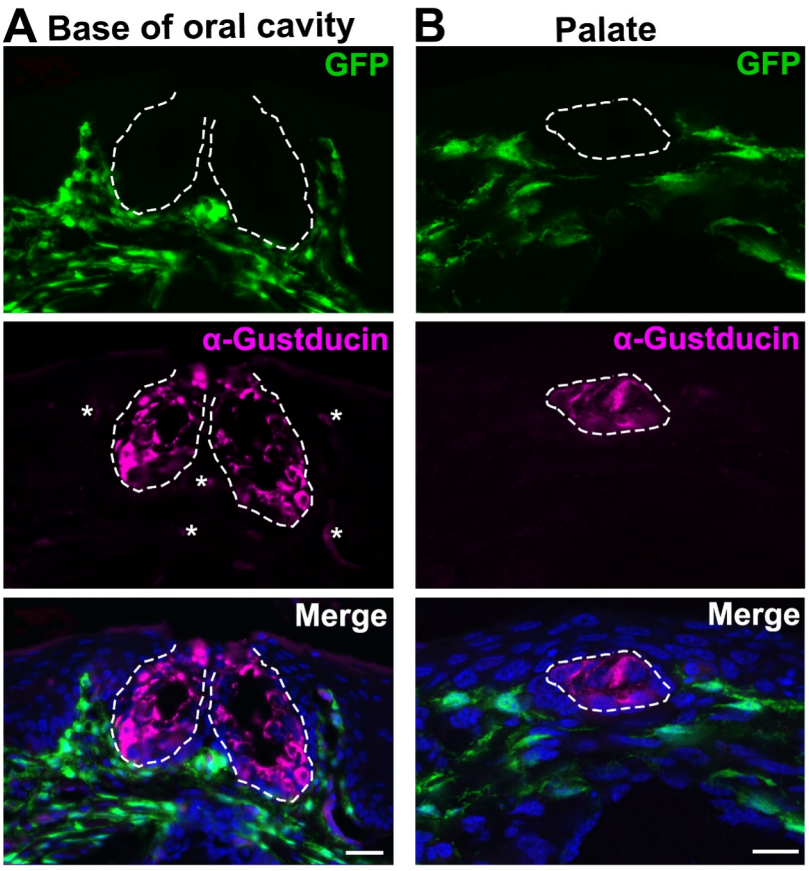
A Base of oral cavity
B Palate
GFP
GFP
α-Gustducin
α-Gustducin
Merge
Merge

***Figure 3.6***. *Mapping neural crest cell lineages in zebrafish.* ***A-C****: Sox10-EGFP expression was in neural crest but not in taste buds.* ***A****: Merges EGFP and bright-field images of lateral views of Sox10-EGFP fish embryos at 7, 10, and 12-somite stages. Arrowheads point to heads and arrows point to truck regions.* ***B****: Photomicrographs of transverse sections of cranial regions of a 12-somite Sox10-EGFP fish embryo. Migrating neural crest cells were immunostained for Sox10 (magenta).* ***C****: Photomicrographs of a sagittal section of a taste bud in lower jaw of a 5.5 dpf fish embryo.* ***D-E****: Sox10-Cre/GFP-RFP labeled known neural crest-derived tissues but not taste buds.* ***D****: Whole mount images of gills (arrows) of Sox10-Cre/GFP-RFP adult zebrafish.* ***E****: Photomicrographs of sagittal sections of lower jaws at 15 dpf, 30 dpf, and adult and adult barbel of Sox10-Cre/GFP-RFP zebrafish. GFP and RFP signals were amplified by applying antibodies against GFP (green) and RFP (magenta). Calretinin (gray) indicates presence of taste buds. Scale bars: 200 μm in A and D; 50 μm in B; 20 μm in C and E (single-plane laser scanning confocal).*

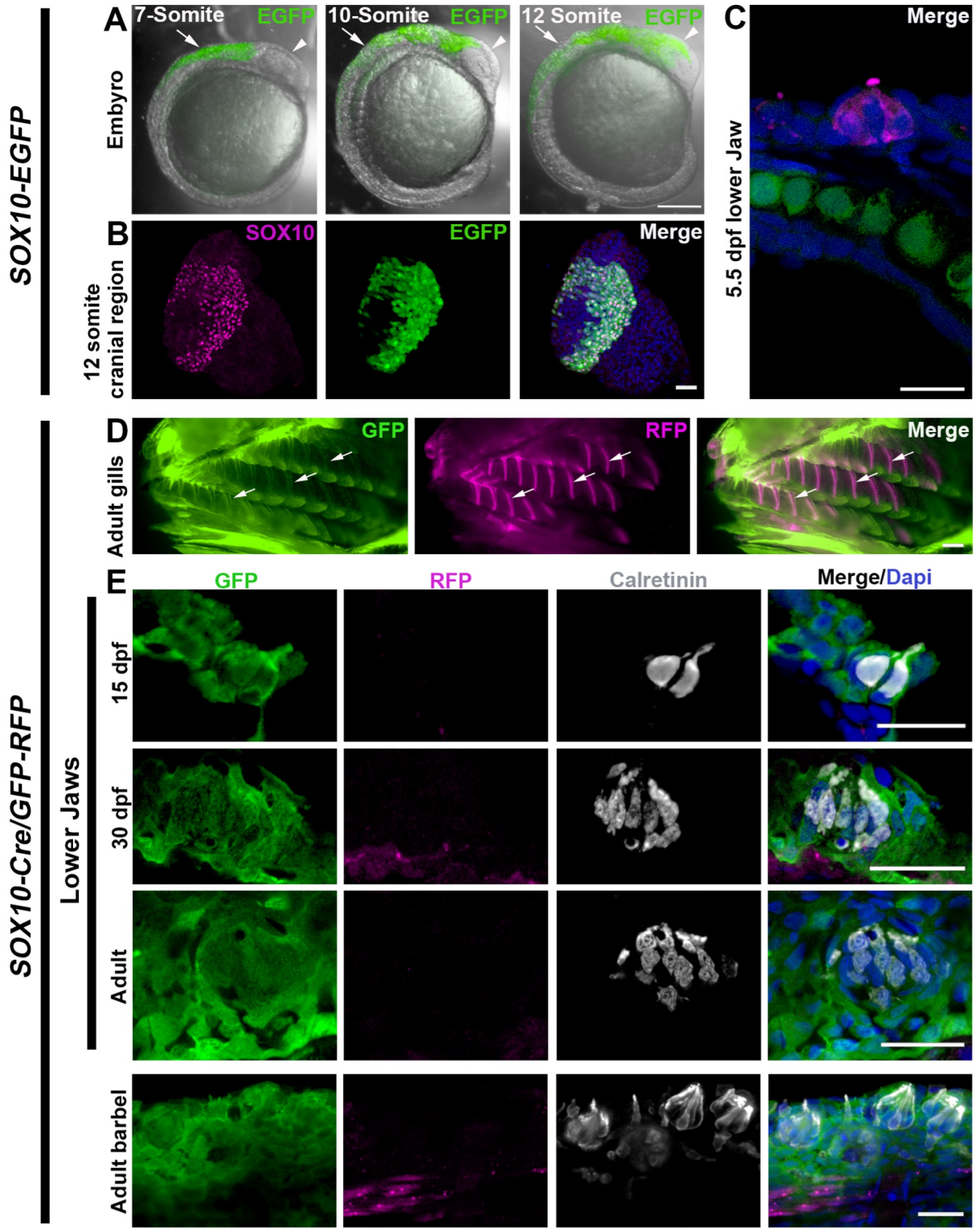
SOX10-EGFP
A
7-Somite
EGFP
10-Somite
EGFP
12 Somite
EGFP
Embyro
B
SOX10
EGFP
Merge
12 somite cranial region
C
Merge
5.5 dpf lower Jaw
SOX10-Cre/GFP-RFP
D
GFP
RFP
Merge
Adult gills
E
GFP
RFP
Calretinin
Merge/Dapi
Lower Jaws
15 dpf
30 dpf
Adult
Adult barbel

## 3.8 Tables

**Table 3.1**. Primary antibodies that were used.

| Antibodies | Dilution | Source |
|---|---|---|
| mouse anti-Calretinin clone 6B3 | 1:5000 (section)<br>1:1000 (whole mount) | Cat No. 010399, Swant, Inc, Switzerland |
| goat anti-Cre | 1:500 | Cat No. sc-83398, Santa Cruz Biotechnology, Inc. Dallas, TX |
| rabbit anti-dsRed | 1:500 | Cat No. ab62341, Abcam, Inc, Cambridge, MA |
| goat anti-E-cadherin | 1:500 | Cat No. AF748, R&D systems, Inc, Minneapolis, MN |
| chicken anti-GFP | 1:500 (section)<br>1:250 (whole mount) | Cat No. GFP-1010, Aves Labs, Inc, Tigard, OR |
| rat anti-Keratin 8 (Krt8) | 1:1000 | Cat No. TROMA-1, Developmental Studies Hybridoma Bank, Iowa city, IA |
| goat anti-SOX10 | 1:500 | Cat No. sc-365692, Santa Cruz Biotechnology, Inc, Dallas, TX |
| mouse anti-HNK1(1C10) | 1:10 | Cat No. AB_10570406, Developmental Studies Hybrydoma Bank, Iwoa city, IA |
| rabbit anti-Epithelial Cell Adhesion Molecule markers (EpCAM) | 1:200 | Cat No. MBS2027145, Mybioresource Inc, San Diego, CA |
| rabbit anti-α-Gustducin | 1:500 | Generated by Dr. Shoji Tabata's lab |
| mouse anti-Vimentin (Vim3B4) | 1:250 | Cat No. ab28028, Abcam, Inc, Cambridge, MA |

# CHAPTER 4

# REGION- AND STAGE-SPECIFIC ROLES OF EVC2 IN REGULATING HEDGEHOG SIGNALING AND THE DEVELOPMENT OF TASTE ORGANS[1]

[1] Zhonghou Wang, Mohamed Ishan, Honghao Zhang, Ruchi Shah, Stephanie Nguyen, Yuji Mishina, Hong-Xiang Liu. To be submitted to *Development.*

## 4.1 Abstract

The number and spacing of taste buds at anterior tongue associated with taste sensitivity in humans. Understanding of cellular and molecular mechanisms governing taste papilla placode induction and patterning remains incomplete. Hedgehog signaling plays essential roles in taste organ development and disruption of Hedgehog signaling causes a number of defects. Patients of Ellis–van Creveld syndrome, which is a rare genetic disorder caused by mutations of *Evc* or *Evc2* and with impaired Hedgehog signaling activities in several organs, experience loss of taste papillae. To define region- and stage-specific roles of EVC2 in development of taste organs and determine how taste bud development is affected in Ellis–van Creveld syndrome, we employed histology and immunohistochemistry, ultrastructural imaging, next-generation sequencing, quantitative and in situ approaches for mRNA characterization to analyze phonotypes of taste organ development in E18.5 *Evc2*$^{-/-}$ mice. Taste papillae increased in number and size but with normal innervation in *Evc2*$^{-/-}$ tongues. Hedgehog signaling was impaired in tongue epithelial cells specifically in tongue tip region at E12.5. And RNA-seq experiment revealed that extracellular matrix (ECM) genes were dramatically up-regulated in *Evc2*$^{-/-}$ tongue epithelium. Moreover, enlarged and flatten fungiform papillae are observed in E18.5 *Evc2*$^{-/-}$ mice. BCL11B, a transcription factor essential for taste papilla morphogenesis, was missing or down-regulated in the abnormal fungiform papillae in *Evc2*$^{-/-}$ mice. Together our data revealed that EVC2 regulates Hedgehog signaling and the development of taste organs in a region- and stage-specific manner.

## 4.2 Introduction

Taste buds are the peripheral sensory organs for taste that is important for animals and humans to take nutrients and avoid toxins. Number and spacing of taste buds at anterior tongue have been associated with taste sensitivity in humans [1, 2]. However, understanding of cellular

and molecular mechanisms governing taste papilla placode induction and patterning remains incomplete. With development and availability of inducible gene-modified mouse lines, numerous advances regarding taste bud development have been made in the last two decades. Multiple conserved signaling pathways like Hedgehog (Hh) [3], Wnt/β-catenin [4, 5], bone morphogenetic protein (BMP) [6], fibroblast growth factor (FGF) [7], have been proved to be involved in papilla placode induction and/or patterning.

Hedgehog signaling pathway is a conserved signaling pathway that regulates cell proliferation and cell differentiation. In vertebrates, the primary cilium is the key organelle and location for the transduction of the Hedgehog signaling pathway. There are three types of Hedgehog proteins (ligands) in vertebrates: Sonic hedgehog (HH), Indian Hedgehog (IHH), and Desert Hedgehog (DHH). Hedgehog proteins can bind to the receptor protein Patched-1 (PTCH1), which in turn releases inhibition of Smoothened (SMO). Once the inhibition of SMO is gone, SMO migrates and interacts with a series of intracellular components including EVC and EVC2, thus activating the cascade that eventually affects proteolysis of the transcriptional effectors of Hedgehog signaling pathway, GLI proteins.

Hedgehog signaling regulates development of taste organs in a tissue- and stage-specific manner. First, Hedgehog signaling regulates taste papilla placode specification. Specifically hedgehog signaling inhibits this process. Both *in vitro* cultures and *in vivo* studies revealed that blocking hedgehog signaling pathway increased number of fungiform papillae [8, 9]. *in vitro* tongue cultures treated with cyclopamine even developed ectopic SHH-expressing taste papilla placodes in intermolar eminence (IE) region, which is free from taste papillae in normal mouse tongues [8]. However, region-specific differences between anterior tongue and IE regarding hedgehog signaling transduction are elusive. Specific roles of Hedgehog signaling is also less

characterized at papilla morphogenesis stage than taste papilla placode specification stage. Also, the downstream targets of Hedgehog signaling during papilla placode specification remains unknown.

Second, Hedgehog signaling is also required for proper tongue development. Roles of Hedgehog signaling in tongue development are stage-specific. Treating E12 rat tongue (equals to E10.5 mouse tongue) cultures with cyclopamine *in vitro* prevents tongue growth while treating E14 rat tongue (equals to E12.5 mouse tongue) cultures with cyclopamine *In vitro* does not affect tongue growth [8]. Roles of Hedgehog signaling in tongue formation are also tissue-specific. Knocking-out *Smo*, the coding gene for an essential Hedgehog modulator, by tongue mesenchyme-specific Cre driver *Wnt1*-Cre caused small and cleft tongues. In contrast, Knocking-out *Smo* by tongue epithelium-specific Cre driver *Shh*-Cre does not cause obvious defects in tongue development [9].

Mis-regulation of Hedgehog signaling in embryos caused a number of birth defects. Ellis–van Creveld syndrome, which is a rare genetic disorder characterized by short limb dwarfism, polydactyly, abnormal development of fingernails as well as regional loss of taste papillae [10], is caused by mutations of *Evc* or *Evc2*. EVC and EVC2 were characterized as essential components transducing Hedgehog signaling pathway. EVC and EVC2 proteins form a complex with Smoothed (Smo) at the base of primary cilia, which is an important step for Hedgehog signaling activation [11, 12]. However, unlike Smoothened, which is absolutely required for Hedgehog signaling transduction, EVC and EVC2 are not always required for development of Hedgehog-regulated organs. So tissue-specific roles of EVC or EVC2 needed to be further defined in taste organs. Moreover, there is no clear explanation about the papilla loss in Ellis–

van Creveld syndrome patients, even though stage-specific roles of Hedgehog signaling has been defined at multiple stages.

To understand how taste bud development is affected in Ellis–van Creveld syndrome and further study how EVC2 and Hedgehog signaling regulates taste papilla and taste bud development, *Evc2*$^{-/-}$ mice and Gli1-CreER/RFP mice were employed for molecular and cellular mechanisms underlying taste papilla and taste bud development. We found that 1) expression of taste bud progenitor marker, SHH, was increased in *Evc2*$^{-/-}$ tongues at taste papilla placode induction stage (E12.5); 2) spacing and increased number of taste papillae significantly decreased with normal innervation in *Evc2*$^{-/-}$ tongues at the stage of papilla morphogenesis (E15.5); 3) Hedgehog signaling activity was slightly impaired in *Evc2*$^{-/-}$ tongues revealed by qRT-PCR and in situ hybridization with *Gli1* and *Ptch1*; 4) RNA-seq experiment revealed that a number of extracellular matrix (ECM)-related genes were turned up in E12.5 *Evc2*$^{-/-}$ tongue epithelium; 5) the number of taste buds increased and epithelial hyperplasia was observed at the taste bud differentiation stage (E18.5), which partially resembled the phenotype in tongues of Ellis–van Creveld syndrome patients; 6) decreased expression of essential transcription factor for papilla morphogenesis, BCL11B, in epithelial hyperplasia regions. 7) loss of taste buds and mis-oriented filiform papillae postnatally (3 weeks) in *Evc2* knockout mice; 8) Hedgehog-responsive cells in embryonic tongues stayed outside taste buds in embryos but populated the whole fungiform papillae postnatally. Overall, we provide strong evidences supporting that EVC2-modulated Hedgehog signaling regulates multiple developmental events of lingual epithelium in mice.

## 4.3 Materials and methods

### *4.3.1 Animals*

Animal use was approved by The University of Georgia Institutional Animal Care and Use Committee and was in compliance with the National Institutes of Health Guidelines for care and use of animals in research.

Heterozygous mice (*Evc2*$^{+/-}$ or *Evc2*$^{LacZ/+}$) [13] carrying one copy of lac-Z in *Evc2* locus were used to characterize expression of *Evc2* by X-gal staining. To generate *Evc2* global knockout embryos and pups, heterozygous mice (*Evc2*$^{+/-}$) were mated with heterozygous mice (*Evc2*$^{+/-}$). C57BL/6J mice (#000664, The Jackson Laboratory, Bar Harbor, ME, USA) were used for colony maintenance as wild type mice.

*Gli1*-CreER$^{T2}$ mice (# 007913, hereafter *Gli1*-CreER mice) and B6.Cg-Gt(ROSA)$^{26Sortm14(CAG-tdTomato)Hze}$/J mice (# 007914, hereafter RFP mice) were obtained from The Jackson Laboratory. *Gli1*-CreER mice were bred with RFP breeders to generate Gli1-CreER/RFP mice. FVB/NJ mice (#001800, The Jackson Laboratory, Bar Harbor, ME, USA) were used to foster cesarean born pups which were administrated with Tamoxifen at embryonic stages.

### *4.3.2 Tamoxifen (TAM) treatment and tissue harvest and processing*

1% (w/v) Tamoxifen solution were prepared by dissolving Tamoxifen (T5648, Sigma Aldrich) in a mixture of autoclaved corn oil and 100% ethanol (volume ratio at 8:1). 0.1 ml Tamoxifen solution was administrated per mouse, per day at embryonic day (E)12.5, E14.5, or E16.5.

Mouse embryonic tongues at desired stages were dissected followed by freshly freezing on dry ice after embedding or fixed in 4% paraformaldehyde (PFA) for 2 hr or 24 hr. Fixation time

was adjusted according to the primary antibody used for immunohistochemistry. Cryoprotection was performed by immersing tissue in 30% sucrose for PFA-fixed tissue to be sectioned. Fixed tissues were embedded in Optimal Cutting Temperature (O.C.T) compound and rapidly frozen.. All tissues were sectioned at 8-10 μm in thickness and mounted onto charged glass slides.

Tongue epithelial sheets was peeled after injection of 1 mg/mL collagenase A and 2.5 mg/mL dispase II under the tongue epithelium and incubation for 30 min at 37 °C. Detailed procedure has been described previously [14].

Tissue for scanning electron microscopy (SEM) was fixed with 2.5% glutaraldehyde and 4% PFA in 0.1 M PBS overnight at 4°C. After rinsed in PBS, tissue was postfixed in 1% OsO4, 1% Tannic acid and 1% OsO4 sequentially. Then tissue was dehydrated by a series of ethanol at ascending concentrations and HMDS. Air dried tissue specimens were mounted on stubs and sputter coated with gold. Imaging were performed by The Thermo Fisher Scientific (FEI) Teneo$^{TM}$ scanning electron microscope.

*4.3.3 Immunohistochemistry and immunofluorescence*

Sections The following primary antibodies were used for immunofluorescence: anti-BCL11B (1:500, #18465, Abcam, Cambridge, MA), anti-cleaved Caspase-3 (1:500, #9661s, Cell Signaling, Danvers, ME), anti-E-Cadherin (1:500, #AF748, R&D Systems, Minneapolis, MN), anti-Keratin 8 (Krt8) (1:1000, TROMA-I, Developmental Studies Hybridoma Bank, IA), anti-Ki67 (1:200, #15580, Abcam, Cambridge, MA), anti-Ki67 (1:500, AF7649, R&D Systems, Minneapolis, MN), anti-neurofilament mediate protein (NF-M) (1:500, # NB300-133, Novus Biologicals, Centennial, CO) and anti-SHH (1:100, #AF464, R&D Systems, Minneapolis, MN).

Slides were air dried for 30 mins ~ 1 hr at room temperature, followed by rehydration in 0.1 M PBS. Nonspecific binding was blocked by 10% normal donkey serum (NDS) followed by

incubation with primary antibodies in a carrier solution of 1% NDS in PBS-X (PBS with 0.3% Triton-X) overnight at 4°C. Slides were rinsed in 0.1 M PBS three times, then incubated with secondary antibodies, i.e., Alexa Fluor 647 conjugated donkey anti-rabbit secondary antibody (1:500, 711-605-152; Jackson Immuno Research Laboratories, West Grove, PA), Alexa Fluor 488 conjugated donkey anti-rat (1:500, 715-545-150, Jackson Immuno Research Laboratories, West Grove, PA), and Alexa Fluor 546 conjugated donkey anti-goat (1:500, A10036, Life Technologies, Inc., Carlsbad, CA), in carrier solution for 1 hr at room temperature. After rinsing in PBS, cell nuclei were counter-stained with DAPI (200 ng/ml in PBS) for 10 min at room temperature. Slides were then thoroughly rinsed, air-dried and cover-slipped using Prolong® Diamond Antifade mounting medium (P36970, Life Technologies, Inc., Carlsbad, CA)

Whole mount The following primary antibodies were used for whole mount staining: anti-Keratin 8 (Krt8) (1:1000, TROMA-I, Developmental Studies Hybridoma Bank, IA), anti-SHH (1:100, #AF464, R&D Systems, Minneapolis, MN), and anti-βIII-tubulin (ab18207, Abcam, Cambridge, United Kingdom). Non-specific binding was blocked 10% NDS in PMS/MT (PBS with 2% instant milk power and 0.1% Triton-X) for 2 hr and then tissue was incubated with primary antibodies for 2 days. After rinsed in PBS/MT 5 times, 1 hr each, tissue was incubated in fluorophore- or biotin-conjugated antibodies (Rabbit Anti-Goat IgG, 1:500, BA-5000, Vector Laboratories, Cambridge, MA) overnight at 4°C. For tissues with DAB reaction, endogenous peroxidase activity of the tissue was blocked with 6% $H_2O_2$ in methanol at room temperature for 5 hr followed by blocking in 10% NDS. VECTASTAIN® Elite® ABC HRP Kit (PK-6100, Vector Laboratories, Burlingame, CA) was used following the incubation with biotin-conjugated antibodies to label biotin with peroxidase. And DAB HRP Substrate Kit (SK-4100, Vector Laboratories, Burlingame, CA) was used to visualize immune signals.

*4.3.4 In situ hybridization*

*Gli1* (# 311001) and *Ptch1* (# 402811) probes were obtained from Advanced Cell Diagnostics. RNAscope® Intro Pack 2.5 HD Reagent Kit Brown (#322371,) was used for hybridization. Procedure of hybridization and tissue processing were performed according to manufacturer's instructions.

*4.3.5 X-Gal staining*

Tissue sections on slides were air dried, rehydrated with PBS, then incubated in 1 mg/ml X-Gal (03117073001, Roche, Indianapolis, IN, USA) for 1-3 days. Cell nuclei were counter-stained with Neutral Red Solution (N2889, Sigma-Aldrich, St. Louis, MO) on tissue sections.

*4.3.6 Microscopy*

Bright-field microscopy was performed under Zeiss Axio Vert. A1 microscope. All fluorescence-labeled sections were thoroughly examined under a light microscope (EVOS FL, Life Technologies). Representative images of immunosignals were taken using Zeiss LSM 810 laser scanning confocal microscope. SEM images were taken using FEI Teneo FE-SEM (FEI, Inc., Hillsboro OR USA) at Georgia Electron Microscopy Core. Images were assembled using Photoshop (Adobe, San Jose, CA).

*4.3.7 Transcriptomic profiling (RNA-seq)*

E12.5 tongue epithelium and underlying mesenchyme were separated after enzyme digestion by a mixture of collagenase A (1 mg/ml) and Dispase II (2.5 mg/mL). RNA was isolated and purified by Hybrid-R™ RNA isolation kit (#305-101, GeneAll). Purified RNA was converted into cDNA using Tribo™ Reverse Transcription Reaction Kit (#TBS4006, Tribioscience, Carlsbad, CA). cDNA libraries were prepared with Kapa Stranded mRNA-seq kit (KAPA Biosystems, Wilmington, MA) and sequenced on NextSeq 500 system (Illumina). All

library preparation and sequencing were conducted by Georgia Genomics and Bioinformatics Core. Raw reads were mapped to mouse reference genome GRCm38 (mm10) using STAR [15]. Transcripts were assembled, quantified and reported with FPKM (fragments per kilobase per million) by StringTie [16]. Differentially expressed genes (DEGs) were identified using R package DESeq2 [17].

*4.3.9 Analysis of public data of single-cell transcriptomic profiling (scRNA-seq) of mice.*

scRNA-seq data sets from two independent research [18, 19] were involved for analysis. The first data set used in present study is part of *Tabula Muris* [18], which includes 7538 adult anterior tongue epithelial cells. The second data set used in present study is part of 'mouse organogenesis cell atlas' (MOCA) [19], which includes 7874 branchial arch epithelial cells collected at stages ranging from E10.5 to E13.5.

Depending on how the public scRNAseq data sets were pre-processed by the owner, distinct but similar tools were used. Adult data set was analyzed using R package Seurat (V3.1.5) [20] while embryonic data set was analyzed using R package Monocle 3 [21]. Clusters of cells were identified by unbiased machine learning algorisms. Principal component analysis (PCA) was applied for dimension reduction, and Uniform Manifold Approximation and Projection (UMAP) was used to visualize data at low-dimensions.

*4.3.10 Real-Time Quantitative Reverse Transcription PCR (qRT-PCR)*

After tissue harvest and collection, RNA was isolated and purified by Hybrid-RTM RNA isolation kit (#305-101, GeneAll, Seoul, Korea). Purified RNA was converted into cDNA using Tribo™ Reverse Transcription Reaction Kit (#TBS4006, Tribioscience, Carlsbad, CA). The following primers were used for qRT-PCR: *Gli1*-Forward: GAAGGCTGTCGGAAGTCC TA; *Gli1*-Reverse: GATCTGTGTAGCGCTTGGTG; *Ptch1*-Forward: TCATTGTCATGGT

CCTGGCT; *Ptch1*-Reverse: AGCATAGCCCTGTGGTTCT T; *Evc2*-Forward: CATGGAGGAAGCAGAAGAGG; *Evc2*-Reverse: TGTGTGCTTGAGCAAAGTCC. *Gapdh*-Forward: CATCACTGCCACCCAGAAGACTG; *Gapdh*-Reverse: ATGCCAGTGAGCTTCAG. *Gapdh* served as internal control. mRNA levels of genes of interest were measured using Tribo™ 2x Fast Sybr Green qPCR Master Mix (#TBS4001-20, Tribioscience, Carlsbad, CA) with QuantStudio™ 5 Real-Time PCR System (#A34322, Thermo Fisher Scientific, Waltham, MA, USA).

*4.3.11 Quantification & statistical analysis*

Quantification of fungiform papilla from SEM experiments and transcripts from RNAscope® *In situ* hybridization experiments, and measurement of fungiform papilla size and length of tongues were performed using Photoshop and/or ImageJ.

Transcripts of *Gli1* and *Ptch1* are quantified by counting dots of DAB signals in bright-field microscopy images of RNAscope® *In situ* hybridization. Transcripts of Gli1 and Ptch1 are quantified in the following three regions for both epithelium and mesenchyme: Tongue tip (TIP), intermediate regions (ID), and intermolar eminence (IE). Transcripts per cell was calculated to be used to quantitively evaluate gene expression. 3 mice from each genotype were included for quantification and statistical analysis. At least 3 representative images of tongue sections from each mice were included for quantification. For each region in each tongue section, an 50 μm X 100 μm area including all layers of epithelial cells and 4-7 layers of underlying mesenchymal cells was chose for quantification. In total, 7470 cells from E12.5 tongues and 4595 cells from E14.5 tongues were included for quantification of *Gli1* transcripts. 9262 cells from E12.5 tongues and 4529 cells from E14.5 tongues were included for *Ptch1* transcripts.

A one-way ANOVA analysis followed by Tukey analysis was implemented to test differences in number and size of taste papillae, and length of embryonic tongues across genotypes (knockout, heterozygous, and wild type) and differences in ΔCt values of *Evc2, Gli1* and *Ptch1* under four different tissue compartments from qRT-PCR experiments. Student's T-test was used to assess differences in means of ΔCt values of *Gli1* and *Ptch1* between genotypes (knockout and wild type) from qPCR experiments and differences in means of transcripts of *Gli1* and *Ptch1* between genotypes (knockout and wild type) from *in situ* hybridization experiments. A nominal P-value smaller than 0.05 was used to declare statistical significance. All analyses were implemented in R [22].

## 4.4 Results

### *4.4.1 Evc2 is dynamically expressed in embryonic mouse tongues over the developmental course*

We first detected expression of *Evc2* relative to housekeeping gene *Gapdh* using qRT-PCR in multiple tissue compartments including epithelium of anterior tongue region (E_A), epithelium of posterior region (E_P) which including intermolar eminence and pharyngeal tongue, mesenchyme of anterior tongue region (M_A), and mesenchyme of posterior region (M_P) at E12.5 (Figure 4.1A). It showed that expression of *Evc2* in E_P region was significantly higher than the rest tissue compartments. At E15.5, expression of *Evc2* was quantified in following tissue compartments: epithelium of anterior tongue region (E_A), epithelium of intermolar eminence region (E_I), mesenchyme of anterior tongue region (M_A), and mesenchyme of intermolar eminence region (M_I) (Figure 4.1B). Neither epithelium (E_A and E_I) nor mesenchyme displayed differences between anterior tongue and intermolar eminence regarding *Evc2* expression.

To further validate and characterize temporal and spatial pattern of *Evc2* expression in mouse tongue, X-gal staining was performed to detected activity of β-galactosidase (β-gal) which represents *Evc2* expression on tongue sections of $Evc2^{LacZ/-}$ mice. And $Evc2^{LacZ/-}$ mice have very minor phenotype compared with littermate control mice [13]. At E12 β-gal signals were only observed in anterior epithelium and intermediate epithelium (Figure 4.2A, 4.2B2 and 4.2B3). There were no or extremely weak β-gal signals in IE epithelium (Figure 4.2B1) or mesenchyme of all three regions (Figure 4.2B). At E14.5 β-gal signals were observed broadly in tongues including all three regions: IE, intermediate and anterior tongue (Figure 4.2C and 4.2D). Notably there were strong β-gal signals within fungiform papillae (Figure 4.2D2 and 4.2D3). At E18.5, β-gal signals were detected throughout tongue epithelium, including taste papilla cells, taste bud cells and non-taste epithelial cells. In mesenchyme, the β-gal signals were sporadically distributed (Figure 4.2E and 2F).

*4.4.2 Taste papillae were increased in number and size in the $Evc2^{-/-}$ tongue.*

Taste papilla placodes were specified at E12.5 and taste placode cells express SHH [23]. To evaluate how specification of taste placodes was affected in $Evc2^{-/-}$ mice, whole-mount Immunohistochemistry again SHH were performed. Larger $SHH^{+}$ patches were found in $Evc2^{-/-}$ tongues compared to the tongues of littermate controls (Figure 4.3A). Correspondingly, SEM analysis of E12.5 tongues revealed that papilla placodes were more elevated in $Evc2^{-/-}$ tongues than tongues in littermate controls (Figure 4.3B). At E15.5, SHH expression was more constricted to fungiform papilla cells in the anterior tongues [24]. Whole-mount Immunohistochemistry again SHH revealed that more fungiform papillae were developed on dorsal surface of $Evc2^{-/-}$ tongues than littermate controls (Figure 4.3C). In SEM data of E15.5 tongues, fungiform papillae in $Evc2^{-/-}$ mice were larger in size than those in littermate controls

(Figure 4.3C and 4.3D). And there was no significant difference between wild type (*Evc2*$^{+/+}$) and heterozygous (*Evc2*$^{+/-}$) in terms of number and size of fungiform papillae (Figure 4.3C and 3D). The length of oral tongues did not change in *Evc2*$^{-/-}$ tongues compared to littermate controls. Notably, all the fungiform papillae were well-patterned and no ectopic fungiform papillae developed in intermolar eminence(IE) regions (Figure 4.3C).

At lateral posterior tongue Evc2 deletion led to enhanced expression of SHH in foliate papillae (Figure 4.4D). No apparent changes were detected in *Evc2*$^{+/-}$ circumvallate papillae (Figure 4.4A, 4.4B, and 4.4C)

*4.4.3 Hedgehog signaling activities were impaired in Evc2*$^{-/-}$ *tongues in a region-specific manner*

Subcellularly EVC2 is located at primary cilium of mammalian cells and EVC2 has been reported to be a positive modulator of Hedgehog signaling *in vitro* and in bones and teeth *in vivo* [11, 12]. The roles of Hedgehog signaling in papilla placode specification have been defined. However, how EVC2 modulating hedgehog signaling during papilla placode specification remains unclear. We hypothesized that Hedgehog signaling activities decreased in *Evc2*$^{-/-}$ tongues in a tissue-specific manner. To test this hypothesis, we first characterized expression of *Gli1* and *Ptch1*, two read-out genes of Hedgehog signaling activity, in multiple regions of wild type mouse tongues at E12.5 (Figure 4.5A) and E14.5 (Figure 4.5B). At E12.5, no significant difference of *Gli1* or *Ptch1* expression were detected among four tissue compartments. At E14.5, the epithelium of anterior tongue (E_A) had a higher expression of *Gli1* and *Ptch1* than the rest of tissue compartments. Due to experimental challenges of getting enough RNA after dissecting into particular epithelium into three regions, whole epithelial sheets and mesenchyme masses were used to compare *Gli1* and *Ptch1* expression between *Evc2*$^{-/-}$ and control tongues. qRT-PCR results (Figure 4.5C and 5D) showed that expression of *Gli1*, not *Ptch1* was significantly lower

in *Evc2*$^{-/-}$ tongue epithelium than control tongue epithelium at E12.5 (Figure 4.5C). And expression of both *Gli1* and *Ptch1* decreased in *Evc2*$^{-/-}$ tongue mesenchyme compared to control tongues (Figure 4.5D).

To spatially characterize Hedgehog signaling activity in *Evc2*$^{-/-}$ tongues, RNAScope™ *in situ* hybridization with *Gli1* and *Ptch1* probes were performed in embryonic tongues at E12.5 and E14.5. And transcripts were quantified in three regions for both epithelium and mesenchyme: Tongue tip (TIP), intermediate regions (ID), and intermolar eminence (IE). At both E12.5 and E14.5, *Ptch1* and *Gli1* transcripts were broadly detected in both *Evc2*$^{-/-}$ tongues and littermate control tongues (Figure 4.6 - 9). However, transcripts of *Gli1* (Figure 4.6 and Figure 4.10A), not *Ptch1* (Figure 4.7 and Figure 4.10C), in epithelial cells at tongue tip region were significantly less abundant in *Evc2*$^{-/-}$ tongue than littermate control tongues at E12.5. At E14.5 no significant differences between *Evc2*$^{-/-}$ tongue and control tongues were detected in terms of *Gli1* or *Ptch1* expression in either tissue compartments at any regions (Figure 4.8, 9 and 10).

*4.4.4 Distribution of Evc2 and Hedgehog signaling targets in individual cells*

Since global deletion of *Evc2* decreased Hedgehog signaling activities only in tongue tip epithelial cells, not in other tissue compartments of tongues, there are likely both EVC2-dependent and EVC2-independent Hedgehog signaling in taste organs. So to support this idea, we checked expression of genes encoding Hedgehog signaling components at single cell level. Using public single cell transcriptome data sets of branchial arch epithelial cells at embryonic stages ranging from E10.5 to E13.5 [19] and adult anterior tongue epithelial cells [18] (Figure 4.11 to 4.15), we found that *Evc2* is expressed in cells almost in all cell clusters. However, in all data sets the expression of *Evc2* had a lower frequency than *Smo* whose protein product binds to

EVC2. Not all the *Evc2*-expressing cells express *Smo* and not all the *Smo*-expressing cells express *Evc2.* Regarding the two indicators of Hedgehog signaling activity, *Gli1* and *Ptch1*, in embryonic data sets *Ptch1* is expressed in a higher frequency than *Gli1* (Figure 4.11 to 4.14) while in adult data set *Gli1* is expressed in a higher frequency than *Ptch1* (Figure 4.15). It is also noteworthy that not all the *Evc2*-expressing cells express *Ptch1* and *vice versa*. Regarding the two effectors of Hedgehog signaling activity, *Gli2* and *Gli3*, in embryonic data sets *Gli3* is expressed in a higher frequency than *Gli2* (Figure 4.11 to 4.14) while in adult data set *Gli3* is expressed in a higher frequency than *Ptch2* (Figure 4.15). Not all the *Evc2*-expressing cells express *Gli2* and *vice versa.*

To closely look at how many Hedgehog-responsive cells express *Evc2* and how many *Evc2*-expressing cells are with activated Hedgehog signaling activity, we filtered *Gli1*-expressing cells and *Evc2*-expressing cells, respectively, from both embryonic (Figure 4.16) and adult (Figure 4.17) scRNA-seq data sets. With analyses of *Gli1*-expressing cells only (Figure 4.16 A and B, Figure 17A and B) and *Evc2*-expressing cells only (Figure 4.16 C and D, Figure 17C and D), it is clear that very few *Gli1*-expressing cells express *Evc2* and very few *Evc2*-expressing cells express *Gli1* in both embryonic branchial arch epithelial cells and adult tongue epithelial cells.

### *4.4.5 Transcriptomic profiling revealed a significant up-regulation of extracellular matrix (ECM)-related genes in Evc2$^{-/-}$ tongue epithelium*

To identify novel gene targets downstream EVC2/Hedgehog signaling, E12.5 *Evc2*$^{-/-}$ and control tongue epithelium were isolated for RNA-seq analyses (Figure 4.18A). A total of 31 down-regulated and 151 up-regulated differentially expressed genes (DEGs) were identified in E12.5 *Evc2*$^{-/-}$ tongue epithelium (Figure 4.18B). To obtain general functions of the DEGs, gene

ontology (GO) analysis were conducted and enrichment results were shown in heatmaps (Figure 4.18C and 18D). For down-regulated DEGs, only 4 items were enriched ($P<0.01$) due to the limited number of genes. Cell fate specification (GO: 001708) was the top hit in the analysis. For up-regulated DEGs, 50 GO terms were identified ($P<0.01$, Figure 4.18D, not showing all). Of note, several ECM-related GO terms were identified, including extracellular matrix (GO: 001708), collagen trimer (GO: 005581), basement membrane (GO: 005604), etc. Other than ECM-related GO terms, development-related GO terms were also among top hits, e.g. sensory organ development (GO: 007423), vasculature development (GO: 001944).

*4.4.6 Evc2 deletion resulted in regional epithelial metaplasia and defects of taste papillae*

At E18.5, early taste buds emerge in the apex of fungiform papilla epithelium over a defined mesenchymal core. SEM analysis clearly revealed that *Evc2* deletion resulted in severe region-specific defects on fungiform papilla development (Figure 4.19A). We noticed that fungiform papillae in the intermediate (ID) regions of *Evc2*$^{-/-}$ tongues were larger in size than those in other anterior regions, like tongue tip (TIP) of *Evc2*$^{-/-}$ tongues and those in littermate control tongues (Figure 4.19B). To examine the morphology of region-specific phenotype, H&E staining was performed in E19.5 sagittal tongue sections. In the tongue tip (TIP), there were no detectable changes regarding morphology of taste buds and fungiform papillae (Figure 4.19$D_2$ and 19$D_4$). However, corresponding to the larger papillae from SEM images, epithelium in intermediate (ID) regions became thicker in *Evc2*$^{-/-}$ tongues (Figure 4.19$D_1$ and 19$D_3$). Moreover, a few filiform papillae were found misoriented and pointing to anterior tongue in *Evc2*$^{-/-}$ mice (star, Figure 4.19C) while almost all filiform papillae in control mice were pointing posteriorly.

To find out whether all the fungiform papillae develop taste buds in *Evc2*$^{-/-}$ tongues, whole-mount staining against Keratin 8 were performed in epithelial sheets. It revealed that consistently with increased number of fungiform papillae at E15.5, more Keratin 8$^{+}$ taste buds were seen in *Evc2*$^{-/-}$ mice at E18.5 (Figure 4.19E). In the high power images which were merged with bright field images, taste buds were found to be extremely close to each other in *Evc2*$^{-/-}$ tongues while taste buds were spaced regularly in control tongues (Figure 4.19E, insets).

*4.4.7 Filiform papillae were misoriented and taste buds were lost regionally in 3-week-old Evc2*$^{-/-}$*mice.*

Most *Evc2*$^{-/-}$ mice die neonatally. So postnatal *Evc2*$^{-/-}$ tongues were examined only at one stage: 3-week-old with limited samples. Regional abnormal fungiform papillae were obvious in 3-week-old *Evc2*$^{-/-}$ mice (Figure 4.20A, 20B$_2$ and 20C$_2$). However, taste buds were missing in *Evc2*$^{-/-}$ mice, and some fungiform papillae became filiform papilla-like in shape (Figure 4.20 B$_3$ and C$_3$). Further, as the most abundantly distributed papillae, filiform papillae at anterior tongue in control mice were uniformly oriented towards back (Figure 4.20 B$_1$ and C$_1$) while, filiform papillae were misorientated in *Evc2*$^{-/-}$mice (Figure 4.20 B$_4$ and C$_4$).

*4.4.8 Ectopic proliferating cells were observed in Evc2*$^{-/-}$ *lingual epithelium*

Given that enlarged fungiform papillae in *Evc2*$^{-/-}$ tongues were observed, we hypothesize that cell proliferation could be affected in *Evc2*$^{-/-}$ tongues. To understand whether the enlarged fungiform papillae was caused by increased cell proliferation, double-labeling of taste bud cell marker Keratin 8 with proliferation marker Ki67 was conducted in E18.5 tongue sections. There were abundant Ki67$^{+}$ cells in both in *Evc2*$^{-/-}$ tongues and control tongues. In the control tongues, Ki67$^{+}$ proliferating cells were primarily located in the basal epithelium of the tongue (Figure 4.21B and 21C). In contrast, *Evc2*$^{-/-}$ mouse tongues depicted abundant Ki67$^{+}$ proliferating cells in

suprabasal layers of the epithelium in intermediate regions (Figure 4.21F), but not anterior regions (Figure 4.21E).

*4.4.9 Cell apoptosis were decreased in the superficial layer of Evc2$^{-/-}$ tongue epithelium*

Cell apoptosis plays essential roles in organogenesis, but has been poorly characterized in lingual papilla development. Here we did triple immunostaining against apoptosis marker cleaved Caspase 3, epithelial cell marker E-cadherin, and taste bud cell marker Keratin 8 in E18.5 tongue sections. In controls, cleaved Caspase 3 signals were found in superficial layer of epithelium and mesenchymal cores (Figure 4.22 A, B, and C). In *Evc2*$^{-/-}$ tongues, fewer cleaved Caspase 3 signals were detected in both tissue compartments (Figure 4.22 D, E, and F).

*4.4.9 BCL11B were absent in the abnormal fungiform papillae in Evc2$^{-/-}$ tongues*

Regulation of fungiform papilla morphogenesis has been largely unexplored. BCL11B was identified as an essential regulator for lingual papilla morphogenesis and *Bcl11b* deletion resulted in "smooth tongues" which is lack of apparent papilla structure [25]. The smooth and bigger fungiform papillae in *Evc2*$^{-/-}$ tongues at E18.5 partially were reminiscent of the "smooth tongues" in *Bcl11b* $^{-/-}$ mice. immunostaining with BCL11B antibody showed regional absence of BCL11B in the abnormal fungiform papillae in intermediate region (Figure 4.23F), but not anterior regions (Figure 4.23E), of *Evc2*$^{-/-}$ tongues while BCL11B was consistently expressed throughout tongue basal epithelium in controls (Figure 4.23B and 23C).

*4.4.11 SHH-responsive (Gli1$^{+}$) cells were located surrounding taste buds in embryonic tongues and its derived cells entered taste buds postnatally*

Considering that Hedgehog signaling pathway inhibits taste bud development in embryos but promote cell differentiation in adult tongues, we hypothesize that SHH-responsive cells in embryonic tongues do not differentiate into early taste bud cells but differentiate into taste bud

cells postnatally. To test this hypothesis, we first located *Gli1*-expressing cells in embryonic tongues at three embryonic stages by performing two-day lineage-tracing experiments using *Gli1*-CreER/RFP mice. Tamoxifen was administrated at E12.5, E14.5 and E16.5, followed by tissue harvest two days post tamoxifen treatment. In E14.5 tongues (tamoxifen at E12.5), $RFP^+$ cells located between taste papillae ( taste progenitors) in tongue epithelium (Figure 4.25A). In E16.5 tongues (tamoxifen @E14.5, Figure 4.25B) and E18.5 tongues (tamoxifen @ E16.5, Figure 4.25C), $RFP^+$ cells also located between early taste bud cell progenitors but adjacent to fungiform papillae. Next we chose E14.5 to do tamoxifen treatment, and did tissue harvest at 5 days and 33 days later. At E19.5, 5 days post tamoxifen, we saw bigger $RFP^+$ clusters than E16.5 tongues (tamoxifen @ E14.5, Figure 4.25D), suggesting *Gli1*-expressing cells were dividing outside early taste papillae and taste buds before birth. However, in P28 tongues (tamoxifen @ E14.5, Figure 4.25E), bigger cell clones were observed in fungiform papillae, including both taste bud cells and cells outside taste buds.

## 4.5 Discussion

In the present study, we are the first to show that EVC2, an important component of hedgehog signaling pathway [11, 12], has a dynamic expression pattern along taste organogenesis and exerts stage- and region-specific roles in the development of taste papillae and taste buds. The *Evc2* expression represented by β-gal signals were only observed in anterior tongue epithelium at E12.5 but were broadly distributed in tongues at E14.5. Genetic deletion of *Evc2 in vivo* affected various events of development and organization of tongue epithelium in a stage- and region-specific manner, including increased number and size of taste papillae, defected morphology of fungiform and filiform papillae, and increased number of early taste buds at E18.5 but decreased number of mature taste buds postnatally. However, the initial

formation and growth of the tongue and epithelial cell fate in the IE region were not apparently affected in *Evc2*$^{-/-}$ mice which is in contrast to the profound alterations by Hedgehog signaling disruption *In vitro*.

*4.5.1 Involvement of EVC2 in Hedgehog signaling and regulation of taste organ development in a region-specific manner.*

Hedgehog signaling in tongue mesenchyme [3] is required for tongue development in a stage-specific manner. Addition of cyclopamine or SHH blocking antibody in mandible cultures within a narrow time window (E12 in rats) suppressed tongue formation [26]. Small and cleft tongues developed if Hedgehog signaling is conditionally interrupted in tongue mesenchyme using *Wnt1*$^{Cre}$/*Smo*$^{fl/fl}$ [3, 27]. In contrast, global deletion of *Evc2* didn't affect tongue formation and growth at least at examined stages (E12.5 - E18.5), which indicates EVC2 is not required for tongue formation and initial out-growth. However, the shape of *Evc2*$^{-/-}$ tongue tip is more rounded than that of wild type tongues (Figure 4.3A), indicating very minor defects of Hedgehog signaling in *Evc2*$^{-/-}$ knockout tongue mesenchyme.

*In vitro* studies have demonstrated that Hedgehog signaling plays an inhibitory role in taste papilla formation, in which disruption of Hedgehog signaling lead to an increased number of papilla placodes and ectopic placodes in intermolar eminence (IE), a normally papilla-free region [3]. Here we report that *Evc2*$^{-/-}$ mice displayed a region-specific phenotypes. *Evc2*$^{-/-}$ mice developed more fungiform papillae in the papilla regions but did not develop ectopic papilla placodes in IE region.

We have two speculations regarding the reason why discrepancies occur. First, it is possible that Hedgehog signaling transduction depends on EVC2 to various extents in different tissue regions ("context-dependent" model). This model suggests that both Evc2-dependent

(anterior tongue epithelium) and -independent (IE epithelium and mesenchyme) Hedgehog signaling existing during tongue and taste papilla development. Second, the EVC/EVC2 complex can only enhance Hedgehog signaling activity but are not indispensable for Hedgehog signaling transduction ("quantitative effect" model). Different levels of Hedgehog activities are required for different target gene expression [15]. Since Hedgehog activities are impaired, but not abrogated in *Evc2*$^{-/-}$ mice, expression of target genes regulating fungiform papilla placode specification which need higher levels of hedgehog signaling is more likely to be affected than expression of those regulating tongue formation in mesenchyme and those inhibiting taste papilla fate in IE epithelium (Figure 4.5B).

In present study, the broad distribution of *Evc2* in developing tongues (Figure 4.1 and Figure 4.2) ruled out the possibility that *Evc2* was exclusively turned on in anterior tongue epithelium. Next we evaluated Hedgehog signaling activities in both wild type and *Evc2*$^{-/-}$ tongues. In wild type tongues, anterior epithelium where fungiform papillae developed had the highest Hedgehog signaling activities measured by qRT-PCR (Figure 4.5B). And in *Evc2*$^{-/-}$ tongues, Hedgehog signaling activities decreased in all four tissue compartments examined using qRT-PCR (Figure 4.5C and 4.5D). So evidences from qRT-PCR suggest that the reason why anterior epithelium is the only region showing phenotypes in global deletion of *Evc2* is due to the highest requirement of Hedgehog signaling in anterior tongue, which supports "quantitative effect" model. However, RNAScope *in situ* hybridization data suggested that only in tongue tip, but not in any other tissue compartments, hedgehog signaling activity is impaired, which supports "context-dependent" model. Further, expression of genes encoding hedgehog signaling components in individual cells supports "context-dependent" model. Not all the *Ptch1*- or *Gli1*-expressing cells express *Evc2* suggest that there is *Evc2*-independent hedgehog signaling

activities. Moreover, the fact that not all the *Evc2*-expressing cells express *Gli1* or *Ptch1* suggests that *Evc2* may play some roles unrelated to Hedgehog signaling.

*4.5.2 EVC2/Hedgehog signaling inhibits transcription of ECM-related genes during papilla placode specification*

Roles of ECM has been implicated in a variety of physiological and developmental processes [28]. But the roles of ECM in taste bud and taste papilla development are largely unexplored. By treating E12.5 tongue culture with heparinase which can cleave glycosidic linkage between hexosamines and uronic acids, Wnt signaling pathway was activated in a bigger area than tongue culture without treatment [7]. In present studies, using high-throughput methodology we found that a number of ECM-related genes were upregulated in $Evc2^{-/-}$ tongue epithelium, suggesting that Hedgehog signaling pathway can negatively modulate number of taste papilla placodes and taste buds via inhibiting transcription of ECM-related genes. Future functional analyses on the specific ECM-genes that were identified in present study during papilla placode specification will advance our understanding of molecular mechanisms underlying taste organ development.

*4.5.3 Evc2 knockout leads to increased number of early taste buds but decreased number of taste buds postnatally*

Due to the limited survival period of taste organs in *in vitro* tissue culture [29] and early lethality of *Shh* knockouts [30], how Hedgehog signaling affects early taste bud development at E18.5 has not been well-characterized. With multiple conditional and inducible knockout mouse lines, previous longitudinal studies conducted by others [3] and us in the present study indicated that deletion of Hedgehog signaling components resulted in increased number of taste buds as well as number of taste papillae. For example, More $K8^{+}$ clusters were found in $Shh^{CreER}/Shh^{flox}$

mice which were exposed to tamoxifen at E11 when compared with controls [3]. In this study, we detected more taste buds labeled by K8 in *Evc2*$^{-/-}$ mice than littermate controls (Figure 4.12E). Collectively, these data supported that differentiation of taste bud cells from taste bud progenitors within papillae was not affected by *Evc2* deletion or Hedgehog signaling interruption, even though EVC2 and Hedgehog signaling regulates number of cell clusters of taste bud progenitors at early stages.

Although the differentiation of taste bud progenitors in papilla placodes seems not to be regulated by Hedgehog signaling, recent attempts revealed that Hedgehog signaling regulated differentiation of basal lingual epithelial cells. Merkel cells were detected in tongue epithelium using the marker Rab3c in basal lingual epithelium in *Shh*$^{Cre}$*/Smo*$^{fl/fl}$ mice, but not in control or *Shh*$^{CreER}$*/Shh*$^{flox}$ mice [3]. Similarly, K8$^{+}$ cells were also detected in anterior basal lingual epithelium in *Evc2*$^{-/-}$ mice while K8$^{+}$ cells were only detected within fungiform papillae in anterior lingual epithelium in control mice. Further characterizing the fate of K8$^{+}$ basal epithelial cells is necessary. Discrepancies of phenotypes among different Hedgehog signaling-interrupted models revealed the complexity of Hedgehog signaling.

*4.5.4 EVC2/Hedgehog signaling regulated papilla morphogenesis potentially via regulating expression of BCL11B in a region-specific manner*

Most clinical reports overlook tongue or taste phenotypes of Ellis–van Creveld syndrome until that recently regionally papilla loss was reported [10]. Considering stage-specific roles of Hedgehog signaling in taste bud development, how and when *Evc2* mutation causes this phenotype is a mystery. Here by employing *Evc2*$^{-/-}$ mice, we partially but successfully phenocopied it and identified the stage when the defects emerge. Regional loss of papillae emerged at E18.5 in *Evc2*$^{-/-}$ mice (Figure 4.12). Our data suggests that in addition to decreasing

number of fungiform papillae, *Evc2* also play essential roles in papilla morphogenesis. Papilla morphogenesis which happens between E15.5 and E19.5 are less understood compared to other developmental events, such as papilla placode specification and taste bud maintenance. BCl11B has been identified as an key transcription factor for papilla morphogenesis. *Bcl11b*$^{-/-}$ mice loss all lingual papillae and develops tongues with smooth surface [25]. So in present study, we tested the hypothesis that EVC2 regulates papilla morphogenesis by modulating BCL11B expression. Regional absence of BCL11B in the abnormal fungiform papillae in *Evc2*$^{-/-}$ mice (Figure 4.16) suggests that EVC2 regulates papilla morphogenesis by controlling BCL11B expression in a region-specific manner. Future studies could focus on elucidating why *Evc2* deletion causes reginal absence of BCL11B.

*4.5.5 Potential roles of EVC2 in filiform papillae development*

As the most dominant type of papillae in the tongue surface [31], filiform papillae are responsible for somatosensory, not for taste sensory (refs). Pax9 is required for filiform papilla development and epithelium differentiation. In Pax9-deficinet mice, tongue is more smoother than controls and the cornified layer is missing [32]. LGN is another essential factor regulating papilla morphogenesis by promoting perpendicular divisions [33]. Moreover, bmp signaling is also involved in filiform papilla morphogenesis. Over-expressing BMP antagonist, Noggin, in K14-expressing cells *in vivo* transformed filiform papillae from rounded to pointed shape in anterior tongue [34]. In the present study, anterior-posterior polarity of filiform papillae in anterior tongue was dramatically interrupted by *Evc2* deletion (Figure 4.4 $B_4$ and $C_4$). However, roles of Hedgehog signaling in filiform papilla development has not yet been reported, which needs to be further characterized in future studies.

## 4.6 References


1. Delwiche, J.F., Z. Buletic, and P.A.S. Breslin, *Relationship of papillae number to bitter intensity of quinine and PROP within and between individuals.* Physiology & Behavior, 2001. **74**(3): p. 329-337.
2. Yackinous, C.A. and J.-X. Guinard, *Relation between PROP (6-n-propylthiouracil) taster status, taste anatomy and dietary intake measures for young men and women.* Appetite, 2002. **38**(3): p. 201-209.
3. El Shahawy, M., et al., *Cell fate specification in the lingual epithelium is controlled by antagonistic activities of Sonic hedgehog and retinoic acid.* PLoS Genetics, 2017. **13**(7): p. e1006914.
4. Liu, F., et al., *Wnt-β-catenin signaling initiates taste papilla development.* Nature Genetics, 2007. **39**(1): p. 106-112.
5. Iwatsuki, K., et al., *Wnt signaling interacts with Shh to regulate taste papilla development.* Proceedings of the National Academy of Sciences of the United States of America, 2007. **104**(7): p. 2253-2258.
6. Beites, C.L., et al., *Follistatin modulates a BMP autoregulatory loop to control the size and patterning of sensory domains in the developing tongue.* 2009. **136**(13): p. 2187-2197.
7. Prochazkova, M., et al., *FGF signaling refines Wnt gradients to regulate the patterning of taste papillae.* Development, 2017. **144**(12): p. 2212-2221.
8. Liu, H.-X., et al., *Sonic hedgehog exerts distinct, stage-specific effects on tongue and taste papilla development.* Developmental Biology, 2004. **276**(2): p. 280-300.

9. El Shahawy, M., et al., *Cell fate specification in the lingual epithelium is controlled by antagonistic activities of Sonic hedgehog and retinoic acid.* PLOS Genetics, 2017. **13**(7): p. e1006914.

10. Hassona, Y., et al., *Ellis-Van Creveld syndrome: dental management considerations and description of a new oral finding.* 2015. **35**(6): p. 312-315.

11. Dorn, Karolin V., Casey E. Hughes, and R. Rohatgi, *A Smoothened-Evc2 Complex Transduces the Hedgehog Signal at Primary Cilia.* Developmental Cell, 2012. **23**(4): p. 823-835.

12. Yang, C., et al., *Smoothened transduces Hedgehog signal by forming a complex with Evc/Evc2.* Cell Research, 2012. **22**: p. 1593.

13. Zhang, H., et al., *Generation of Evc2/Limbin global and conditional KO mice and its roles during mineralized tissue formation.* genesis, 2015. **53**(9): p. 612-626.

14. Au - Yu, W., et al., *Cell Dissociation from the Tongue Epithelium and Mesenchyme/Connective Tissue of Embryonic-Day 12.5 and 8-Week-Old Mice.* JoVE, 2021(167): p. e62163.

15. Dobin, A., et al., *STAR: ultrafast universal RNA-seq aligner.* Bioinformatics, 2012. **29**(1): p. 15-21.

16. Pertea, M., et al., *StringTie enables improved reconstruction of a transcriptome from RNA-seq reads.* Nature Biotechnology, 2015. **33**: p. 290.

17. Love, M.I., W. Huber, and S. Anders, *Moderated estimation of fold change and dispersion for RNA-seq data with DESeq2.* Genome Biology, 2014. **15**(12): p. 550.

18. Schaum, N., et al., *Single-cell transcriptomics of 20 mouse organs creates a Tabula Muris.* Nature, 2018. **562**(7727): p. 367-372.

19. Cao, J., et al., *The single-cell transcriptional landscape of mammalian organogenesis.* Nature, 2019. **566**(7745): p. 496-502.

20. Stuart, T., et al., *Comprehensive Integration of Single-Cell Data.* Cell, 2019. **177**(7): p. 1888-1902.e21.

21. Trapnell, C., et al., *The dynamics and regulators of cell fate decisions are revealed by pseudotemporal ordering of single cells.* Nature Biotechnology, 2014. **32**(4): p. 381-386.

22. Ihaka, R. and R. Gentleman, *R: A Language for Data Analysis and Graphics.* Journal of Computational and Graphical Statistics, 1996. **5**(3): p. 299-314.

23. Thirumangalathu, S., et al., *Fate mapping of mammalian embryonic taste bud progenitors.* Development, 2009. **136**(9): p. 1519-1528.

24. Liu, H.X., et al., *Multiple Shh signaling centers participate in fungiform papilla and taste bud formation and maintenance.* Developmental biology, 2013. **382**(1): p. 82-97.

25. Nishiguchi, Y., et al., *Bcl11b/Ctip2 is required for development of lingual papillae in mice.* Developmental Biology, 2016. **416**(1): p. 98-110.

26. Liu, H.-X., et al., *Sonic hedgehog exerts distinct, stage-specific effects on tongue and taste papilla development.* Developmental Biology, 2004. **276**(2): p. 280-300.

27. Jeong, J., et al., *Hedgehog signaling in the neural crest cells regulates the patterning and growth of facial primordia.* Genes & development, 2004. **18**(8): p. 937-951.

28. De Arcangelis, A. and E. Georges-Labouesse, *Integrin and ECM functions: roles in vertebrate development.* Trends in Genetics, 2000. **16**(9): p. 389-395.

29. Mistretta, C.M., et al., *Cyclopamine and jervine in embryonic rat tongue cultures demonstrate a role for Shh signaling in taste papilla development and patterning:*

*fungiform papillae double in number and form in novel locations in dorsal lingual epithelium.* Developmental Biology, 2003. **254**(1): p. 1-18.

30. Chiang, C., et al., *Cyclopia and defective axial patterning in mice lacking Sonic hedgehog gene function.* Nature, 1996. **383**(6599): p. 407-413.

31. Farbman, A.I., *The dual pattern of keratinization in filiform papillae on rat tongue.* Journal of anatomy, 1970. **106**(Pt 2): p. 233-242.

32. Jonker, L., et al., *Pax9 is required for filiform papilla development and suppresses skin-specific differentiation of the mammalian tongue epithelium.* Mechanisms of Development, 2004. **121**(11): p. 1313-1322.

33. Byrd, K.M., et al., *LGN plays distinct roles in oral epithelial stratification, filiform papilla morphogenesis and hair follicle development.* Development (Cambridge, England), 2016. **143**(15): p. 2803-2817.

34. Kawasaki, K., et al., *Bmp signalling in filiform tongue papillae development.* Archives of oral biology, 2012. **57**(6): p. 805-813.

## 4.7 Figures

*Figure 4.1 Histograms of normalized values of Evc2 measured by qRT-PCR in wild type mouse tongues at E12.5 (A) and E15.5 (B). qRT-PCR of Evc2 at E12.5 (A) were performed at in following tissue compartment: anterior epithelium (E_A), intermolar em epithelium (E_P), anterior mesenchyme (M_A), and posterior mesenchyme (M_P). qRT-PCR of Evc2 at E15.5 (B) were performed at in following tissue compartments: anterior epithelium (E_A), Intermolar eminence epithelium (E_I), anterior mesenchyme (M_A), and Intermolar eminence mesenchyme (M_I). NS: not significant, P>0.05; *: 0.01<P<0.05.*

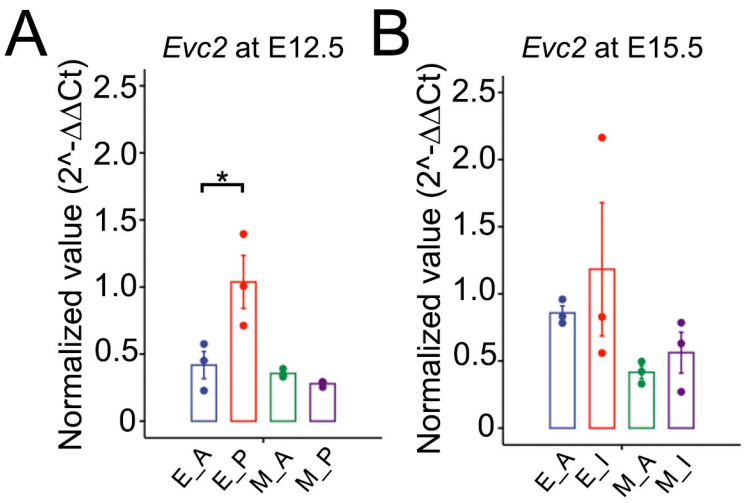
A
Evc2 at E12.5
Normalized value (2^-ΔΔCt)
2.5
2.0
1.5
1.0
0.5
0
*
E_A
E_P
M_A
M_P
B
Evc2 at E15.5
Normalized value (2^-ΔΔCt)
2.5
2.0
1.5
1.0
0.5
0
E_A
E_I
M_A
M_I

*Figure 4.2 Bright field microscopy images of β-gal signals in Evc2$^{LacZ/+}$ tongue sections at E12.5 (A and B), E14.5 (C and D), and E18.5 (E and F). Both low power and high power images are shown here. High power images were took from three regions: anterior tongue ( B3, D3 and F3), intermediate region (B2, D2 and F2), and intermolar eminence (IE, in B1, D1 and F1). Scale bars: 200 μm in A, C and E and 50 μm in B, D and F.*

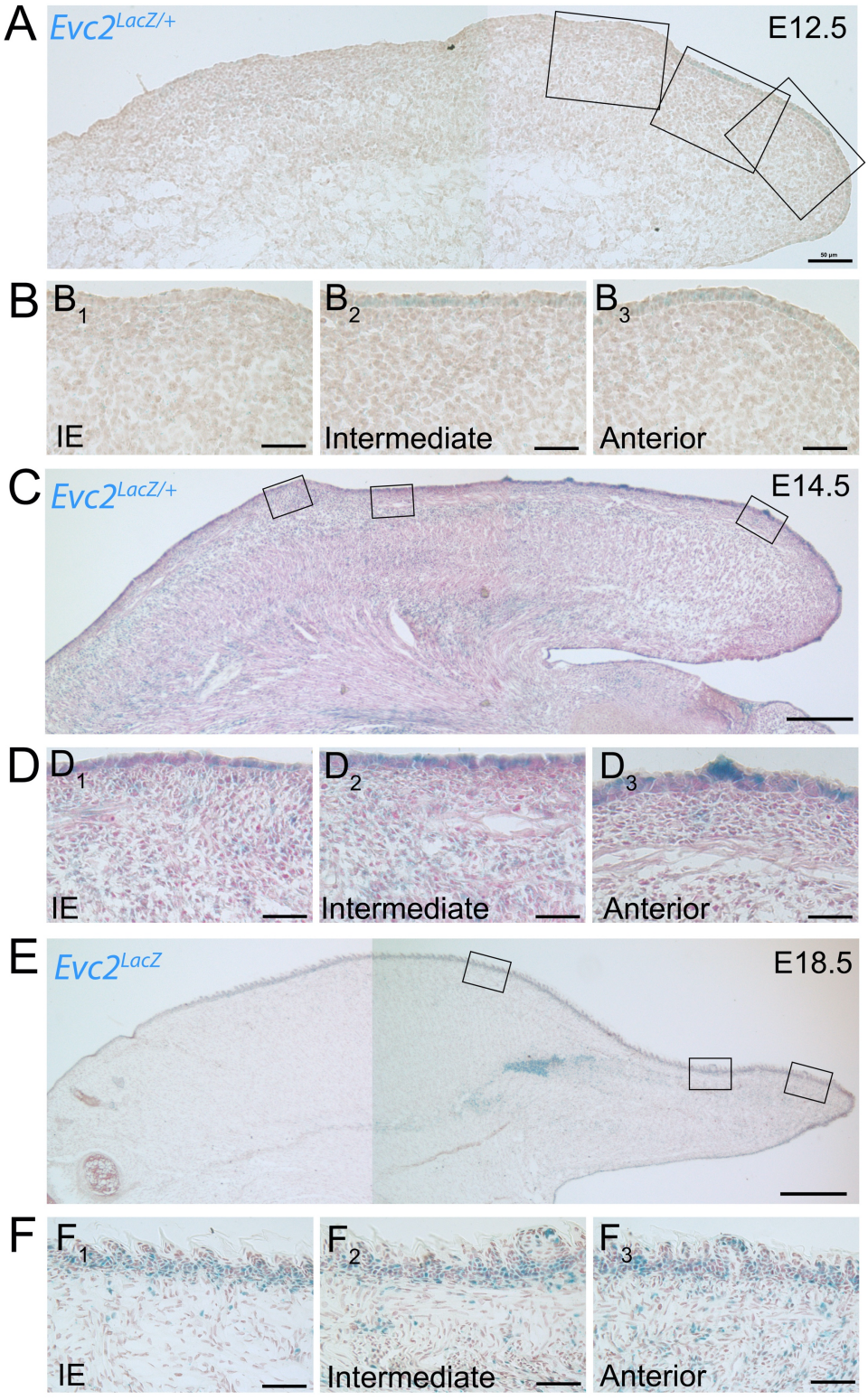
A
Evc2LacZ/+
E12.5
B
B1
IE
B2
Intermediate
B3
Anterior
C
Evc2LacZ/+
E14.5
D
D1
IE
D2
Intermediate
D3
Anterior
E
Evc2LacZ
E18.5
F
F1
IE
F2
Intermediate
F3
Anterior

*Figure 4.3 Whole-mount anti-SHH immunohistochemistry images (A and C) and scanning electron microcopy (SEM) images (B and D) of oral tongues from wild type, heterozygous, and Evc2$^{-/-}$ mice at E12.5 (A and B) and E15.5 (C and D). High power images of fungiform papillae at E15.5 are shown in insets of panel D. Scale bars: 100 μm in A and B, 200 μm in C (20 μm in insets) and D. Histograms of length of oral tongue at E15.5 (left), number of fungiform papillae (FP) (middle), and size of individual fungiform papillae (right) were shown in E. NS: not significant; **: 0.001<P<0.01.*

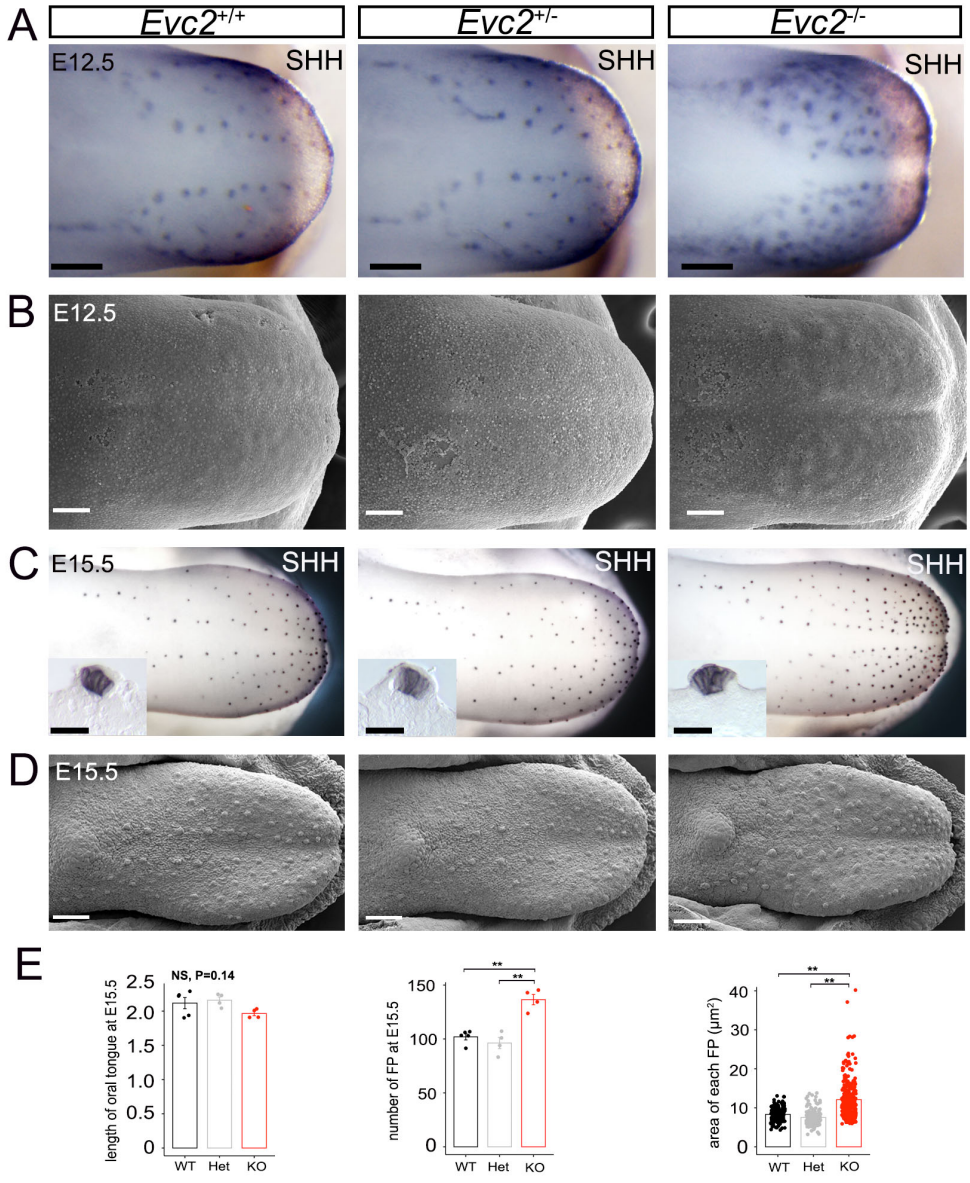
A
Evc2+/+
Evc2+/-
Evc2-/-
E12.5
SHH
B
E12.5
C
E15.5
SHH
D
E15.5
E
NS, P=0.14
length of oral tongue at E15.5
2.5
2.0
1.5
1.0
0.5
0
WT Het KO
number of FP at E15.5
150
100
50
0
**
area of each FP (μm²)
40
30
20
10

*Figure 4.4 Anti-SHH immunohistochemistry images in whole-mount (A, B and D) and sections (C) and scanning electron microcopy (SEM) images (A and B) of circumvallate papillae or foliate papillae from wild type, heterozygous, and Evc2$^{-/-}$ mice at E12.5 (A) and E15.5 (B, C and D). Fol: Foliate papilla. Scale bars: 50 μm in A, 100 μm in B, 25 μm in C, and 100 μm in D.*

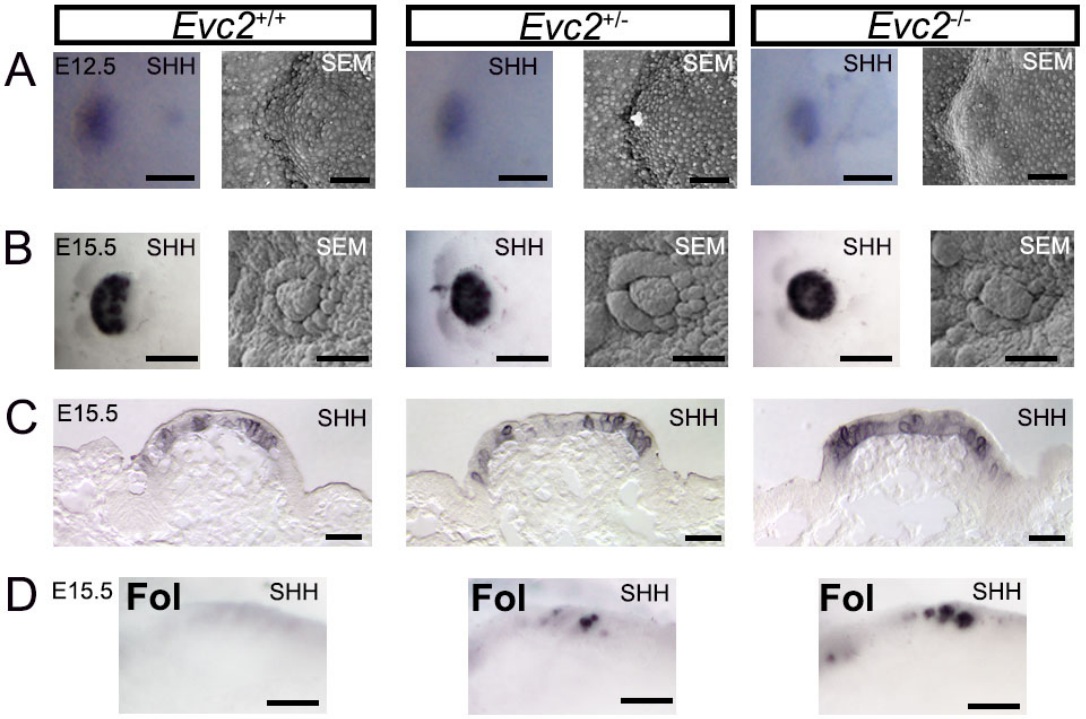
Evc2+/+
Evc2+/-
Evc2-/-
A
E12.5
SHH
SEM
B
E15.5
C
D
Fol

*Figure 4.5 Histograms of normalized values of Gli1 and Ptch1 measured by qRT-PCR in wild type (A and B) and Evc2$^{-/-}$ and control tongues (C and D) at E12.5 (A, C and D) or E15.5 (B). Following four tissue compartments were dissected for E12.5 wild type tongues: qRT-PCR: anterior epithelium (E_A), posterior epithelium (E_P), anterior mesenchyme (M_A), and posterior mesenchyme (M_P). Following four tissue compartments were dissected for E14.5 wild type tongues: anterior epithelium (E_A), Intermolar eminence epithelium (E_I), anterior mesenchyme (M_A), and Intermolar eminence mesenchyme (M_I). Whole epithelial sheets (C) and mesenchyme masses (D) were collected from E12.5 Evc2$^{-/-}$ and control tongues. NS: not significant, P>0.05; *: 0.01<P<0.05; **: 0.001<P<0.01.*

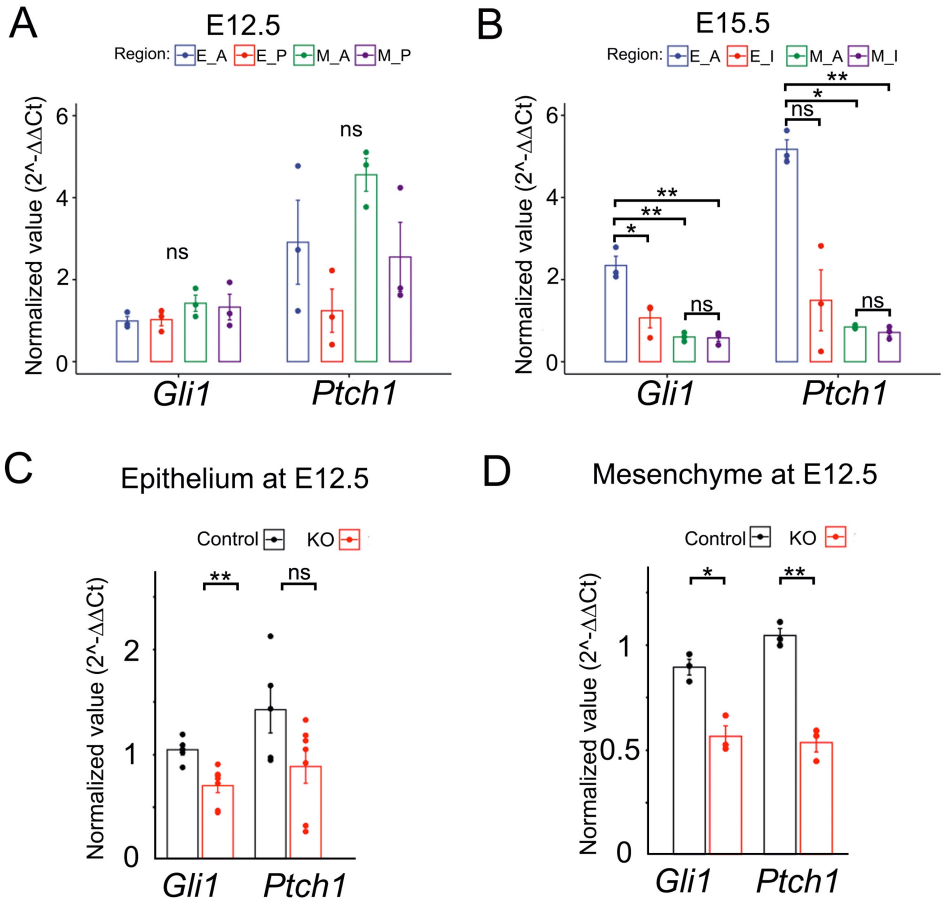
A
E12.5
Region: E_A E_P M_A M_P
Normalized value (2^-ΔΔCt)
ns
ns
Gli1
Ptch1
B
E15.5
Region: E_A E_I M_A M_I
Normalized value (2^-ΔΔCt)
**
*
**
*
ns
ns
ns
Gli1
Ptch1
C
Epithelium at E12.5
Control KO
Normalized value (2^-ΔΔCt)
**
ns
Gli1
Ptch1
D
Mesenchyme at E12.5
Control KO
Normalized value (2^-ΔΔCt)
*
**
Gli1
Ptch1

*Figure 4.6 Bright field microscopy images of Gli1 transcripts (brown dots) detected by RNAScope™ in situ hybridization in Evc2$^{-/-}$ and control tongues at E12.5. Both low power (A1 and B1) and high power images (A2, A3, A4, B2, B3 and B4) are shown here. High power images were took from three regions: intermolar eminence (IE, in A2 and B2), intermediate region (A3 and B3), and anterior tongue (A4 and B4). Scale bars: 100 μm in A1 and B1, and 50um in A2, A3, A4, B2, B3 and B4.*

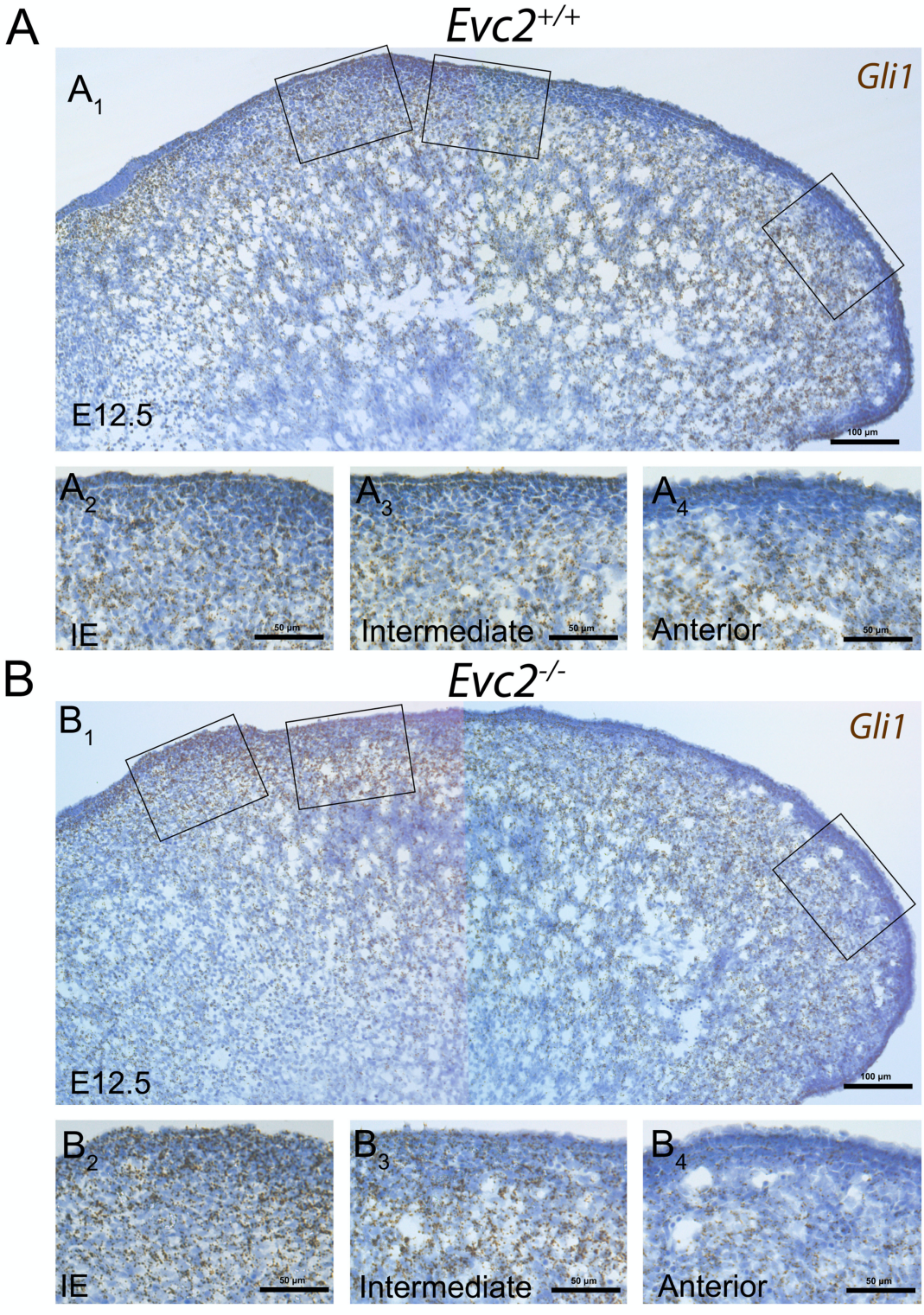
A
Evc2+/+
A1
Gli1
E12.5
100 µm
A2
IE
50 µm
A3
Intermediate
50 µm
A4
Anterior
50 µm
B
Evc2-/-
B1
Gli1
E12.5
100 µm
B2
IE
50 µm
B3
Intermediate
50 µm
B4
Anterior
50 µm

*Figure 4.7 Bright field images of Ptch1 transcripts (brown dots) detected by RNAScope™ in situ hybridization in Evc2$^{-/-}$ and control tongues at E12.5. Both low power (A1 and B1) and high power images (A2, A3, A4, B2, B3 and B4) are shown here. High power images were took from three regions: intermolar eminence (IE, in A2 and B2), intermediate region (A3 and B3), and anterior tongue (A4 and B4). Scale bars: 100 μm in A1 and B1, and 50um in A2, A3, A4, B2, B3 and B4.*

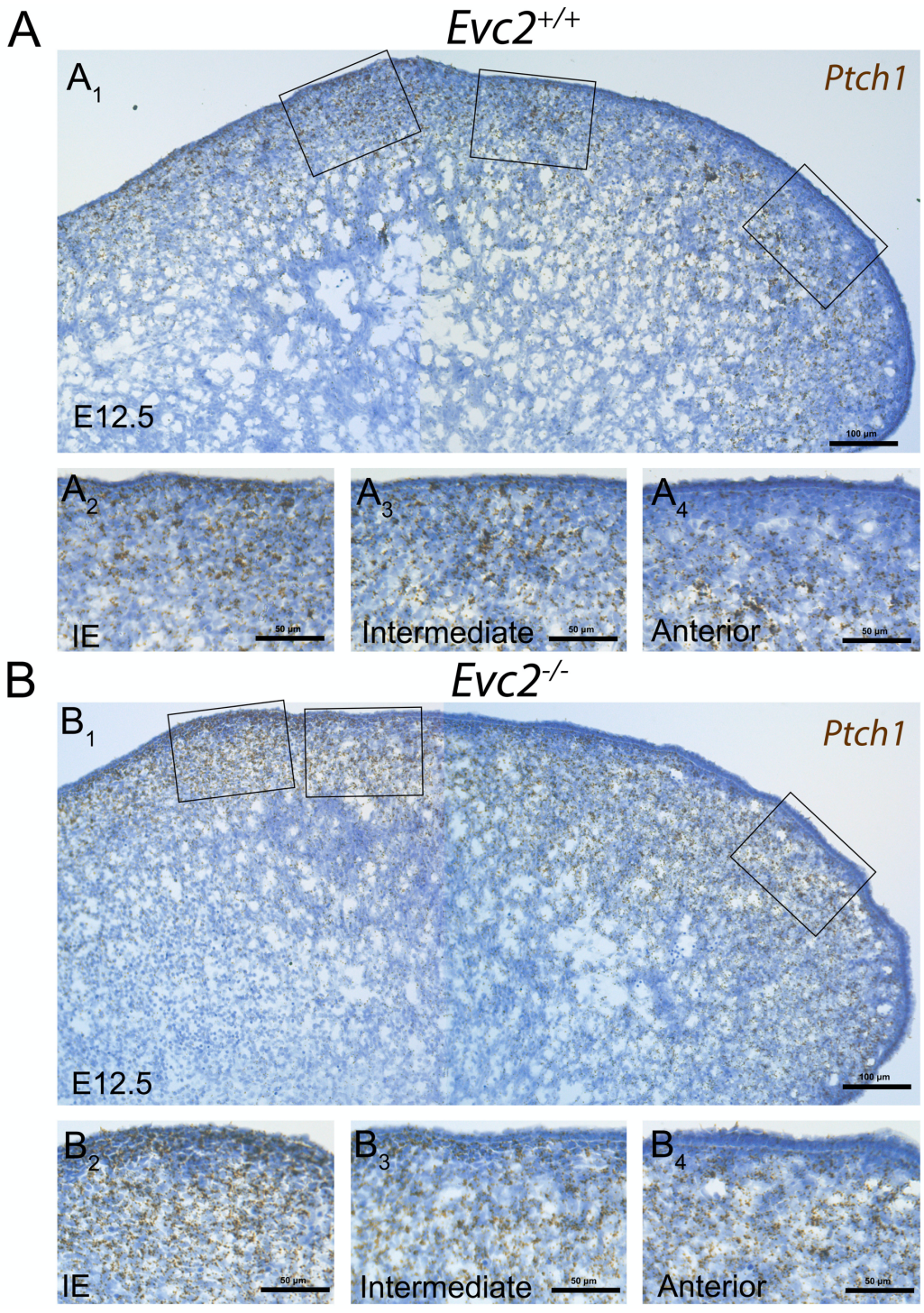
A
Evc2+/+
A1
Ptch1
E12.5
100 µm
A2
IE
50 µm
A3
Intermediate
50 µm
A4
Anterior
50 µm
B
Evc2-/-
B1
Ptch1
E12.5
100 µm
B2
IE
50 µm
B3
Intermediate
50 µm
B4
Anterior
50 µm

*Figure 4.8 Bright field microscopy images of Gli1 transcripts (brown dots) detected by RNAScope™ in situ hybridization in Evc2$^{-/-}$ and control tongues at E14.5. Both low power (A1 and B1) and high power images (A2, A3, A4, B2, B3 and B4) are shown here. High power images were took from three regions: intermolar eminence (IE, in A2 and B2), intermediate region (A3 and B3), and anterior tongue (A4 and B4). Scale bars: 200 μm in A1 and B1, and 50um in A2, A3, A4, B2, B3 and B4.*

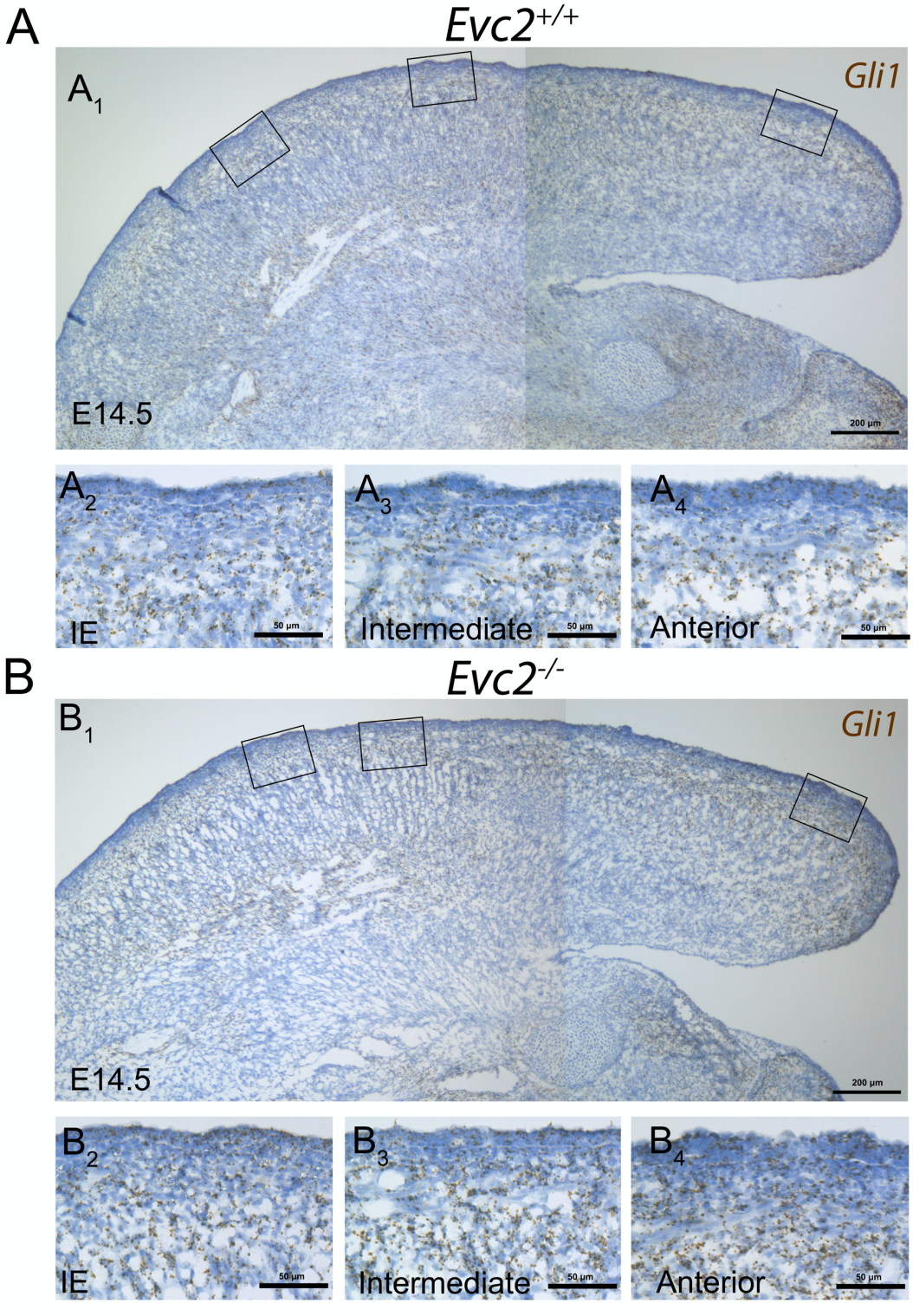
A
Evc2+/+
A1
Gli1
E14.5
200 µm
A2
IE
50 µm
A3
Intermediate
50 µm
A4
Anterior
50 µm
B
Evc2-/-
B1
Gli1
E14.5
200 µm
B2
IE
50 µm
B3
Intermediate
50 µm
B4
Anterior
50 µm

*Figure 4.9 Bright field microscopy images of Ptch1 transcripts (brown dots) detected by RNAScope™ in situ hybridization in Evc2$^{-/-}$ and control tongues at E14.5. Both low power (A1 and B1) and high power images (A2, A3, A4, B2, B3 and B4) are shown here. High power images were took from three regions: intermolar eminence (IE, in A2 and B2), intermediate region (A3 and B3), and anterior tongue (A4 and B4). Scale bars: 200 μm in A1 and B1, and 50um in A2, A3, A4, B2, B3 and B4.*

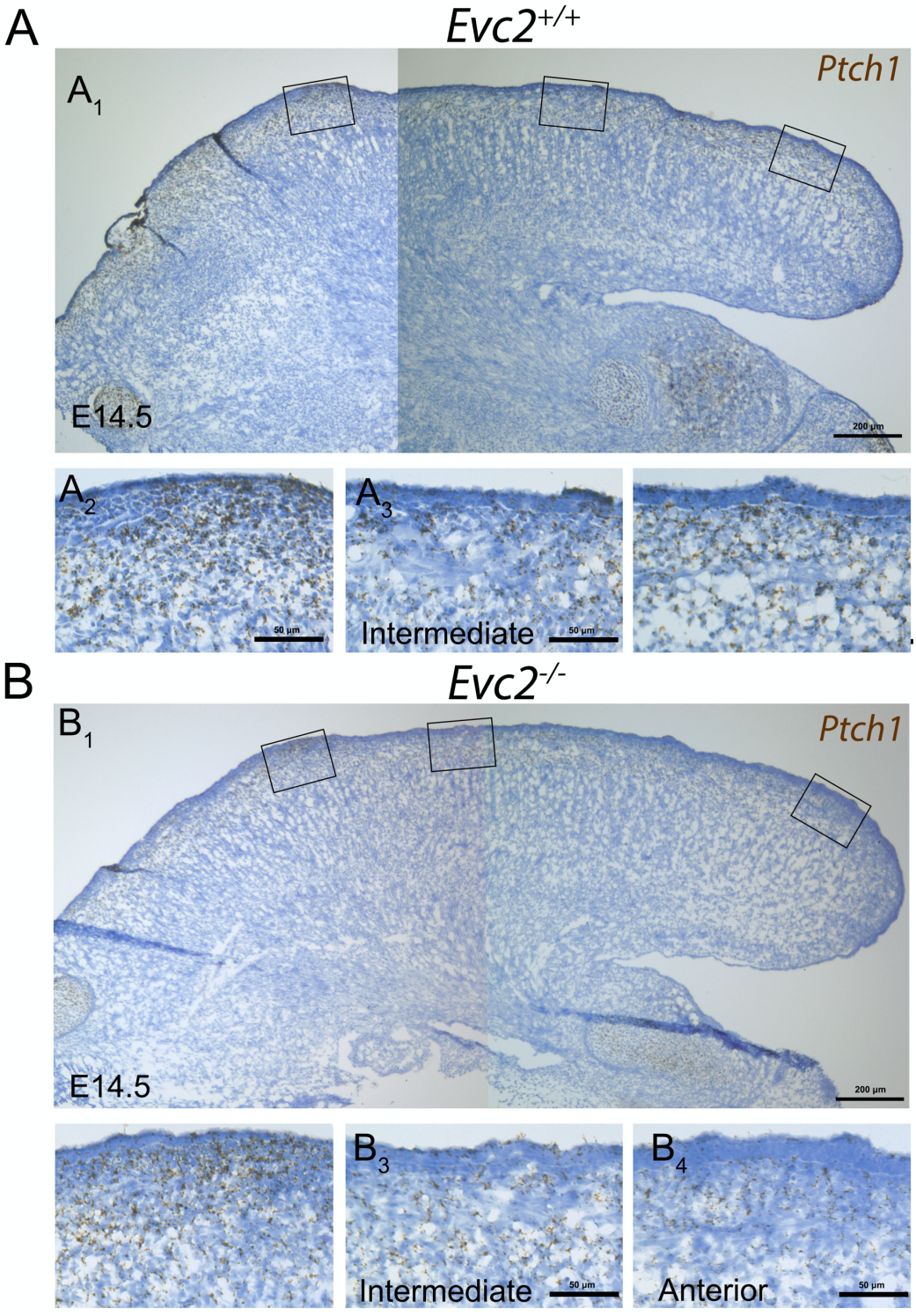
A
Evc2+/+
A1
Ptch1
E14.5
200 µm
A2
50 µm
A3
Intermediate
50 µm
B
Evc2-/-
B1
Ptch1
E14.5
200 µm
B3
Intermediate
50 µm
B4
Anterior
50 µm

*Figure 4.10 Histograms of average number of transcripts of Gli1 (A, B, E and F) and Ptch1 (C, D, G and H) per cell detected by RNAScope™ in situ hybridization in tongue epithelium and tongue mesenchyme from Evc2$^{-/-}$ and control tongues at E12.5 (A - D) and E14.5 (E - H). Each dot in histograms represents a single mouse. Transcripts are quantified as dots in in situ hybridization images (Figure 6 -9). Transcripts of Gli1 and Ptch1 are quantified in the following three regions for both epithelium and mesenchyme: Tongue tip (TIP), intermediate regions (ID), and intermolar eminence (IE). ns: not significant, P>0.05; *: 0.01<P<0.05; **: 0.001<P<0.01.*

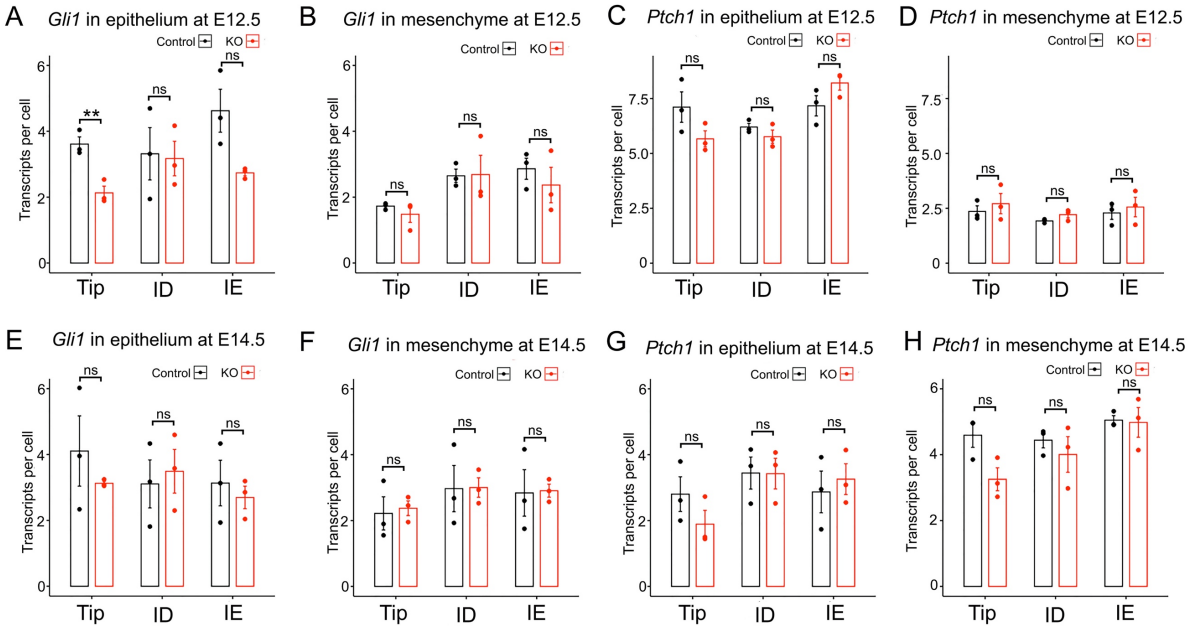
A
Gli1 in epithelium at E12.5
B
Gli1 in mesenchyme at E12.5
C
Ptch1 in epithelium at E12.5
D
Ptch1 in mesenchyme at E12.5
E
Gli1 in epithelium at E14.5
F
Gli1 in mesenchyme at E14.5
G
Ptch1 in epithelium at E14.5
H
Ptch1 in mesenchyme at E14.5
Control
KO
Transcripts per cell
Tip
ID
IE
ns
**

*Figure 4.11 Distribution of genes encoding Hedgehog signaling components in the cell clusters of E10.5 branchial arch (BA) epithelium (2470 cells in total) from scRNAseq data sets published by Junyue Cao et al (2019).* ***A****: A UMAP map to illustrate the 4 cell clusters that were identified from 2470 E10.5 branchial arch (BA) epithelial cells.* ***B****-****H****: UMAP maps to illustrate gene expression (log10(UMIs count /10000)) of Evc (B), Evc2 (C), Smo (D), Ptch1 (E), Gli1 (F), Gli2 (G), and Gli3 (H). In the UMAP maps, each dot represents an individual cell in the dataset and the color gradients of dots represent the expression levels of corresponding genes.* ***I****: A dot plot to illustrate gene expression (log(mean+0.1)) across the 4 cell clusters. 7 genes encoding Hedgehog signaling components are included. The size of dots represents the proportion of gene-expressing cells and color intensity of dots represents the average level expression of the gene expression.*

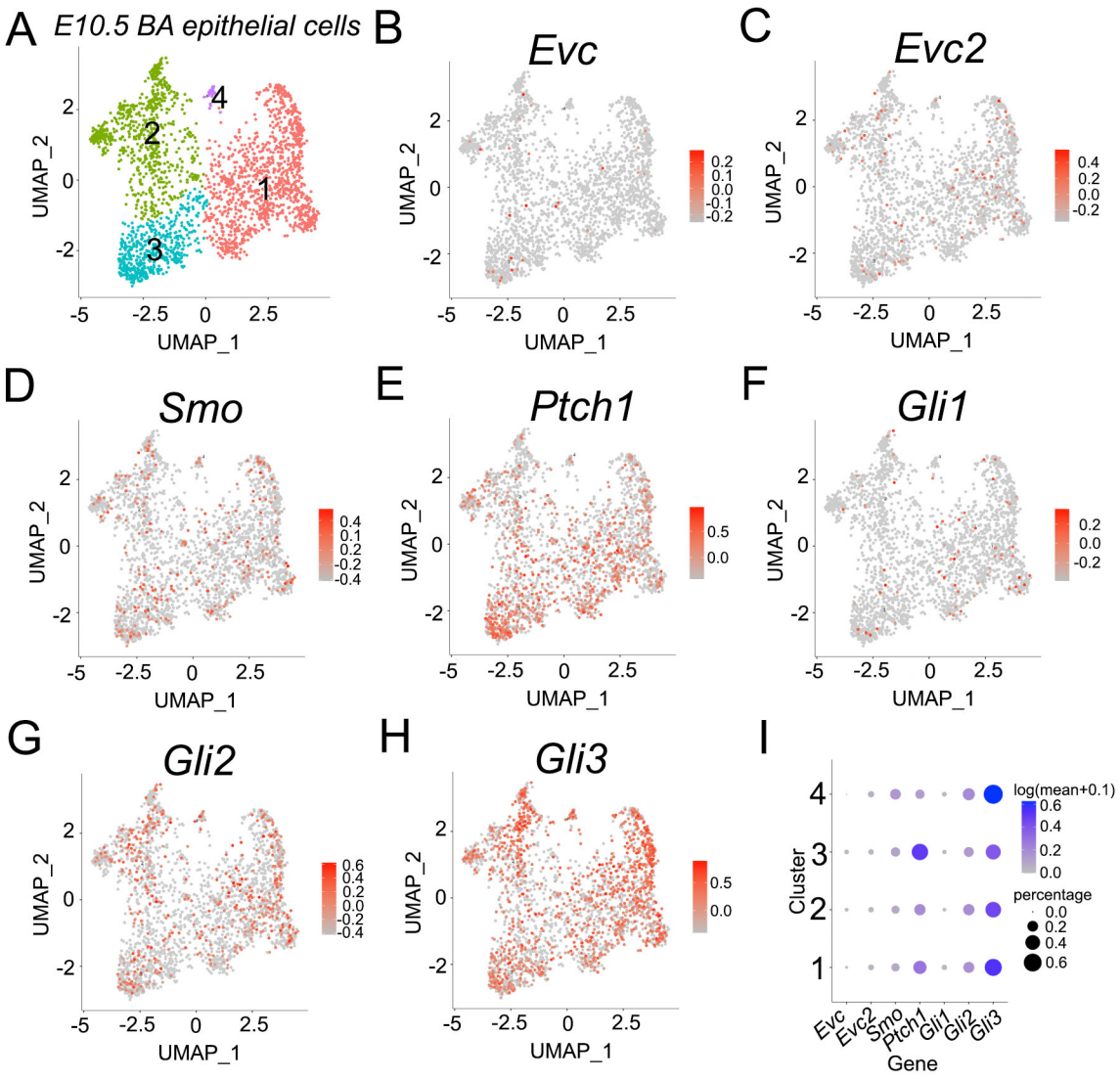
A
E10.5 BA epithelial cells
B
Evc
C
Evc2
D
Smo
E
Ptch1
F
Gli1
G
Gli2
H
Gli3
I
UMAP_1
UMAP_2
Cluster
Gene
log(mean+0.1)
percentage
Evc
Evc2
Smo
Ptch1
Gli1
Gli2
Gli3

*Figure 4.12 Distribution of genes encoding Hedgehog signaling components in the cell clusters of E11.5 branchial arch (BA) epithelium (2502 cells in total) from scRNAseq data sets published by Junyue Cao et al (2019).* ***A****: A UMAP map to illustrate the 4 cell clusters that were identified from 2502 E11.5 branchial arch (BA) epithelial cells.* ***B****-****H****: UMAP maps to illustrate gene expression (log10(UMIs count /10000)) of Evc (B), Evc2 (C), Smo (D), Ptch1 (E), Gli1 (F), Gli2 (G), and Gli3 (H). In the UMAP maps, each dot represents an individual cell in the dataset and the color gradients of dots represent the expression levels of corresponding genes.* ***I****: A dot plot to illustrate gene expression (log(mean+0.1)) across the 4 cell clusters. 7 genes encoding Hedgehog signaling components are included. The size of dots represents the proportion of gene-expressing cells and color intensity of dots represents the average level expression of the gene expression.*

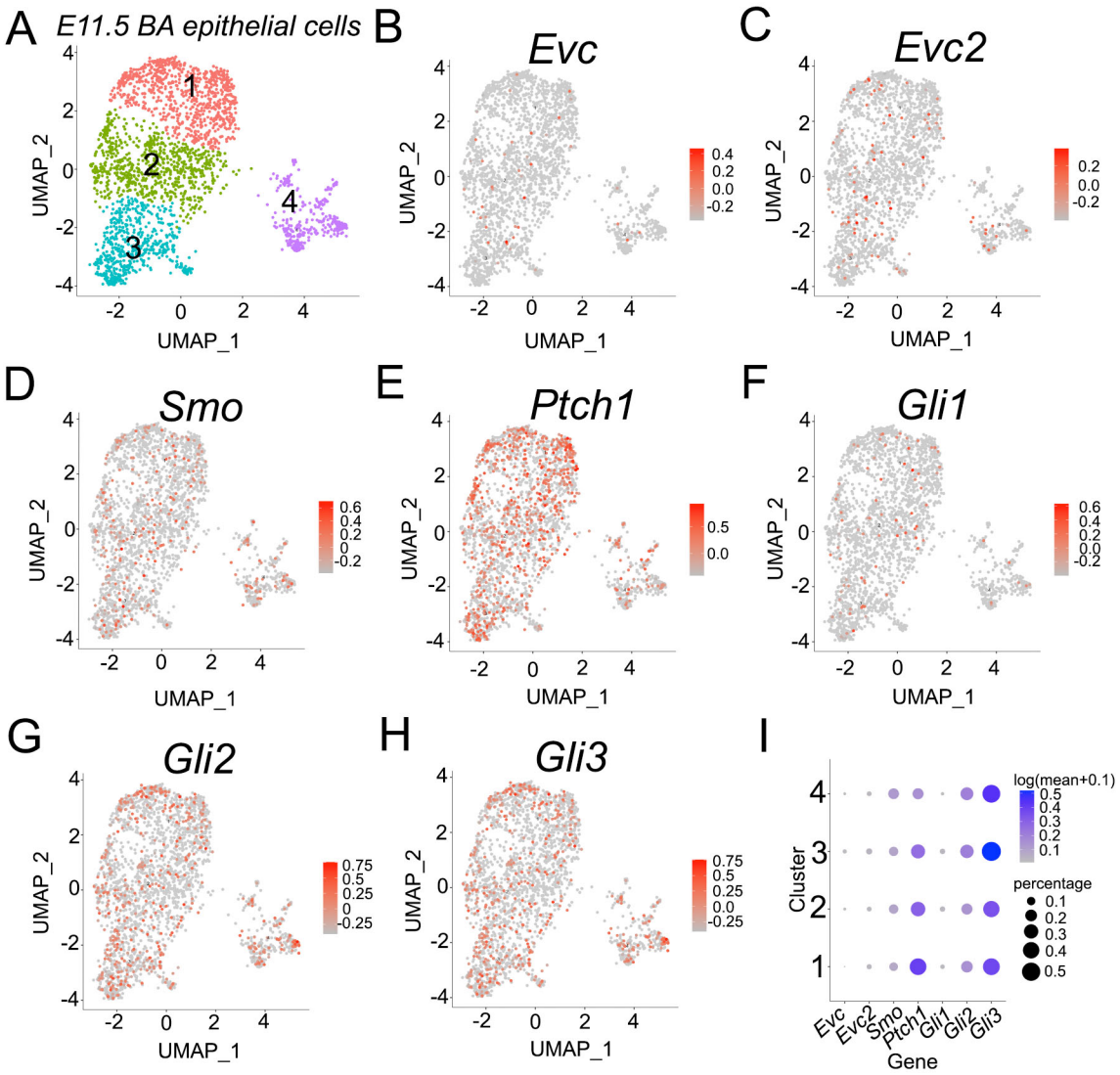
A
E11.5 BA epithelial cells
B
Evc
C
Evc2
D
Smo
E
Ptch1
F
Gli1
G
Gli2
H
Gli3
I
UMAP_1
UMAP_2
Cluster
Gene
log(mean+0.1)
percentage
Evc
Evc2
Smo
Ptch1
Gli1
Gli2
Gli3

*Figure 4.13 Distribution of genes encoding Hedgehog signaling components in the cell clusters of E12.5 branchial arch (BA) epithelium (1395 cells in total) from scRNAseq data sets published by Junyue Cao et al (2019).* ***A****: A UMAP map to illustrate the 4 cell clusters that were identified from 1395 E12.5 branchial arch (BA) epithelial cells.* ***B****-****H****: UMAP maps to illustrate gene expression (log10(UMIs count /10000)) of Evc (B), Evc2 (C), Smo (D), Ptch1 (E), Gli1 (F), Gli2 (G), and Gli3 (H). In the UMAP maps, each dot represents an individual cell in the dataset and the color gradients of dots represent the expression levels of corresponding genes.* ***I****: A dot plot to illustrate gene expression (log(mean+0.1)) across the 4 cell clusters. 7 genes encoding Hedgehog signaling components are included. The size of dots represents the proportion of gene-expressing cells and color intensity of dots represents the average level expression of the gene expression.*

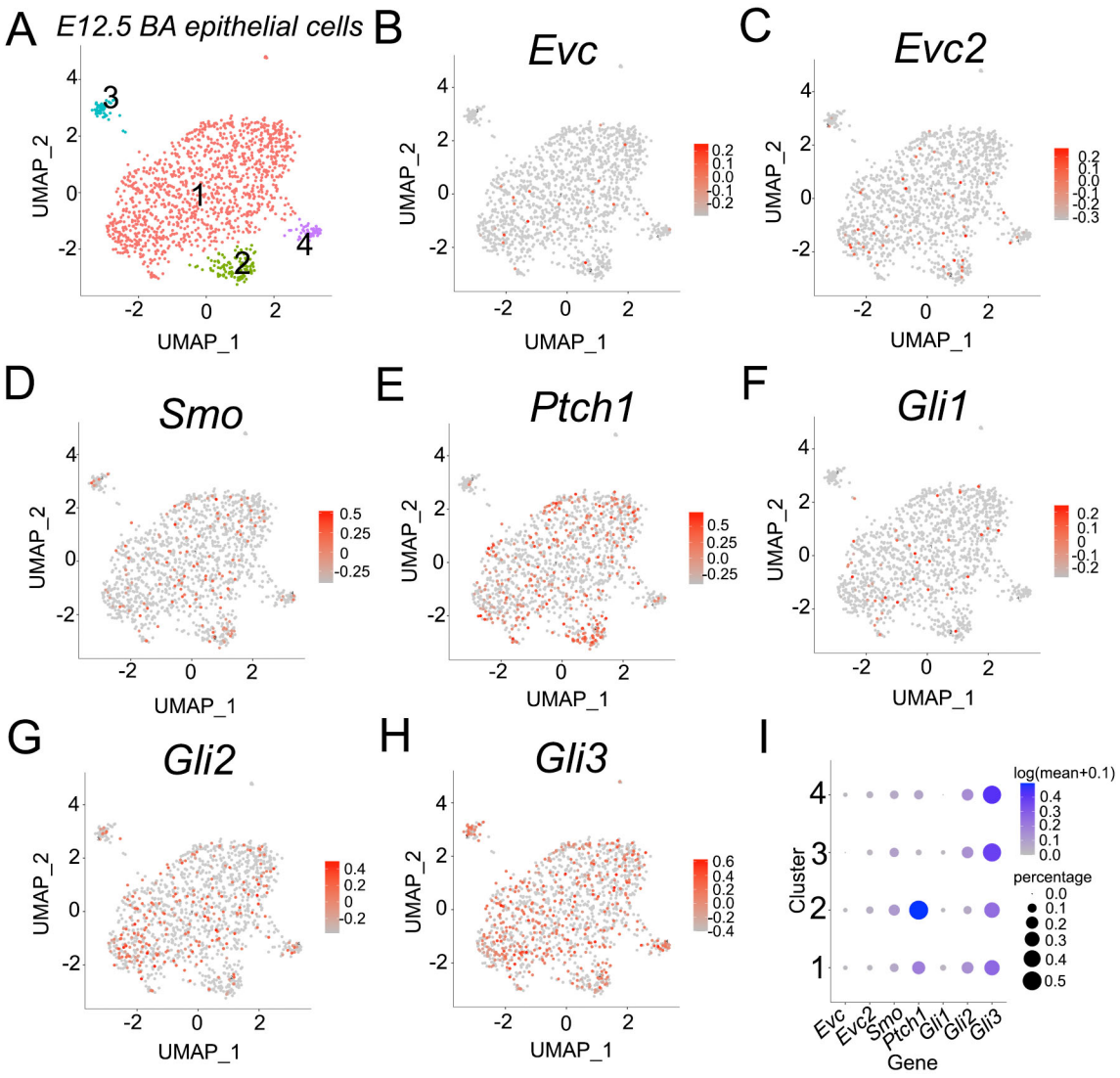
A
E12.5 BA epithelial cells
B
Evc
C
Evc2
D
Smo
E
Ptch1
F
Gli1
G
Gli2
H
Gli3
I
UMAP_1
UMAP_2
Cluster
Gene
Evc
Evc2
Smo
Ptch1
Gli1
Gli2
Gli3
log(mean+0.1)
percentage

*Figure 4.14 Distribution of genes encoding Hedgehog signaling components in the cell clusters of E13.5 branchial arch (BA) epithelium (1480 cells in total) from scRNAseq data sets published by Junyue Cao et al (2019).* ***A****: A UMAP map to illustrate the 4 cell clusters that were identified from 1480 E13.5 branchial arch (BA) epithelial cells.* ***B****-****H****: UMAP maps to illustrate gene expression (log10(UMIs count /10000)) of Evc (B), Evc2 (C), Smo (D), Ptch1 (E), Gli1 (F), Gli2 (G), and Gli3 (H). In the UMAP maps, each dot represents an individual cell in the dataset and the color gradients of dots represent the expression levels of corresponding genes.* ***I****: A dot plot to illustrate gene expression (log(mean+0.1)) across the 4 cell clusters. 7 genes encoding Hedgehog signaling components are included. The size of dots represents the proportion of gene-expressing cells and color intensity of dots represents the average level expression of the gene expression.*

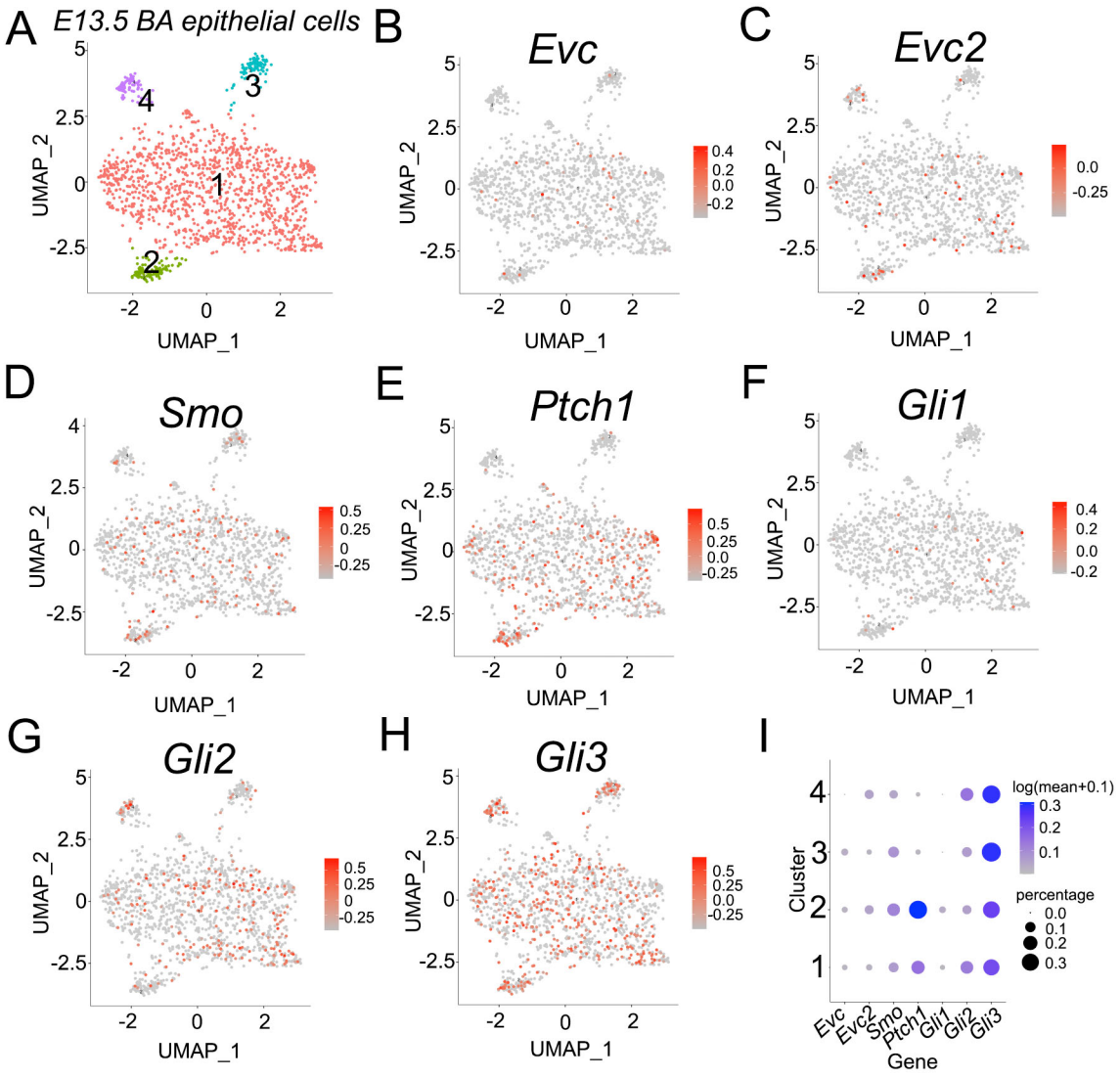
A
E13.5 BA epithelial cells
B
Evc
C
Evc2
D
Smo
E
Ptch1
F
Gli1
G
Gli2
H
Gli3
I
UMAP_1
UMAP_2
Cluster
Gene
log(mean+0.1)
percentage
Evc
Evc2
Smo
Ptch1
Gli1
Gli2
Gli3

*Figure 4.15 Distribution of genes encoding Hedgehog signaling components in the cell clusters of adult tongue epithelium from Schaum et al (2018).* ***A****: A UMAP map to illustrate the 13 cell clusters that were identified in a scRNA-seq dataset (7538 anterior tongue epithelial cells in total) from Schaum et al (2018).* ***B-H****: UMAP maps and dot plots to illustrate gene expression (log(UMIs count /10000+1)) across the 13 cell clusters in the scRNA-seq dataset (7538 cells in total) from Schaum et al. In the UMAP maps, each dot represents an individual cell in the dataset and the color gradients of dots represent the expression levels of corresponding genes.* ***I****: A dot plot to illustrate gene expression (log(UMIs count /10000+1)) across the 13 cell clusters in the scRNA-seq dataset (7538 cells in total) from Schaum et al. 7 genes encoding Hedgehog signaling components are included. The size of dots represents the proportion of gene-expressing cells and color intensity of dots represents the average level expression of the gene expression.*

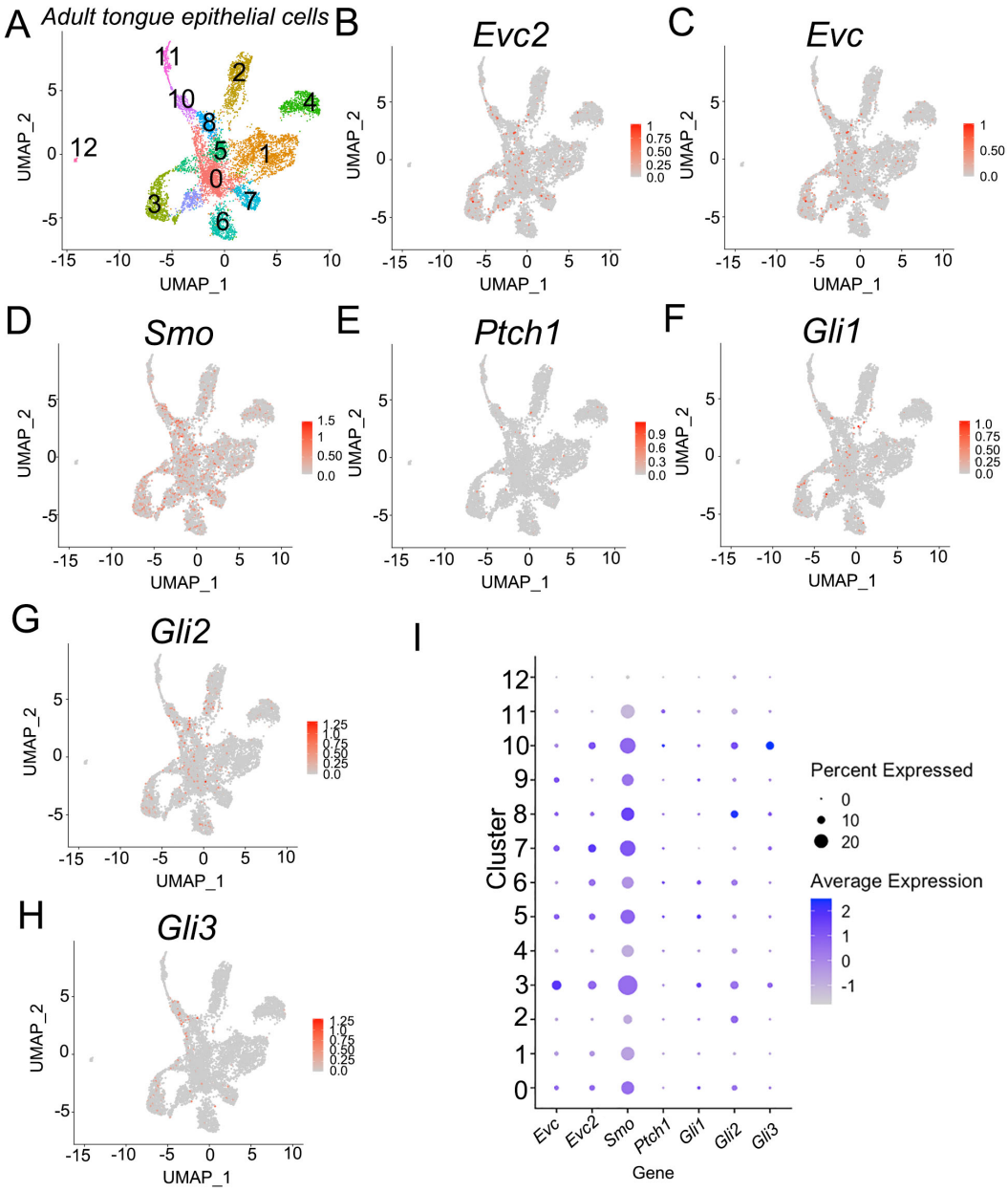
A
Adult tongue epithelial cells
B
Evc2
C
Evc
D
Smo
E
Ptch1
F
Gli1
G
Gli2
H
Gli3
I
UMAP_1
UMAP_2
Cluster
Gene
Evc
Evc2
Smo
Ptch1
Gli1
Gli2
Gli3
Percent Expressed
Average Expression

*Figure 4.16 Distribution of expression of Evc2 in Gli1$^{+}$ branchial arch epithelial cells (A and B) and distribution of expression of Gli1 in Evc2$^{+}$ branchial epithelial cells (C and D).* ***A****: A UMAP map to illustrate the 2 clusters of Gli1$^{+}$ branchial arch epithelial cells in a scRNA-seq dataset from Junyue Cao et al (2019).* ***B****: A UMAP map to illustrate Evc2 gene expression (log(UMIs count /10000)) across the 2 clusters of Gli1$^{+}$ branchial arch epithelial cells.* ***C****: A UMAP map to illustrate the 3 clusters of Evc2$^{+}$ branchial arch epithelial cells in a scRNA-seq dataset from Junyue Cao et al (2019).* ***D****: A UMAP map to illustrate Gli1 gene expression (log(UMIs count /10000+1)) across the 2 clusters of Evc2$^{+}$ branchial arch epithelial cells. In the UMAP maps, each dot represents an individual cell in the dataset and the color gradients of dots represent the expression levels of corresponding genes (B and D).*

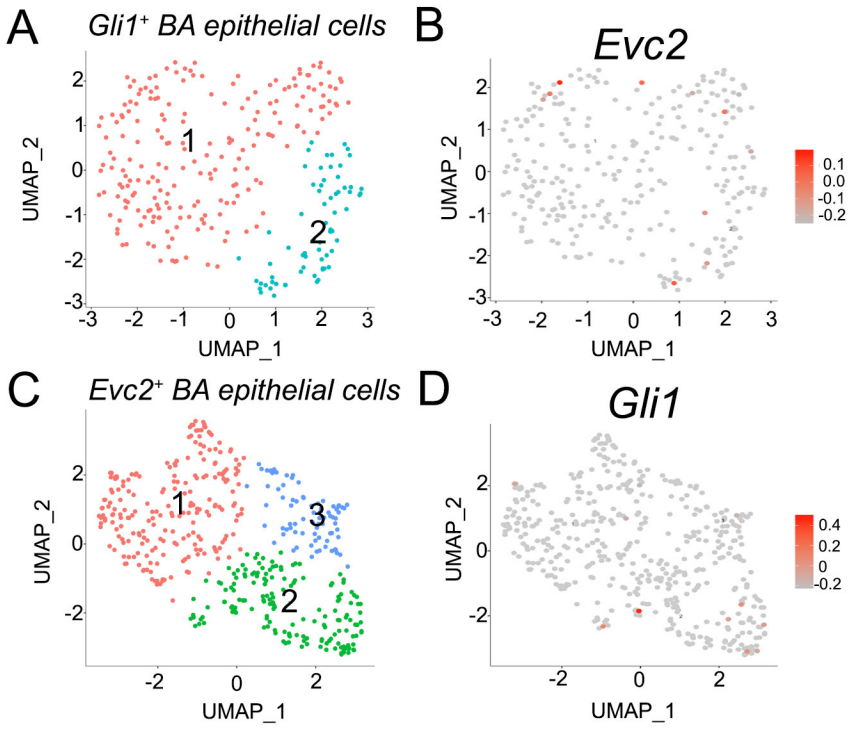
A
Gli1+ BA epithelial cells
UMAP_2
UMAP_1
1
2
B
Evc2
0.1
0.0
-0.1
-0.2
C
Evc2+ BA epithelial cells
3
D
Gli1
0.4
0.2
0
-0.2

*Figure 4.17 Distribution of expression of Evc2 in Gli1$^{+}$ adult tongue epithelial cells (A and B) and distribution of expression of Gli1 in Evc2$^{+}$ adult tongue epithelial cells (C and D).* ***A****: A UMAP map to illustrate the 3 clusters of Gli1$^{+}$ adult tongue epithelial cells in a scRNA-seq dataset from Schaum et al (2018).* ***B****: A UMAP map to illustrate Evc2 gene expression (log(UMIs count /10000+1)) across the 3 clusters of Gli1$^{+}$ adult tongue epithelial cells.* ***C****: A UMAP map to illustrate the 4 clusters of Evc2$^{+}$ adult tongue epithelial cells in a scRNA-seq dataset from Schaum et al (2018).* ***D****: A UMAP map to illustrate Gli1 gene expression (log(UMIs count /10000+1)) across the 4 clusters of Evc2$^{+}$ adult tongue epithelial cells. In the UMAP maps, each dot represents an individual cell in the dataset and the color gradients of dots represent the expression levels of corresponding genes (B and D).*

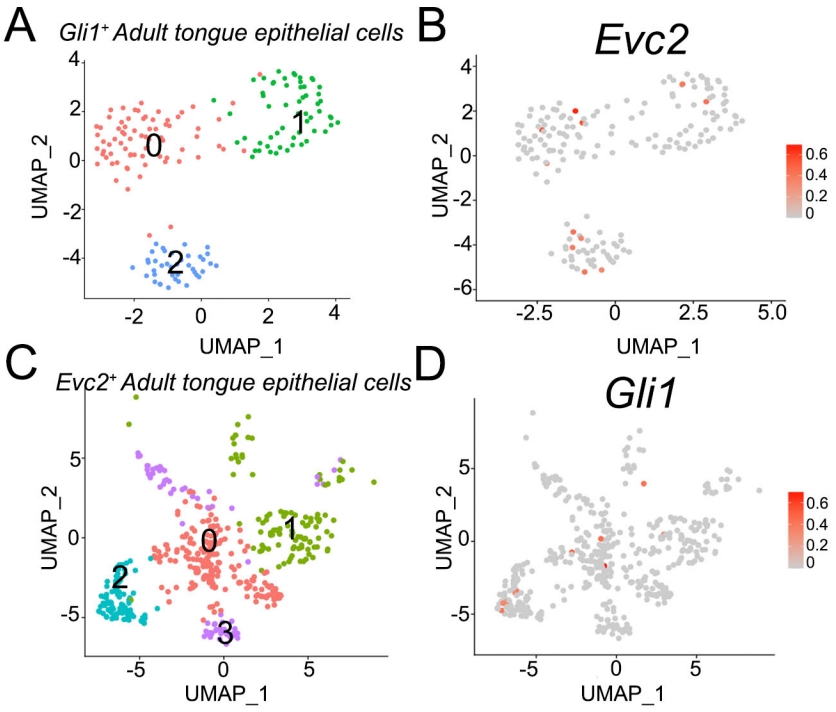
A
Gli1+ Adult tongue epithelial cells
UMAP_2
UMAP_1
0
1
2
B
Evc2
0.6
0.4
0.2
0
C
Evc2+ Adult tongue epithelial cells
3
D
Gli1

*Figure 4.18 Transcriptomic profiling of E12.5 tongue epithelium and mesenchyme from Evc2$^{-/-}$ mice and littermate controls. Strategy for transcriptome profiling of E12.5 tongue epithelium and mesenchyme from Evc2$^{-/-}$ and control mice is depicted here (A). - log10(p value) of each gene is plotted against log2(Foldchange) of all epithelial transcripts in volcano plot (B). Red dots represented differentially expressed genes (DEGs) identified by DEseq2. Histograms of - log10(p value) values of KEGG data base (C) and GO database (D) enrichment analysis of down-regulated epithelial DEGs in Evc2$^{-/-}$ mice were shown.*

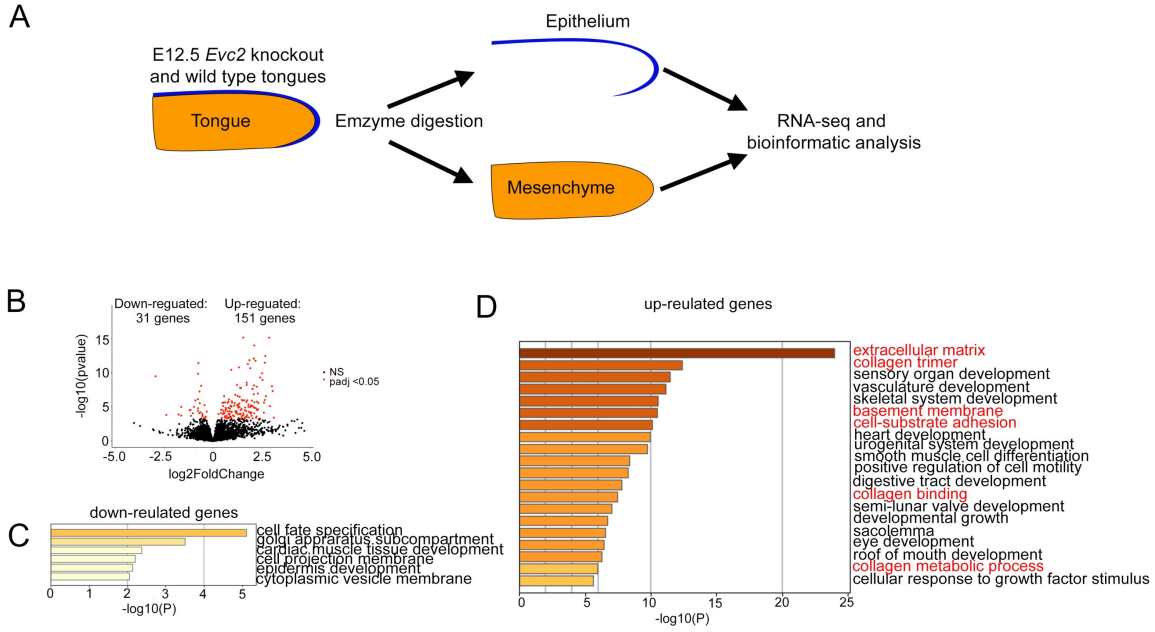
A
E12.5 Evc2 knockout
and wild type tongues
Tongue
Emzyme digestion
Epithelium
Mesenchyme
RNA-seq and
bioinformatic analysis
B
Down-reguated:
31 genes
Up-reguated:
151 genes
-log10(pvalue)
log2FoldChange
NS
padj <0.05
C
down-reulated genes
cell fate specification
golgi apparatus subcompartment
cardiac muscle tissue development
cell projection membrane
epidermis development
cytoplasmic vesicle membrane
-log10(P)
D
up-reulated genes
extracellular matrix
collagen trimer
sensory organ development
vasculature development
skeletal system development
basement membrane
cell-substrate adhesion
heart development
urogenital system development
smooth muscle cell differentiation
positive regulation of cell motility
digestive tract development
collagen binding
semi-lunar valve development
developmental growth
sacolemma
eye development
roof of mouth development
collagen metabolic process
cellular response to growth factor stimulus
-log10(P)

*Figure 4.19 Scanning electron microcopy (SEM) images of tongues (A and B), bright field microscopy images of H&E staining in tongue sections (C and D), and images of whole-mount immunofluorescence against Krt8 of whole tongue epithelial sheets from Evc2-/- and control mice at E18.5 (E). High power images of SEM (B) and H&E staining (D) are shown from two regions of area containing fungiform papillae: tongue tip (TIP) and intermediate region (ID). IE, intermolar eminence. High power whole-mount immunofluorescence merged with bright-field images are shown in insets of panel E. Scale bars: 500 μm in A, 25 μm in B, 200 μm in C, 50 μm in D, and 200 μm in E.*

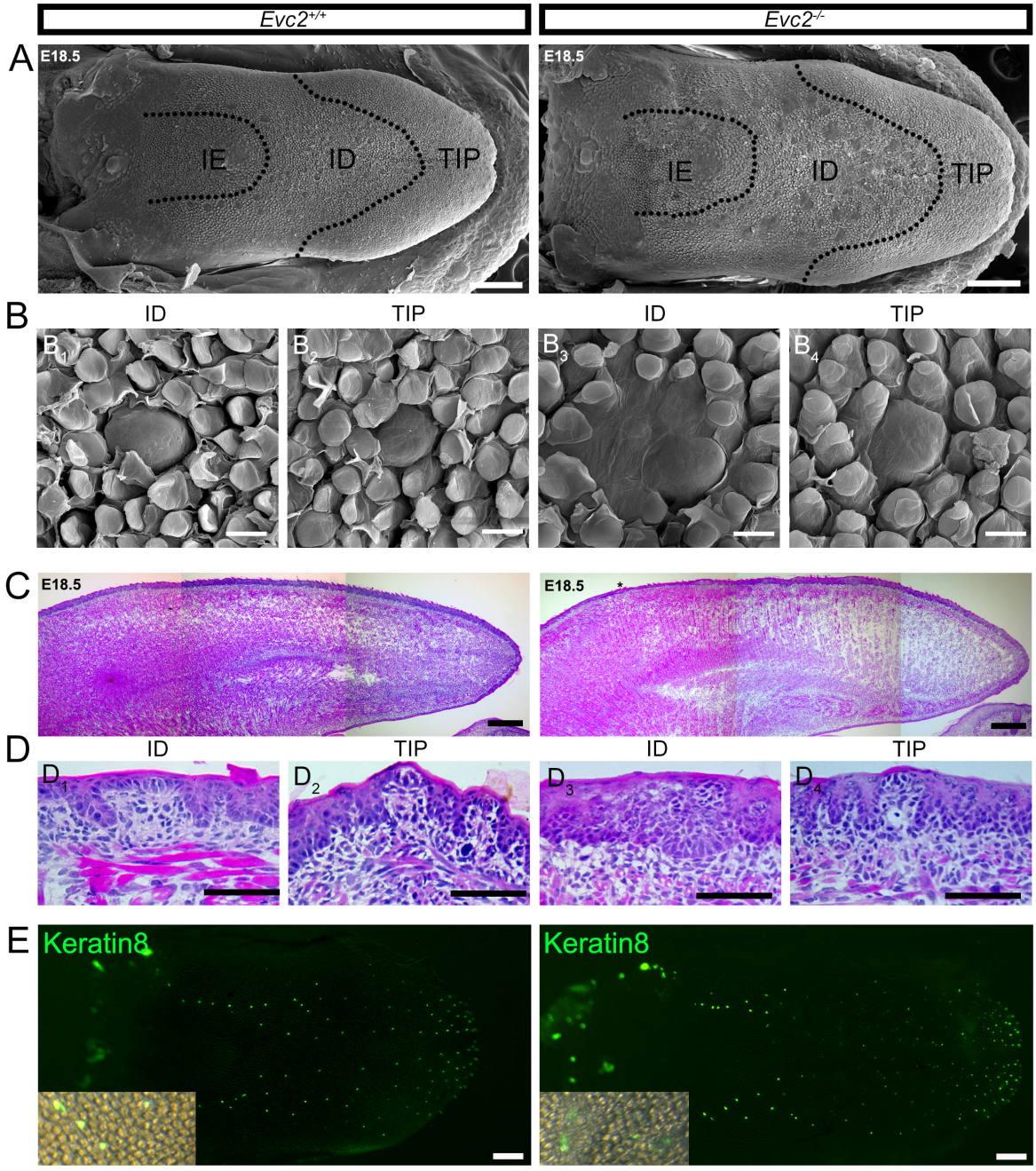
Evc2+/+
Evc2-/-
A
E18.5
IE
ID
TIP
E18.5
IE
ID
TIP
B
ID
TIP
ID
TIP
B1
B2
B3
B4
C
E18.5
E18.5
*
D
ID
TIP
ID
TIP
D1
D2
D3
D4
E
Keratin8
Keratin8

*Figure 4.20 Scanning electron microcopy (SEM) images of tongues (A and B), bright field microscopy images of H&E staining in tongue sections (C) from Evc2$^{-/-}$ and control mice at 3-week-old. High power SEM images and H&E images show morphology of both normal papillae from control mice (A1 and B1) and distinct types of abnormal papillae from Evc2$^{-/-}$ mice (A2 to A4, B2 to B4). Scale bars: 500 μm in A, 20 μm in B, and 50 μm in C.*

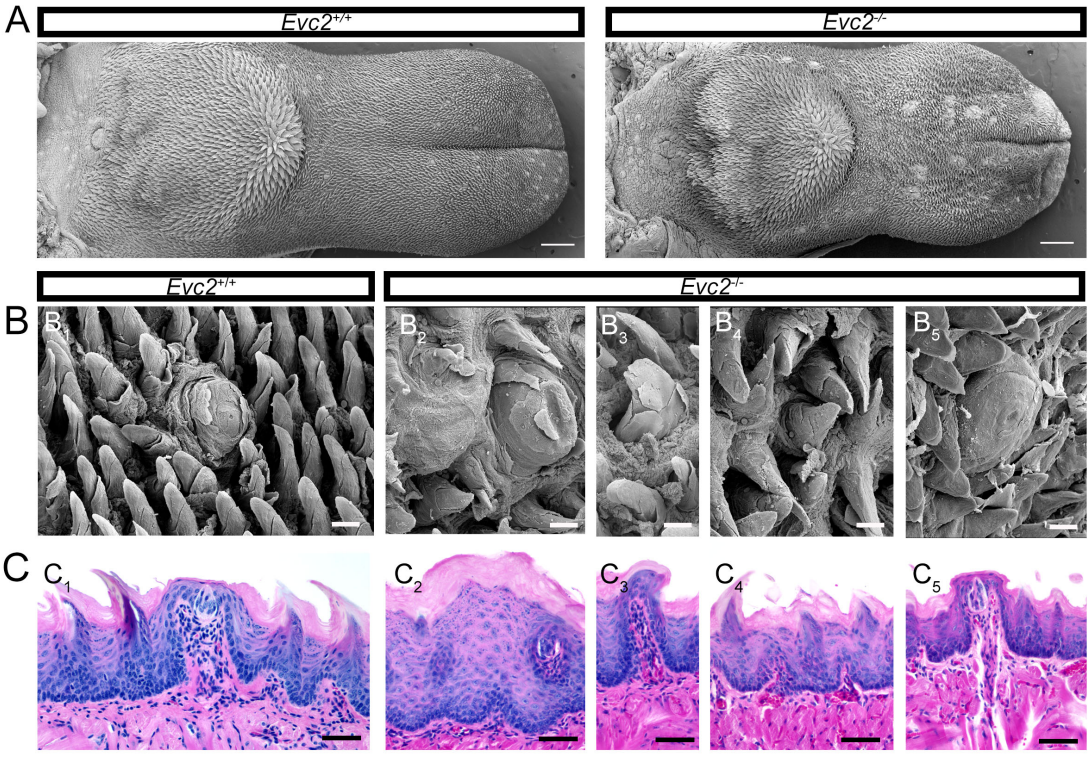
A
Evc2+/+
Evc2-/-
B
Evc2+/+
Evc2-/-
B1
B2
B3
B4
B5
C
C1
C2
C3
C4
C5

*Figure 4.21 Confocal microscopy images of double immunofluorescence with proliferation marker anti-Ki67 and taste bud cell marker anti-Krt8 in tongue sections from Evc2$^{-/-}$ (D, E and F) and control mice (A, B and C) at E18.5. High power images are took from two regions: anterior region (B and E) and intermediate region (C and F). Nuclei were counterstained with DAPI. DAPI signals are merged with the other fluorescent signals (B, C, E and F). Scale bars: 100 μm in A and D, 20 μm in B, C, E and F.*

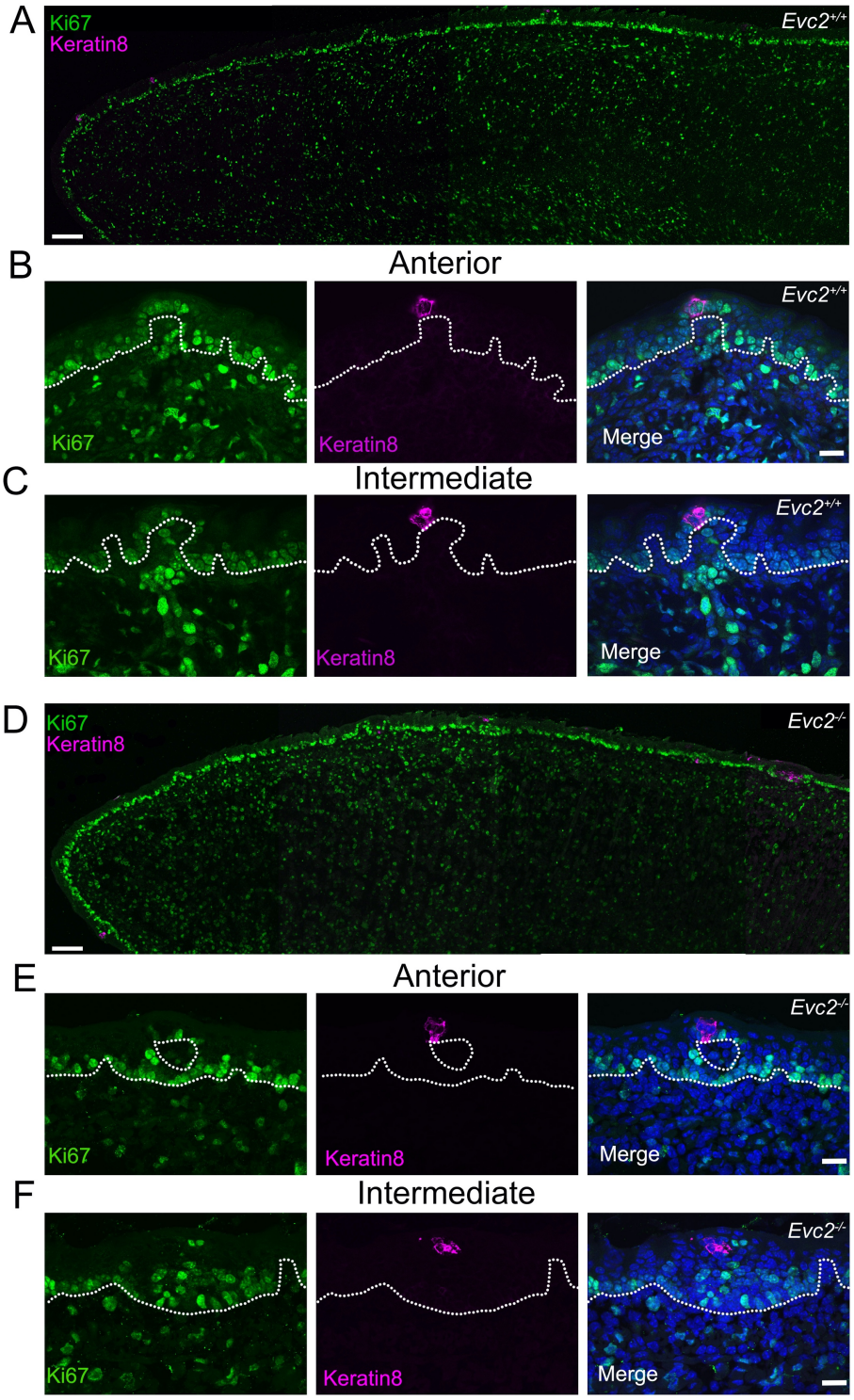
A
Ki67
Keratin8
Evc2+/+
B
Anterior
Ki67
Keratin8
Merge
Evc2+/+
C
Intermediate
Ki67
Keratin8
Merge
Evc2+/+
D
Ki67
Keratin8
Evc2-/-
E
Anterior
Ki67
Keratin8
Merge
Evc2-/-
F
Intermediate
Ki67
Keratin8
Merge
Evc2-/-

*Figure 4.22 Confocal microscopy images of triple immunofluorescence with cell apoptosis marker anti-Caspase3, taste bud cell marker anti-Krt8, and epithelial cell marker anti-E-Cadherin in tongue sections from Evc2$^{-/-}$ (D, E and F) and control mice (A, B and C) at E18.5. High power images are took from two regions: anterior region (B and E) and intermediate region (C and F). Nuclei were counterstained with DAPI. DAPI signals are merged with the other fluorescent signals (B, C, E and F). Scale bars: 100 μm in A and D, 20 μm in B, C, E and F.*

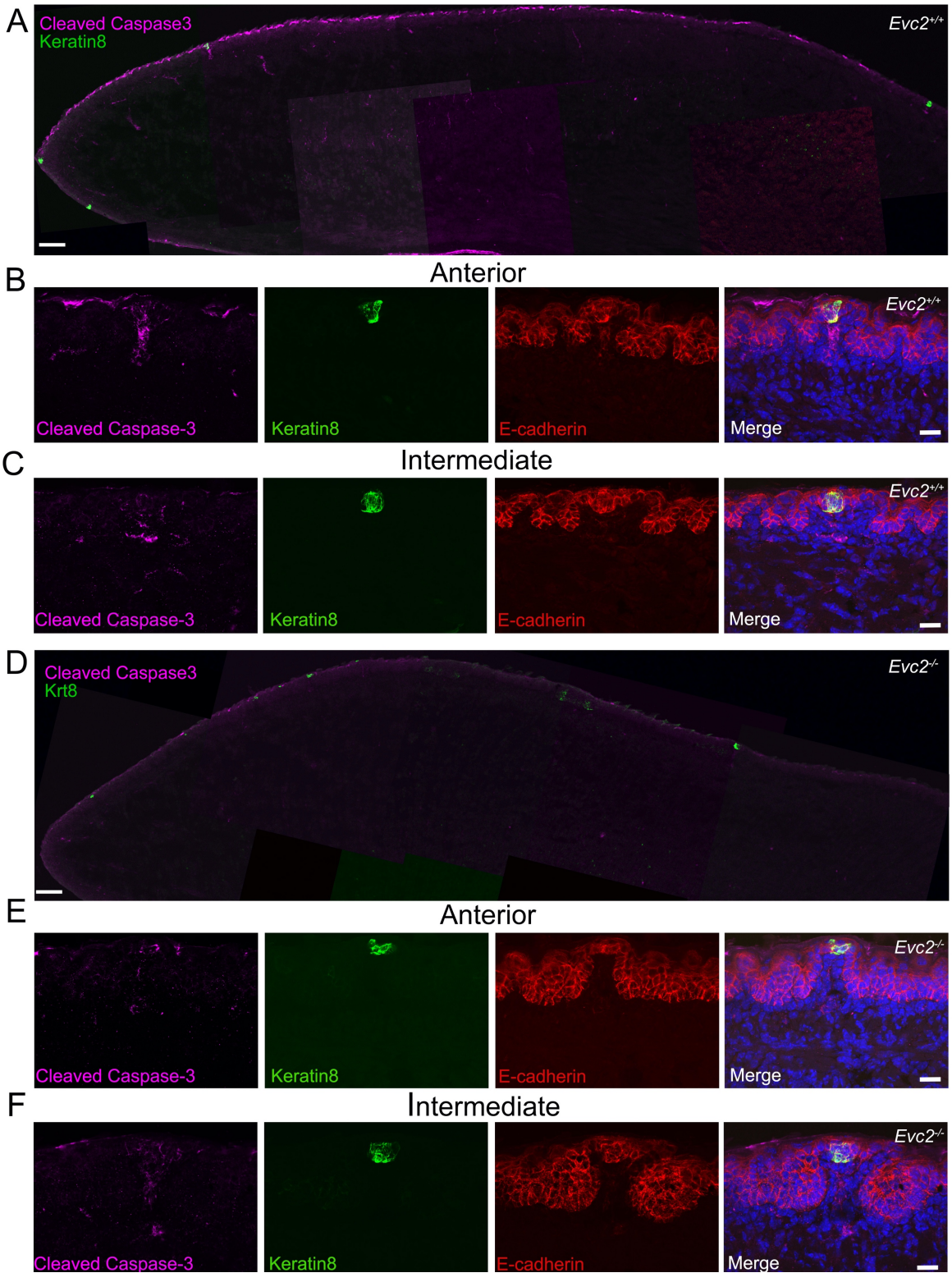
A
Cleaved Caspase3
Keratin8
Evc2+/+
B
Anterior
Cleaved Caspase-3
Keratin8
E-cadherin
Merge
Evc2+/+
C
Intermediate
Cleaved Caspase-3
Keratin8
E-cadherin
Merge
Evc2+/+
D
Cleaved Caspase3
Krt8
Evc2-/-
E
Anterior
Cleaved Caspase-3
Keratin8
E-cadherin
Merge
Evc2-/-
F
Intermediate
Cleaved Caspase-3
Keratin8
E-cadherin
Merge
Evc2-/-

*Figure 4.23 Confocal microscopy images of immunofluorescence with anti-BCL11B in tongue sections from Evc2$^{-/-}$ (D, E and F) and control mice (A, B and C) at E18.5. High power images are took from two regions: anterior region (B and E) and intermediate region (C and F). Nuclei were counterstained with DAPI. DAPI signals are merged with the other fluorescent signals (B, C, E and F). Scale bars: 100 μm in A and D, 20 μm in B, C, E and F.*

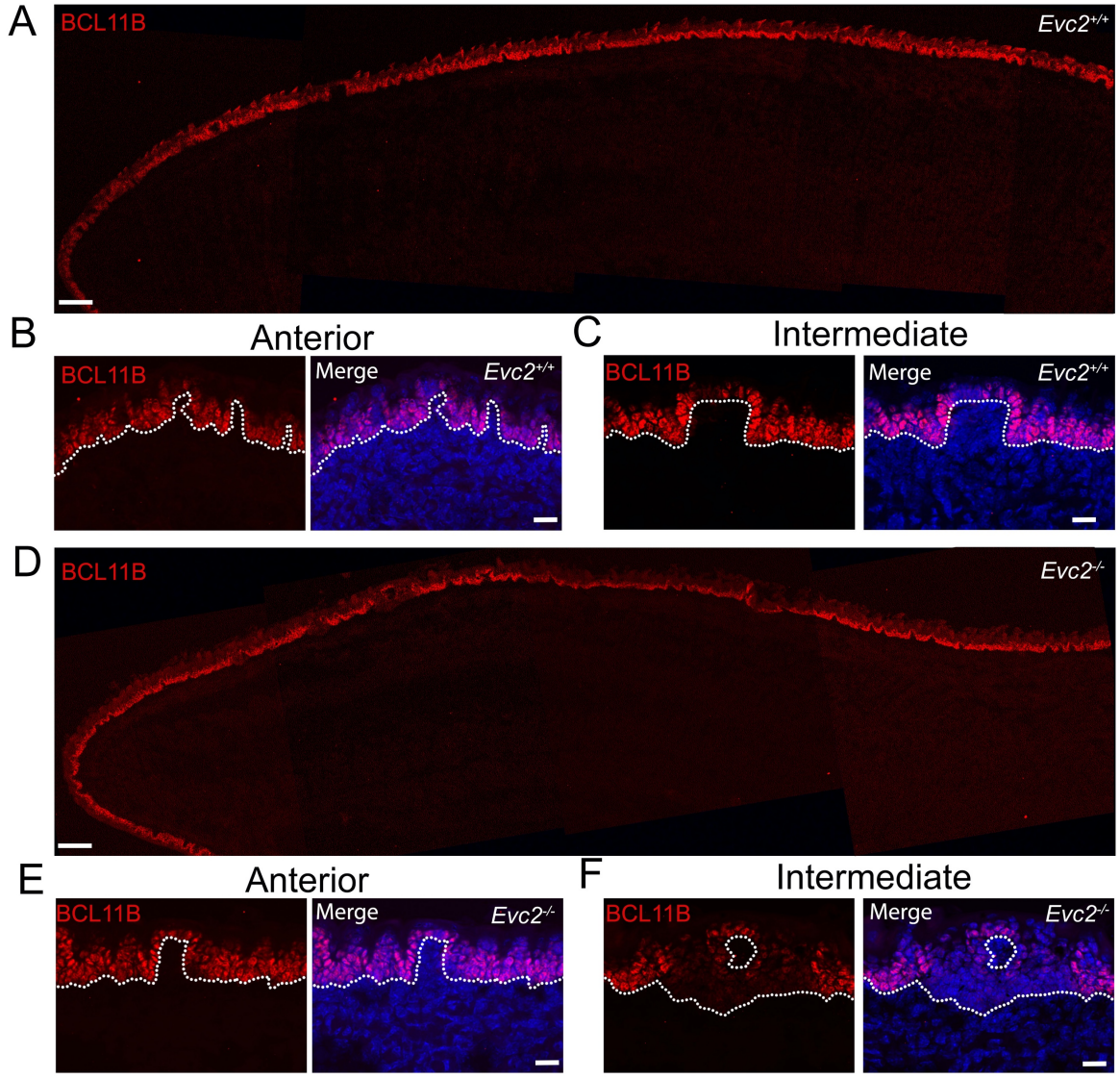
A
BCL11B
Evc2+/+
B
Anterior
BCL11B
Merge
Evc2+/+
C
Intermediate
BCL11B
Merge
Evc2+/+
D
BCL11B
Evc2-/-
E
Anterior
BCL11B
Merge
Evc2-/-
F
Intermediate
BCL11B
Merge
Evc2-/-

*Figure 4.24 Bright field images of whole-mount immunohistochemistry with anti- anti-βIII-Tubulin of whole embryonic tongues (A) and confocal microscopy images of immunofluorescence with anti-NF-M in tongue sections (B) from Evc2$^{-/-}$ and control mice. Nuclei were counterstained with DAPI. DAPI signals are merged with other fluorescent signals. Scale bars: 200 μm in A and 20 μm in B.*

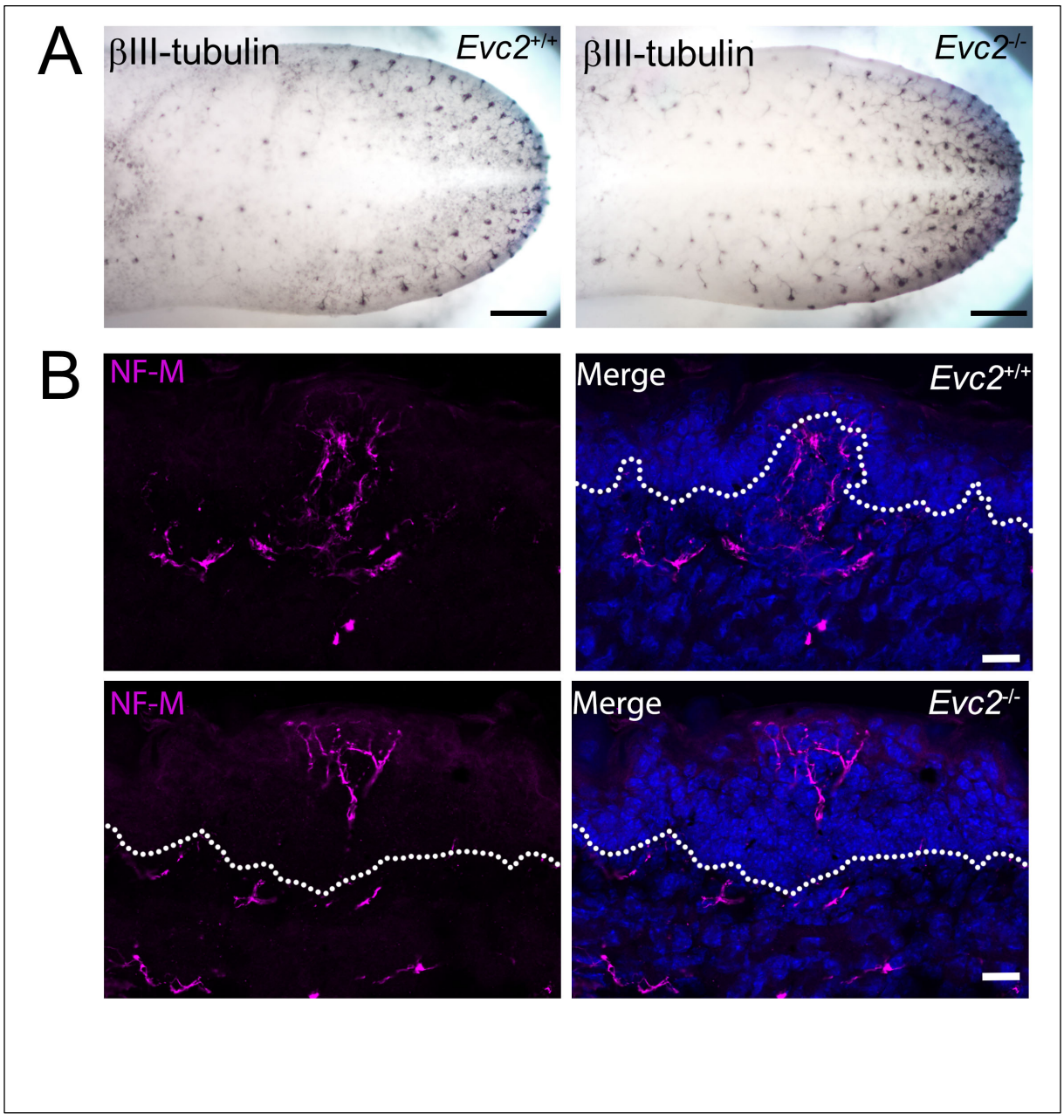
A
βIII-tubulin
Evc2+/+
βIII-tubulin
Evc2-/-
B
NF-M
Merge
Evc2+/+
NF-M
Merge
Evc2-/-

*Figure 4.25 Confocal microscopy images of double immunofluorescence with anti-Keratin 8 and anti-E-Cadherin in tongue sections from Gli1-CreER/RFP mice with tamoxifen treatment. The stages of tamoxifen treatment and tissue collection are illustrated by the schematic to the left of corresponding confocal microscopy images. Scale bars: 20 μm for all images.*

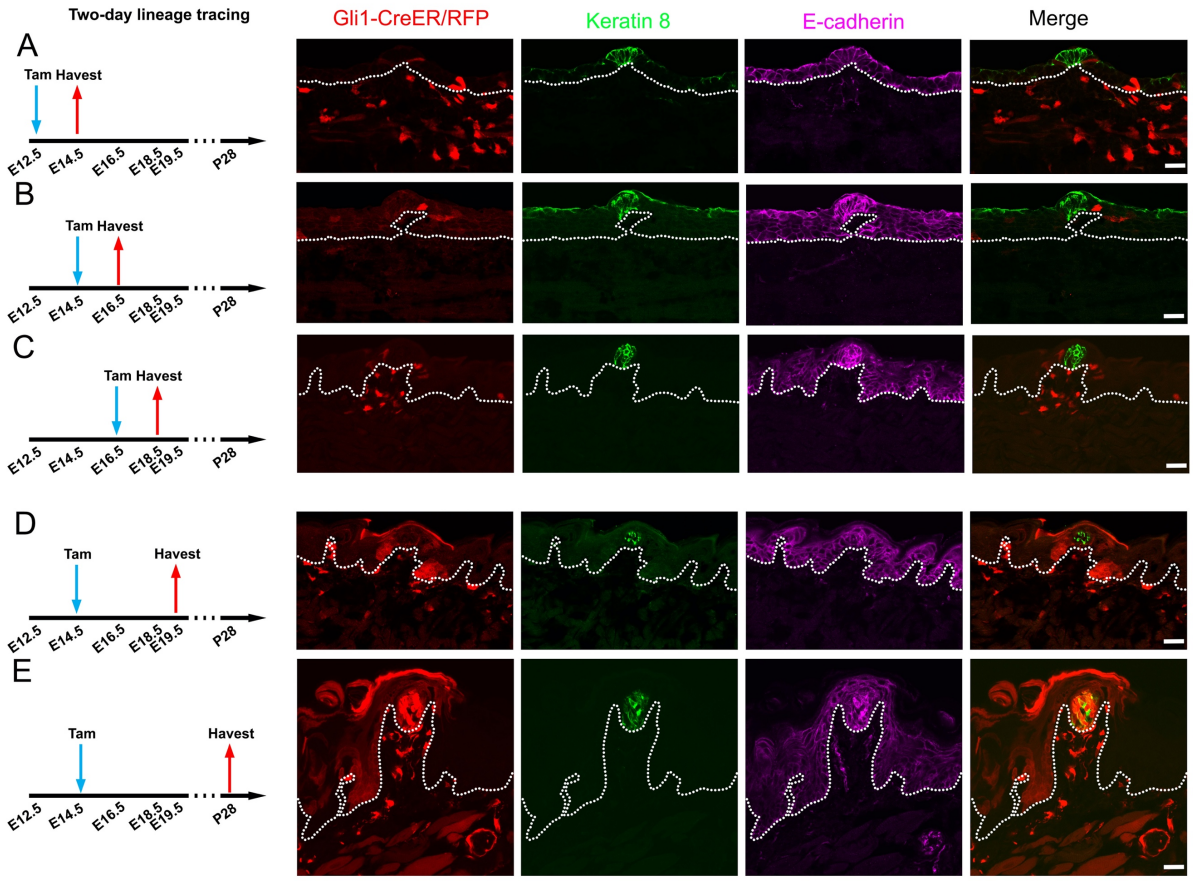
Two-day lineage tracing
Gli1-CreER/RFP
Keratin 8
E-cadherin
Merge
A
Tam Havest
B
Tam Havest
C
Tam Havest
D
Tam
Havest
E
Tam
Havest
E12.5
E14.5
E16.5
E18.5
E19.5
P28

# CHAPTER 5

# SARS-COV-2 RECEPTOR ACE2 IS ENRICHED IN A SUBPOPULATION OF MOUSE TONGUE EPITHELIAL CELLS IN NON-GUSTATORY PAPILLAE, BUT NOT IN TASTE BUDS OR EMBRYONIC ORAL EPITHELIUM[1]

[1]Zhonghou Wang, Jingqi Zhou, Brett Marshall, Romdhane Rekaya, Kaixiong Ye, Hong-Xiang Liu. *ACS Pharmacol. Transl. Sci.* 2020, 3, 4, 749–758. Reprinted here with permission of publisher.

## 5.1 Abstract

As a result of the COVID-19 pandemic, evidence revealed that SARS-CoV-2 infection caused taste loss at a higher rate than influenza. *ACE2*, the entry receptor of SARS-CoV-2, has been identified in the oral epithelium; however, it is unclear at what developmental stage *ACE2* expression emerges and whether *ACE2* is expressed in taste buds. To identify the specific developmental stage, we analyzed RNA-Seq data from embryonic and newborn mouse oral tissue. We found that robust *ACE2* expression was observed in the newborn oral epithelium. In contrast, only extremely low levels, if any, of *ACE2* transcripts in the embryonic stage oral tissue were found (E12.5 and E14.5). Analyses of three public scRNA-seq datasets of adult mouse tongue epithelial cells showed that receptors for various viruses were enriched in distinct clusters of tongue epithelial cells. *ACE2* was enriched in a subpopulation of epithelial cells in the basal region of non-gustatory filiform papillae, but not in the taste papillae or taste buds. Expression of *ACE2* was detected in a small proportion of type III taste cells. Our results indicate that when applied across species, non-gustatory papilla epithelial cells are the prime targets for SARS-CoV-2 infection in the tongue, and thus taste loss in COVID-19 patients is likely not caused by a direct infection of SARS-CoV-2 to taste bud cells. Additionally, fetuses at different stages of development may have distinct susceptibility to the disease.

## 5.2 Introduction

Taste buds are the sensory organs for taste that transduce gustatory stimuli into neural signals conveyed to the central nervous system. In mammals, taste buds are located in the oral cavity, primarily in the lingual taste papillae and the soft palate. Mammalian taste bud cells are post-mitotic and have a short life span (on average 10-12 days in mice) [1-5]. Thus, it is essential

that progenitor cells in the surrounding tissue compartments continuously differentiate into the specific types of taste cells (type I, II and III) for taste bud homeostasis and intact taste sensation.

Deficiencies of taste buds and/or their progenitors cause taste dysfunctions. These deficiencies may be caused by genetic factors, injuries, medical treatments (e.g., radiotherapy and chemotherapy), and illness – including infections in the oral cavity (see review [6]). Upper respiratory and oral cavity viral infections are among the most common causes of taste dysfunction and are frequently associated with taste loss [7-11]. For example, hypogeusia and dysgeusia are often a complaint in patients following an influenza-like illness [11].

Evidence collected during the COVID-19 pandemic revealed that taste and smell loss occurs at a higher rate in patients with COVID-19 symptoms compared to those with influenza-like symptoms [12-17]. Angiotensin-converting enzyme 2 (*ACE2*), the receptor that mediates the entry of SARS-CoV-2 into cells [18-22], is expressed in the oral mucosa and highly enriched in the tongue epithelial cells in humans, thus providing evidence for the infectious susceptibility of the oral cavity [23, 24]. More recent data showed that the *ACE2*-expressing ($ACE2^+$) cells in the tongue of humans are a subpopulation of keratinocytes [23]. In mice, *ACE2* is detected in both gustatory and non-gustatory tongue epithelium [25]. Quantitative data from cellular analyses are currently unavailable. In spite of the valuable knowledge gained recently about ACE2 and COVID-19 infections, several relevant questions remain unanswered. Specifically, 1) where are $ACE2^+$ cells localized in the tongue epithelium? 2) is *ACE2* expression more enriched in taste bud cells such that viral infection directly causes taste bud cell death and subsequently taste loss? and 3) how does ACE2 expression in oral epithelium change during different stages of embryonic development?

Although mouse *ACE2* is not susceptible to SARS-CoV-2 [26], its expression may still provide insights into the development of pathological changes in humans given that mice and humans share similar gene expression patterns. In this study, analyses of available RNA-Seq data from our lab and recent publications [27, 28] indicate that *ACE2* expression was detected in the oral epithelium at birth and not in embryos at E12.5 and E14.5. In adult mice, *ACE2* is enriched in a subpopulation of epithelial cells in the non-gustatory filiform papillae, but not in taste papillae or taste buds. Our mouse data, together with other reports, if true in humans, suggest that: (1) taste loss in COVID-19 patients is likely not directly caused by the transfection of SARS-CoV-2 to taste bud cells; (2) embryos at different stages of development have distinct susceptibility to the disease; and (3) the risk of a maternal-fetal transmission exists given the expression of *ACE2* in organs of late embryos and newborns, placenta and female reproductive system.

## 5.3 Results

### *5.3.1 Expression dynamics of SARS-CoV-2, influenza virus, and inflammation-associated genes in mouse oral cavity at early stages (E12.5, E14.5 and P1)*

To predict how early oral tissues can be susceptible to SARS-CoV-2 and influenza virus, we retrieved our bulk RNA-Seq data regarding the expression of genes associated with SARS-CoV-2 (*ACE2*, *TMPRSS2*) [29], influenza virus (*St3gal4* and *St6gal1*) [30] and inflammation (*Ifngr1* and *Tnfrsf1a*). Four tissue compartments (epithelium and underlying mesenchyme in the tongue and soft palate) were collected at three developmental stages (E12.5, E14.5 and P1). The selected genes showed distinct expression patterns across the four tissue compartments and during the different stages of development. In general, expression level increased for all genes during tissue development except for *St6gal1,* which was decreased at later development stages.

Among the examined genes, *ACE2* was exclusively found in the epithelium, while all other genes were detected in both the epithelium and the mesenchyme.

The expression of *ACE2* was rarely detected in any of the four tissue compartments in embryos (E12.5 and E14.5), however, robust *ACE2* transcripts were found in the epithelium at P1, but not the mesenchyme of the soft palate and tongue (Figure 5.1A). Expression of the protease *TMPRSS2,* that mediates the initial viral entry of SARS-CoV-2, showed a progressive increase over developmental stages in both the epithelium and mesenchyme of the soft palate and in tongue epithelium. Furthermore, the transcripts of *TMPRSS2* were most abundant in the soft palate epithelium (Figure 5.1B). *St3gal4* and *St6gal1*, which are essential for synthesis of sialic acid recognized by influenza virus [30], were detected across all tissue compartments at all three developmental stages. The pattern of expression of these two genes varied across the different developmental stages characterized by a general increased expression for *St3gal4 and* decreased abundance of *St6gal1* transcripts (Figure 5.1C and 5.1D). *Ifngr1* and *Tnfrsf1a*, genes that encode two essential receptors for inflammatory cytokines, were detected in all examined tissue compartments as early as E12.5 and their expression increased during development (Figure 5.1E and 5.1F).

*5.3.2 Enrichment of SARS-CoV-2 receptor gene ACE2 occurs in a subpopulation of tongue epithelial cells of non-gustatory papillae, but not in taste papillae or buds*

Recent studies indicated that *ACE2* is enriched in the tongue epithelial cells in humans [23]. To understand which subpopulation(s) of tongue epithelial cells are the likely target of SARS-CoV-2, we scoured the data in the recently published mouse scRNA-seq atlas [27]. Using the best high-throughput dataset (7538 cells in total), we identified 13 anterior tongue epithelial cell clusters (Figure 5.2A) and their associated signature genes (Figure 5.2B, Table S-1) using a

machine learning approach . Consistent with human data [23], SARS-CoV-2 entry receptor coding gene, *ACE2*, is detected in mouse tongue epithelium and *ACE2*$^{+}$ cells are specifically enriched in 4 of the 13 clusters (No. 1, 2,4 and 11) of anterior tongue epithelial cells (Figure 5.2C). In contrast, the expression of *TMPRSS2* is broadly scattered at a low frequency across all cell clusters (Figure 5.2D).

To identify the type(s) of *ACE2*$^{+}$ cells and answer the question of whether taste bud cells express *ACE2*, we empirically analyzed the *ACE2*$^{+}$ cell-enriched clusters using markers for taste bud cells (*Krt8*$^{+}$), taste bud cell progenitors (*Lgr6*$^{+}$), and basal epithelial cells in fungiform papillae (*Gli1*$^{+}$) in three independent scRNA-seq datasets. In the first dataset (7538 cells in total from the anterior tongue epithelium), *Krt8*$^{+}$, *Lgr6*$^{+}$, and *Gli1*$^{+}$ cells were not enriched in *ACE2*$^{+}$ cell-enriched clusters (No. 1, 2, 4 and 11) (Figure 5.3A-C). To confirm the previous results, a second dataset (1432 anterior tongue epithelium cells) was analyzed. Consistent with the results shown above (Figure 5.2C-D), *ACE2*$^{+}$ cells were especially enriched in one cell cluster (No. 5) while some positive cells were found in other clusters (Figure 5.3D). Again, *ACE2*$^{+}$ cell-enriched clusters had few or no cells expressing *Krt8* or *Lgr6* or *Gli1* (Figure 5.3D-G).

To further confirm that *ACE2* is not expressed in taste bud cells, a third independent scRNA-seq dataset (52 taste bud cells in total) [28] was analyzed. As shown in Figure 5.3H, most taste bud cells from distinct types ( *Gad1*$^{+}$ type III, *Gustducin*$^{+}$ type II, *T1r3*$^{+}$ sweet and umami type II, and manually selected type III) and taste bud progenitors (*Lgr5*$^{+}$) did not express *ACE2* (Figure 5.3H). Out of the 53 analyzed cells, only 8% showed robust *ACE2* transcripts (higher than 160 FPKM), and all of them were type III cells. Collectively, *ACE2* is not enriched in most taste bud cells, or the surrounding taste bud progenitors and taste papilla epithelial cells.

To further characterize the identity of *ACE2*-expressing cells, we examined the genes that have been reported to be exclusively expressed in the non-gustatory filiform papillae of the dorsal surface of the tongue. *Hoxc13*$^{+}$ cells, distributed in the basal region of filiform papillae [31], were enriched in 3 out 13 cell clusters (No. 2, 10, and 11). It is noteworthy that *Hoxc13*$^{+}$ and *ACE2*$^{+}$ cell enrichment overlapped in two (No.2 and 11) of the cell clusters (Figure 5.4A). An additional two genes (*Krt36* and *Krt84),* that are expressed in filiform papillae, were enriched in the same cell clusters as *Hoxc13* and *ACE2*. Jointly, our data suggest that a proportion of *ACE2*$^{+}$ cells are distributed in the epithelium at the basal region of filiform papillae.

*5.3.3 Potential for distinct tropism of multiple viruses in the tongue epithelium*

To understand the relevance of the distribution of viral receptor expression in oral epithelium and the vulnerability of taste sensation to infectious diseases, we performed a head-to-head comparison of the frequency and the abundance of key viral entry factors for SARS-CoV-2, HCoV-229E, influenza virus, and MERS-CoV45 across all 13 cell clusters identified in the first scRNA-seq dataset [27]. The two most *TMPRSS2*-enriched cell clusters (No.2 and No.11) were also *ACE2*-enriched, although the proportion of *TMPRSS2*$^{+}$ cells was generally low. The HCoV-229E's entry factor Anpep [32] shared one cell-enriched cluster (No.4) with *ACE2*. However, the *St3gal4* -enriched clusters (essential for influenza virus entry) were totally separate from those for *ACE2*. The expression of *Dpp4*, which is essential for MERS-CoV infection [32], is very low in cell clusters throughout the tongue epithelium (Figure 5.5).

Given that a strong innate immune response was activated by SARS-CoV-2 infection [33] and the resulting inflammation that may affect taste bud homeostasis [2, 34], the response of the innate immune system of the host may be involved in taste loss in COVID-19 patients.

Strikingly, tumor necrosis factor receptor 1 gene, *Tnfrsf1a*, displays abundant expression across all cell clusters. Moreover, the expression of IFN receptor genes *Ifngr1* and *Ifngr2* (but not the Il1 receptor gene *Il1r1*) was detected broadly in the tongue epithelium. Expression of *Tlr3*, which is essential for the recognition of viral pathogen and activation of the immune system, was very low (Figure 5.5).

## 5.4 Discussion

COVID-19, caused by the infection of SARS-CoV-2 [35], is highly contagious and often life threatening due to severe acute respiratory syndrome and the failure of other organs [36, 37]. The entry of the virus into cells is through the obligatory receptor, *ACE2* [18-22], and the protease TMPRSS2 [29]. Several studies showed that COVID-19 viral infections occur through multiple potential routes including respiratory, oral, and contact [38-40]. The symptoms vary among patients including sore throat, cough, fever, difficulty breathing, and loss of taste and smell [36]. In this report, we provide a new understanding of loss of taste in COVID-19 patients and a potential correlation of the susceptibility with the gestational stages. We acknowledge that mouse *ACE2* is, unlike humans, not susceptible to SARS-CoV-2 [26]; however, provided that mice and humans share similar gene expression patterns, *ACE2* expression in mice may still provide insights into how pathological changes develop in humans.

*Taste loss in COVID-19 patients is likely not due to an initial direct viral infection in taste bud cells*

Another matter of particular interest is that taste loss, often together with smell loss, is one of the common symptoms of COVID-19, even when there are no other apparent symptoms [16, 41]. Recently reported data showed that *ACE2* is enriched in tongue epithelial cells in humans [23], and *ACE2* mRNA is detected in both the gustatory and non-gustatory tongue epithelium in

mice [25]. However, it remains unclear what specific types of cells highly express *ACE2* and where they are localized in the tongue epithelium.

Taste buds are primarily located in the tongue, and lingual taste buds reside in the epithelium of the taste papillae. The three types of taste papillae (fungiform, foliate and circumvallate) are stereotypically distributed on the tongue, i.e., fungiform located among the non-gustatory filiform papillae on the anterior 2/3 oral tongue, foliate on the two lateral edges of the posterior oral tongue, and circumvallate papillae (8-12 in humans and 1 in rodents) are located in the border between the oral and pharyngeal tongue [42]. Mammalian taste bud maintenance and homeostasis require the surrounding progenitor cells to continuously renew the differentiated taste bud cells (type I, II and III) for intact taste function [6]. Multiple lineages of taste bud cell progenitors have been reported including $K14^+$ [43], $Lgr5^+$ [44], $Lgr6^+$ [45], $SOX2^+$ [46], and $Gli1^+$ [47] epithelial cells that surround taste buds.

To dissect the heterogeneity of gustatory epithelial cells, rapidly developing scRNA-seq techniques provide a powerful tool. In this report, the mining of two independent sets of data from a single cell RNA-Seq of anterior tongue epithelium provides insights into the molecular heterogeneity of these cells (Table S-1 and Table S-2). Our results indicate that *ACE2* is expressed in a subpopulation of tongue epithelial cells. The $ACE2^+$ cells are enriched in 4 out of 13 clusters of these tongue epithelial cells. Two of the four clusters highly express markers (*Hoxc13, Krt36, Krt84*) that are restricted to a subpopulation of epithelial cells in the basal region of filiform (non-gustatory) papillae [31, 48]. However, $ACE2^+$ cell-enriched clusters do not frequently overlap with those clusters in which markers are expressed in taste bud cells and the surrounding taste papilla epithelial cells, i.e., *Krt8* [49], *Lgr6* [45], and *Gli1* [47]. Furthermore, scRNA-seq data of taste bud cells [28] confirm that most taste bud cells have no or

extremely low expression level of *ACE2*. Expression of *ACE2* was detected in a small proportion of type III taste cells, which is consistent with mRNA detection in taste buds using RT-PCR [25]. Collectively, these scRNA-seq data provide a more precise information than the previously reported[24] regarding *ACE2*$^{+}$ cell types and enriched tissue compartments. The enrichment of *ACE2* in non-gustatory papillae, but not taste buds, indicates that taste loss in COVID-19 patients is not, at least initially, primarily due to a direct viral infection of taste bud cells.

We hypothesize that taste loss in COVID-19 patients may result indirectly from multiple potential causes. First, local and/or systematic immune responses to SARS-CoV-2-induced inflammation may disrupt taste bud homeostasis [6]. It has been recently reported that deletion of TNFα prevents taste bud loss caused by the chronic inflammation [50]. Thus, abundant expression of *Tnfrsf1a*, the gene encoding tumor necrosis factor receptor 1 (TNFR1), in single cell transcriptomic analyses of anterior mouse tongue epithelium suggests that TNF signaling may be a mediator in taste loss during SARS-CoV-2 infection. In addition, systemic IFNs can trigger IFN-mediated signaling cascades in taste buds at posterior tongues [34]. Detection of both *Ifngr1* and *Ifngr2* expression in our single cell-level analysis of anterior tongue epithelium indicate the involvement of IFN-mediated signaling in regulating fungiform taste bud homeostasis in the anterior tongue. Secondly, infections of SARS-CoV-2 in the nervous system may damage the innervation of taste buds which leads to taste bud degeneration [51]. Finally, if *ACE2* expression in taste buds can be activated by IFN [40] after the virus first enters into a host in mice as recently reported in the olfactory epithelium in humans [40], then there is a possibility that SARS-CoV-2 in the blood and saliva [52] may infect taste bud cells via the subsequently expressed *ACE2* in these cells. This possibility requires further experimental testing.

*Fetuses may have developmental stage-dependent susceptibilities to the infection of SARS-CoV-2*

The available pandemic data shows that elderly people are more susceptible to SARS-CoV-2 infection and more likely to have a poor prognosis, including death [53]. A recent report showed that the *ACE2* protein level in some organs, e.g., olfactory epithelium, increases with age [54], thus providing a possible explanation as to why the severity and mortality rate are higher in older people. Though young people are also susceptible to infection when exposed to the virus, the symptoms are mostly mild [55]. The youngest COVID-19 patient reported was only four weeks old [56].

To understand whether fetuses are also susceptible to COVID-19 through maternal transmission, thorough examinations on *ACE2* expression in the body of fetus and placenta are needed. It has been reported that *ACE2* is highly expressed in early ovum-phase human embryos (2- and 4-cell stages) and the expression level drops afterwards [57]. Further, the presence of *ACE2* in the urine of 23 week human fetuses suggests the expression in the body [58]. In mouse pancreas, *ACE2* is detected in embryos and peaked at E16.5 [59]. In the present study, we analyzed the expression of *ACE2* receptor and co-receptor TMPRSS2 in different tissue compartments of the oral cavity in mouse embryos and newborns. Although the transcripts of TMPRSS2 for SARS-CoV-2 entry were detected in the lingual and palatal epithelium of both embryos and newborns, the receptor *ACE2* was only detected in newborns, not in embryos at examined developmental stages (E12.5 and E14.5). Together, these findings indicate that the susceptibility of fetuses to SARS-CoV-2 infections is likely to be stage-dependent (i.e., high level immediately after fertilization and during late fetal stages). Given that *ACE2* is highly expressed in the fetal part of placenta (labyrinth and basal zones) [60] and female reproductive

tract including uterus and vagina [61], potential risk of maternal-fetal transmission exists before and during birth, although SARS-CoV-2 infections were not found in neonates of infected pregnant mothers in a recent report [62].

*Different viral infections transmit through distinct cell targeting in the tongue epithelium*

It is known that various viral infections affect taste function to different extents, e.g., at distinct incidence and severity levels of taste dysfunction [6]. Taste loss occurs more frequently in COVID-19 patients than in other patients with influenza-like symptoms [12]. The underlying mechanisms in these infectious disease conditions remain elusive at the cellular level. In this study, scRNA-seq profiling of anterior tongue epithelial cells that are heterogeneous structurally, molecularly and functionally revealed that molecules for various viruses' entries into cells are enriched in different cell clusters. We hypothesize that different viral infections may cause impairments of different subpopulations of tongue epithelial cells and may trigger various immune responses leading to distinct taste deficiencies. To better understand how taste bud cells and/or progenitors are affected in various disorders, further experimental studies are needed. The available data from our analysis and others [27] will be useful in these future studies.

We are aware of the seemingly different expression levels of some genes between our study and literature reports. Il1r1, the gene encoding Interleukin 1 Receptor Type 1, and *Tlr3*, the gene encoding toll-like receptor 3, were detected at a low level in the scRNA-seq dataset of anterior mouse tongue epithelium. However, detection of proteins of IL1-β and IL1-RI receptor has been reported in taste buds in rats [63]. Moreover, multiple TLRs were detected in taste buds from posterior tongues using RT-PCR [64]. These discrepancies may be due, in part, to the difference of innate immune system components between the anterior vs. posterior tongue. Furthermore, loss-of-function analysis of one or more innate immune components under

different conditions will be beneficial for understanding the effects of inflammation on taste bud maintenance and function.

Overall, our results show that different viral infections may affect distinct cell targets in the tongue epithelium. We identified the basal region of epithelial cells in non-gustatory filiform papillae as the prime targets for SARS-CoV-2 infection in tongue epithelium. We revealed that *ACE2* was detected in newborns, but little to no expression was found in mouse fetal oral tissues. Thus, the results in mouse tissues suggest that, when applied across species and organs, taste loss in COVID-19 patients is likely not caused by an initial direct infection of taste bud cells by SARS-CoV-2, fetal susceptibility to SARS-CoV-2 is stage-dependent during prenatal development, and risks of maternal-fetal transmission exist. .

## 5.5 Methods

### *5.5.1 Animals*

Animal use was approved by The University of Georgia Institutional Animal Care and Use Committee and was in compliance with the National Institutes of Health Guidelines for care and use of animals in research.

Timed pregnant and newborn mice (C57BL/6J, The Jackson Laboratory, stock# 000664,) were used to collect tissues for the in-house bulk RNA-Seq. Noon on the day in which a vaginal plug was detected was designated embryonic day (E) 0.5. The day when the pups were born was noted as postnatal day (P) 1.

### *5.5.2 Transcriptomic profiling of oral tissues (bulk RNA-Seq) in mouse embryos and newborns*

Pregnant mice at E12.5, E14.5 were euthanized with $CO_2$, followed by cervical dislocation, and newborn (P1) mouse decapitation. Tongues and soft palates were dissected. To separate the epithelium and underlying mesenchyme, E12.5 tissues were incubated with 2.5 mg/ml Dispase II

(#04942078001, Roche Diagnostics), a 1 mg/ml Collagenase A (#10103578001, Roche Diagnostics) was added for the E14.5 tissues. In the P1 tissues, the enzyme mixture was injected into the sub-epithelial space. After the enzyme incubation at 37°C for 30 min, the epithelium and mesenchyme of tongue and soft palate were separated for RNA extraction using Trizol and RNeasy Plus kits (Qiagen). RNA Quality was assessed on an Agilent 2100 Bioanalyzer (Agilent Technologies, Santa Clara, CA). Each group of tissues included 3 biological replicates and each sample of the replicate contained up to 10 (E12.5), 3 (E14.5) and 1 (P1) tongues or soft palates for sufficient RNA.

cDNA libraries were prepared with Kapa Stranded mRNA-seq kit (KAPA Biosystems, Wilmington, MA). Library quality and quantity were measured by Fragment Analyzer Automated CE (Advanced Analytical, Evry Cedex, France) and Qubit (Thermo Fisher) systems, respectively. Libraries were subsequently subjected to 2 × 75 bp paired-end sequencing on a NextSeq 500 system (Illumina). All samples were pooled and sequenced on one lane. The RNA quality check, library preparation, and sequencing were conducted at the University of Georgia Genomics and Bioinformatics Core (Athens, GA). The raw RNA-Seq data of each sample was aligned to mouse reference genome (GRCm37.1) via STAR [65] and the transcripts were quantified via StringTie [66]. Gene expression was calculated in fragments per kilobase of exon model per million reads mapped (FPKM) and presented as FPKM ($X \pm SE$, n=3). Raw read counts were quantified by HTSeq and subsequently analyzed for differentially expressed genes (DEGs) between stages via DESeq2 [67]. Significance was declared when the adjusted *P* value was less than 0.05.

All raw sequencing data and processed data were deposited in Gene Expression Omnibus (GSE151205).

*5.5.3 Analysis of public data from single-cell transcriptomic profiling (scRNA-seq) of adult mouse tongue epithelium*

Three independent datasets were used. Two sets of tongue scRNA-seq data were downloaded from *Tabula Muris* [27], including one that was based on microfluid platform and contained 7538 adult anterior tongue epithelial cells (for unique molecular identifiers (UMIs)) , and another based on the FACS method and contained 1432 tongue epithelial cells (for reads). Genes detected in less than three cells were filtered out. Cells in which less than two hundred genes were detected were removed.

The third set of data (SRP094673) contained 52 available cells: 47 circumvallate taste bud cells from different types (11 *Gad1*$^+$ cells, 10 *Gustducin*$^+$ cells, 17 type III cells, and 9 *Tas1r3*$^+$ cells) and 5 taste bud cell progenitors (*Lgr5*$^+$) [28]. The raw sequencing data for each cell from Sukumaran *et al* (2017) was aligned to a mouse reference genome using STAR [65] and the transcripts of genes were quantified using RSEM [68]. Gene expression was calculated in fragments per kilobase of exon model per million reads mapped (FPKM).

Analysis of scRNA-seq datasets were performed with R package Seurat (V3.1.5) [69]. Expression matrix from Schaum *et al* (2018) underwent logistic transformation and scaling. Clusters of cells were identified by unbiased machine learning algorisms. Principal component analysis (PCA) was applied for dimension reduction, and t-Distributed Stochastic Neighbor Embedding (t-SNE) was used to visualize data at low-dimensions.

*5.5.4 Data visualization*

Visualization of bulk RNA-Seq data was conducted using R package ggpubr. For scRNA-seq analyses, t-SNE maps, heatmaps, violin plots, and dot plots were implemented using the built-in functions of R package Seurat (V3.1.5) [69].

## 5.6 References


1. Perea-Martinez, I., T. Nagai, and N. Chaudhari, *Functional Cell Types in Taste Buds Have Distinct Longevities.* PLOS ONE, 2013. **8**(1): p. e53399.

2. Cohn, Z.J., et al., Lipopolysaccharide-induced inflammation attenuates taste progenitor cell proliferation and shortens the life span of taste bud cells. BMC Neuroscience, 2010. **11**(1): p. 72.

3. Hamamichi, R., M. Asano-Miyoshi, and Y. Emori, *Taste bud contains both short-lived and long-lived cell populations.* Neuroscience, 2006. **141**(4): p. 2129-2138.

4. Farbman, A.I., *Renewal of taste bud cells in rat circumvallate papillae.* Cell Proliferation, 1980. **13**(4): p. 349-357.

5. Beidler , L.M. and R.L. Smallman *RENEWAL OF CELLS WITHIN TASTE BUDS.* Journal of Cell Biology, 1965. **27**(2): p. 263-272.

6. Feng, P., L. Huang, and H. Wang, *Taste bud homeostasis in health, disease, and aging.* Chem Senses, 2014. **39**(1): p. 3-16.

7. Bromley, S.M., *Smell and taste disorders: a primary care approach.* Am Fam Physician, 2000. **61**(2): p. 427-36, 438.

8. Cullen, M.M. and D.A. Leopold, *Disorders of smell and taste.* Med Clin North Am, 1999. **83**(1): p. 57-74.

9. Goodspeed, R.B., J.F. Gent, and F.A. Catalanotto, *Chemosensory dysfunction. Clinical evaluation results from a taste and smell clinic.* Postgrad Med, 1987. **81**(1): p. 251-7, 260.

10. Bartoshuk, L., et al., *Tasting on Localized Areasa.* Annals of the New York Academy of Sciences, 1987. **510**(1): p. 166-168.

11. Henkin, R.I., A.L. Larson, and R.D. Powell, *Hypogeusia, dysgeusia, hyposmia, and dysosmia following influenza-like infection.* Ann Otol Rhinol Laryngol, 1975. **84**(5 Pt 1): p. 672-82.

12. Yan, C.H., et al., Association of chemosensory dysfunction and Covid-19 in patients presenting with influenza-like symptoms. Int Forum Allergy Rhinol, 2020.

13. Vaira, L.A., et al., Anosmia and Ageusia: Common Findings in COVID-19 Patients. Laryngoscope, 2020.

14. Lee, Y., et al., Prevalence and Duration of Acute Loss of Smell or Taste in COVID-19 Patients. J Korean Med Sci, 2020. **35**(18): p. e174.

15. Lechien, J.R., et al., Olfactory and gustatory dysfunctions as a clinical presentation of mild-to-moderate forms of the coronavirus disease (COVID-19): a multicenter European study. Eur Arch Otorhinolaryngol, 2020: p. 1-11.

16. Hjelmesæth, J. and D. Skaare, *Loss of smell or taste as the only symptom of COVID-19.* Tidsskr Nor Laegeforen, 2020. **140**(7).

17. Gautier, J.F. and Y. Ravussin, *A New Symptom of COVID-19: Loss of Taste and Smell.* Obesity (Silver Spring), 2020. **28**(5): p. 848.

18. Yan, R., et al., Structural basis for the recognition of SARS-CoV-2 by full-length human ACE2. Science, 2020. **367**(6485): p. 1444-1448.

19. Shang, J., et al., *Structural basis of receptor recognition by SARS-CoV-2.* Nature, 2020. **581**(7807): p. 221-224.

20. Luan, J., et al., Spike protein recognition of mammalian ACE2 predicts the host range and an optimized ACE2 for SARS-CoV-2 infection. Biochem Biophys Res Commun, 2020. **526**(1): p. 165-169.

21. Guzzi, P.H., et al., Master Regulator Analysis of the SARS-CoV-2/Human Interactome. J Clin Med, 2020. **9**(4).

22. Giron, C.C., A. Laaksonen, and F.L.B. da Silva, On the interactions of the receptor-binding domain of SARS-CoV-1 and SARS-CoV-2 spike proteins with monoclonal antibodies and the receptor ACE2. Virus Res, 2020: p. 198021.

23. Xu, H., et al., High expression of ACE2 receptor of 2019-nCoV on the epithelial cells of oral mucosa. International Journal of Oral Science, 2020. **12**(1): p. 8.

24. Venkatakrishnan, A.J., et al., Knowledge synthesis of 100 million biomedical documents augments the deep expression profiling of coronavirus receptors. eLife, 2020. **9**: p. e58040.

25. Shigemura, N., et al., Expression of Renin-Angiotensin System Components in the Taste Organ of Mice. Nutrients, 2019. **11**(9): p. 2251.

26. Zhou, P., et al., A pneumonia outbreak associated with a new coronavirus of probable bat origin. Nature, 2020. **579**(7798): p. 270-273.

27. Schaum, N., et al., Single-cell transcriptomics of 20 mouse organs creates a Tabula Muris. Nature, 2018. **562**(7727): p. 367-372.

28. Sukumaran, S.K., et al., *Whole transcriptome profiling of taste bud cells.* Scientific Reports, 2017. **7**(1): p. 7595.

29. Hoffmann, M., et al., SARS-CoV-2 Cell Entry Depends on ACE2 and TMPRSS2 and Is Blocked by a Clinically Proven Protease Inhibitor. Cell, 2020. **181**(2): p. 271-280.e8.

30. Broszeit, F., et al., *N-Glycolylneuraminic Acid as a Receptor for Influenza A Viruses.* Cell Rep, 2019. **27**(11): p. 3284-3294.e6.

31. Godwin, A.R. and M.R. Capecchi, *Hoxc13 mutant mice lack external hair.* Genes Dev, 1998. **12**(1): p. 11-20.

32. Yeager, C.L., et al., Human aminopeptidase N is a receptor for human coronavirus 229E. Nature, 1992. **357**(6377): p. 420-422.

33. Mehta, P., et al., COVID-19: consider cytokine storm syndromes and immunosuppression. Lancet, 2020. **395**(10229): p. 1033-1034.

34. Wang, H., et al., *Inflammation Activates the Interferon Signaling Pathways in Taste Bud Cells.* The Journal of Neuroscience, 2007. **27**(40): p. 10703-10713.

35. Organization, W.H. *Naming the coronavirus disease (COVID-19) and the virus that causes it*. 2020; Available from: https://www.who.int/emergencies/diseases/ novel-coronavirus-2019/technical-guidance/naming-the-coronavirus-disease- (covid-2019)-and-the-virus-that-causes-it

36. Chen, L., et al., *Analysis of clinical features of 29 patients with 2019 novel coronavirus pneumonia.* Zhonghua jie he he hu xi za zhi = Zhonghua jiehe he huxi zazhi = Chinese journal of tuberculosis and respiratory diseases, 2020. **43**(0): p. E005.

37. Guan, W.J., et al., *Clinical Characteristics of Coronavirus Disease 2019 in China.* N Engl J Med, 2020. **382**(18): p. 1708-1720.

38. Zou, X., et al., Single-cell RNA-seq data analysis on the receptor ACE2 expression reveals the potential risk of different human organs vulnerable to 2019-nCoV infection. Front Med, 2020. **14**(2): p. 185-192.

39. Sungnak, W., et al., SARS-CoV-2 entry factors are highly expressed in nasal epithelial cells together with innate immune genes. Nature Medicine, 2020.

40. Ziegler, C.G.K., et al., SARS-CoV-2 Receptor ACE2 Is an Interferon-Stimulated Gene in Human Airway Epithelial Cells and Is Detected in Specific Cell Subsets across Tissues. Cell, 2020.

41. Cooper, K.W., Brann, D.H., Farruggia, M.C., Bhutani, S., Pellegrino, R.,, T. Tsukahara, Weinreb, C., Joseph, P.V., Larson, E.D., Parma, V., Albers, M.W., Barlow, L.A., Datta,, and D.P. S.R., A., *COVID-19 and the chemical senses: supporting players take center stage.* Neuron, 2020.

42. Reutter, M.W.a.K., Anatomy of the Tongue and Taste Buds, in Handbook of Olfaction and Gustation, Third Edition, R.L. Doty, Editor. 2015.

43. Okubo, T., C. Clark, and B.L.M. Hogan, Cell Lineage Mapping of Taste Bud Cells and Keratinocytes in the Mouse Tongue and Soft Palate. STEM CELLS, 2009. **27**(2): p. 442-450.

44. Yee, K.K., et al., Lgr5-EGFP Marks Taste Bud Stem/Progenitor Cells in Posterior Tongue. STEM CELLS, 2013. **31**(5): p. 992-1000.

45. Ren, W., et al., *Single Lgr5- or Lgr6-expressing taste stem/progenitor cells generate taste bud cells ex vivo.* Proceedings of the National Academy of Sciences, 2014. **111**(46): p. 16401-16406.

46. Ohmoto, M., et al., Genetic Lineage Tracing in Taste Tissues Using Sox2-CreERT2 Strain. Chemical Senses, 2017. **42**(7): p. 547-552.

47. Liu, H.X., et al., Multiple Shh signaling centers participate in fungiform papilla and taste bud formation and maintenance. Developmental Biology, 2013. **382**(1): p. 82-97.

48. Xu, M., et al., WNT10A mutation causes ectodermal dysplasia by impairing progenitor cell proliferation and KLF4-mediated differentiation. Nat Commun, 2017. **8**: p. 15397.

49. Knapp, L., et al., *Keratins as markers of differentiated taste cells of the rat.* Differentiation, 1995. **58**(5): p. 341-349.

50. Kaufman, A., et al., Inflammation arising from obesity reduces taste bud abundance and inhibits renewal. PLoS Biol, 2018. **16**(3): p. e2001959.

51. Guagliardo, N.A. and D.L. Hill, *Fungiform taste bud degeneration in C57BL/6J mice following chorda-lingual nerve transection.* Journal of Comparative Neurology, 2007. **504**(2): p. 206-216.

52. Xu, R., et al., *Saliva: potential diagnostic value and transmission of 2019-nCoV.* International Journal of Oral Science, 2020. **12**(1): p. 11.

53. Bonafè, M., et al., Inflamm-aging: Why older men are the most susceptible to SARS-CoV-2 complicated outcomes. Cytokine Growth Factor Rev, 2020.

54. Bilinska, K., et al., Expression of the SARS-CoV-2 Entry Proteins, ACE2 and TMPRSS2, in Cells of the Olfactory Epithelium: Identification of Cell Types and Trends with Age. ACS Chem Neurosci, 2020.

55. CDC, Coronavirus disease 2019 (COVID-19): people who need to take extra precautions. 2020.

56. Minnesota's youngest COVID-19 patient is 4 weeks old, in hospital. 2020, Fox 9.

57. Li, Y., H. Li, and L. Zhou, *EZH2-mediated H3K27me3 inhibits ACE2 expression.* Biochemical and Biophysical Research Communications, 2020. **526**(4): p. 947-952.

58. Rocha, N.P., et al., The protective arm of the renin–angiotensin system may counteract the intense inflammatory process in fetuses with posterior urethral valves. Jornal de Pediatria, 2019. **95**(3): p. 328-333.

59. Wang, L., J. Liang, and P.S. Leung, The ACE2/Ang-(1-7)/Mas Axis Regulates the Development of Pancreatic Endocrine Cells in Mouse Embryos. PLOS ONE, 2015. **10**(6): p. e0128216.

60. Levy, A., et al., *ACE2 expression and activity are enhanced during pregnancy.* American Journal of Physiology-Regulatory, Integrative and Comparative Physiology, 2008. **295**(6): p. R1953-R1961.

61. Jing, Y., et al., *Potential influence of COVID-19/ACE2 on the female reproductive system.* Molecular human reproduction, 2020. **26**(6): p. 367-373.

62. Karimi-Zarchi, M., et al., Vertical Transmission of Coronavirus Disease 19 (COVID-19) from Infected Pregnant Mothers to Neonates: A Review. Fetal Pediatr Pathol, 2020: p. 1-5.

63. Shi, L., et al., *Functional role for interleukin-1 in the injured peripheral taste system.* Journal of Neuroscience Research, 2012. **90**(4): p. 816-830.

64. Wang, H., et al., *Inflammation and taste disorders: mechanisms in taste buds.* Ann N Y Acad Sci, 2009. **1170**: p. 596-603.

65. Dobin, A., et al., *STAR: ultrafast universal RNA-seq aligner.* Bioinformatics, 2012. **29**(1): p. 15-21.

66. Pertea, M., et al., StringTie enables improved reconstruction of a transcriptome from RNA-seq reads. Nature Biotechnology, 2015. **33**(3): p. 290-295.

67. Love, M.I., W. Huber, and S. Anders, Moderated estimation of fold change and dispersion for RNA-seq data with DESeq2. Genome Biology, 2014. **15**(12): p. 550.

68. Li, B. and C.N. Dewey, RSEM: accurate transcript quantification from RNA-Seq data with or without a reference genome. BMC Bioinformatics, 2011. **12**(1): p. 323.

69. Butler, A., et al., Integrating single-cell transcriptomic data across different conditions, technologies, and species. Nature Biotechnology, 2018. **36**(5): p. 411-420.

## 5.7 Figures

*Figure 5.1 Histograms of FPKM values (mean ± SE, n=3) to illustrate the expression of SARS-CoV-2- (A and B), Influenza- (C and D) and inflammation- (E and F) related genes. The epithelium (Epi) and mesenchyme (Mes) were separately collected from E12.5, E14.5 and P1 mouse tongue (T) and soft palate (SP), the two main regions that host taste buds. Dots in each histogram represent the individual data points of the biological replicates. FPKM: fragments per kilobase million reads. Statistical analysis of differential expression in the same tissue compartment across stages was performed based on read counts using DESeq2. *P<0.05, **P<0.01 (adjusted P value).*

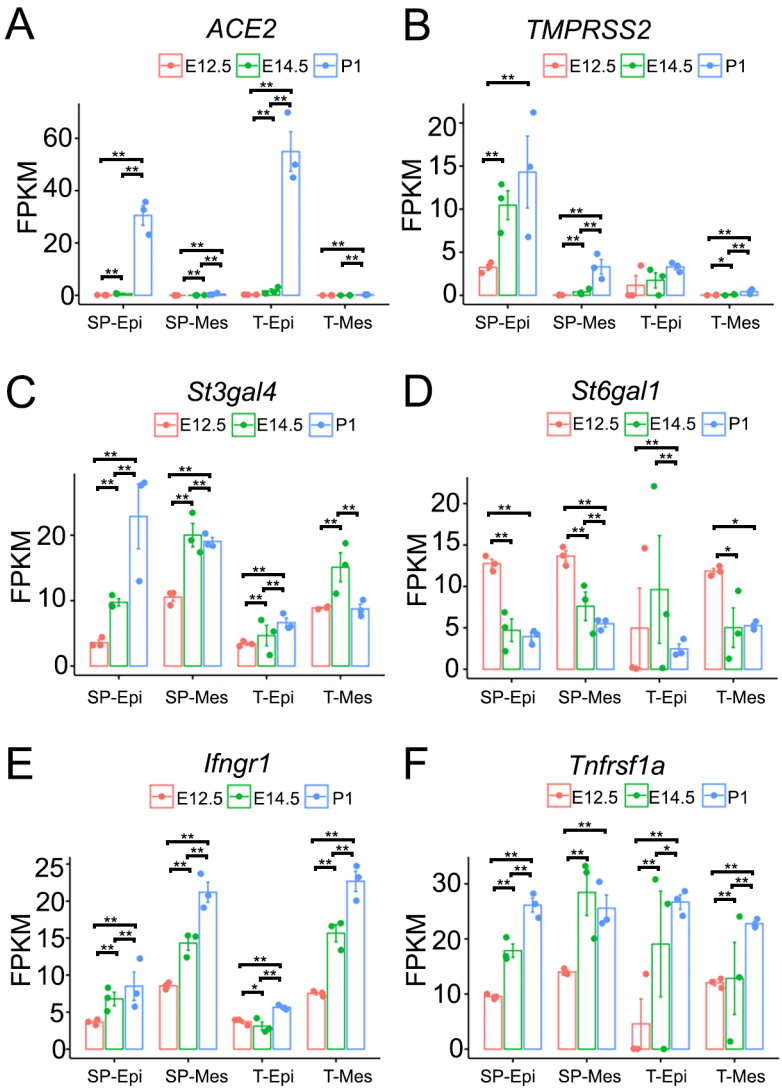
A
ACE2
E12.5 E14.5 P1
FPKM
SP-Epi SP-Mes T-Epi T-Mes
B
TMPRSS2
C
St3gal4
D
St6gal1
E
Ifngr1
F
Tnfrsf1a

*Figure 5.2 Distribution of SARS-CoV-2-associated genes, ACE2 and TMPRSS2, in the cell clusters of anterior tongue epithelium.* ***A****: A t-SNE map to illustrate the 13 cell clusters that were identified in a scRNA-seq dataset (7538 anterior tongue epithelial cells in total) from Schaum et al (2018). Each dot represents a single cell in this dataset.* ***B****: A heatmap to show the 13 cell clusters identified with the most significantly different gene from other clusters. The colors represent expression (log (UMIs count/10000+1)) of marker genes as the legend indicates.* ***C-D****: t-SNE maps and violin plots to illustrate the expression (log(UMIs count/10000+1)) of ACE2 (C) and TMPRSS2 (D). In the t-SNE maps, each dot represents an individual cell in the dataset and the color gradients of dots represent the expression levels of ACE2 (C) or TMPRSS2 (D) in cells. In the violin plots, each dot represents an individual cell that expressed ACE2 (C) or TMPRSS2 (D).*

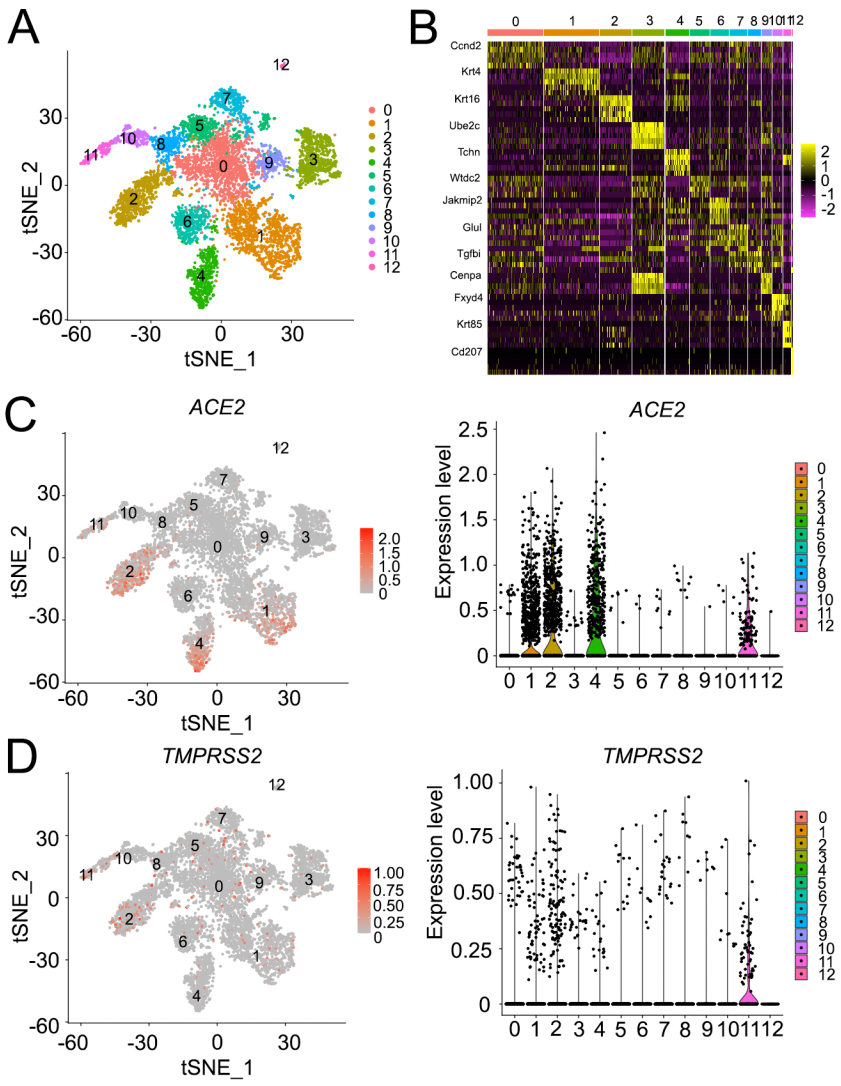
A
B
C
D
tSNE_1
tSNE_2
ACE2
TMPRSS2
Expression level
Ccnd2
Krt4
Krt16
Ube2c
Tchn
Wtdc2
Jakmip2
Glul
Tgfbi
Cenpa
Fxyd4
Krt85
Cd207

*Figure 5.3 ACE2 is not enriched in taste papilla epithelium and taste buds.* ***A-C****: t-SNE maps and violin plots to illustrate expression (log(UMIs count /10000+1)) of taste bud cell marker, Krt8 (A), taste bud cell progenitor marker, Lgr6 (B), and fungiform papilla cell marker, Gli1 (C) in distinct cell clusters in dataset from Schaum et al. (7538 cells in total).* ***D-G****: t-SNE maps and violin plots to illustrate expression (log(read counts/10000+1)) of ACE2 (D), taste bud cell marker, Krt8 (E), taste bud cell progenitor marker, Lgr6 (F), and fungiform papilla cell marker, Gli1 (G) in Schaum et al. dataset (1432 cells in total). In the t-SNE maps, each dot represents an individual cell in the dataset and the color gradients of dots represent the expression levels of the gene indicated in the tittle. In the violin plots, each dot represents an individual cell that expressed the gene indicated in the tittle.* ***H****: A boxplot to illustrate expression (FPKM) of ACE2 of 47 taste bud cells and 5 taste bud progenitors in Sunil K Sukumara et al. dataset. Note that almost all the lines standing for first quartile, median, and third quartile of boxplots stack at zero.*

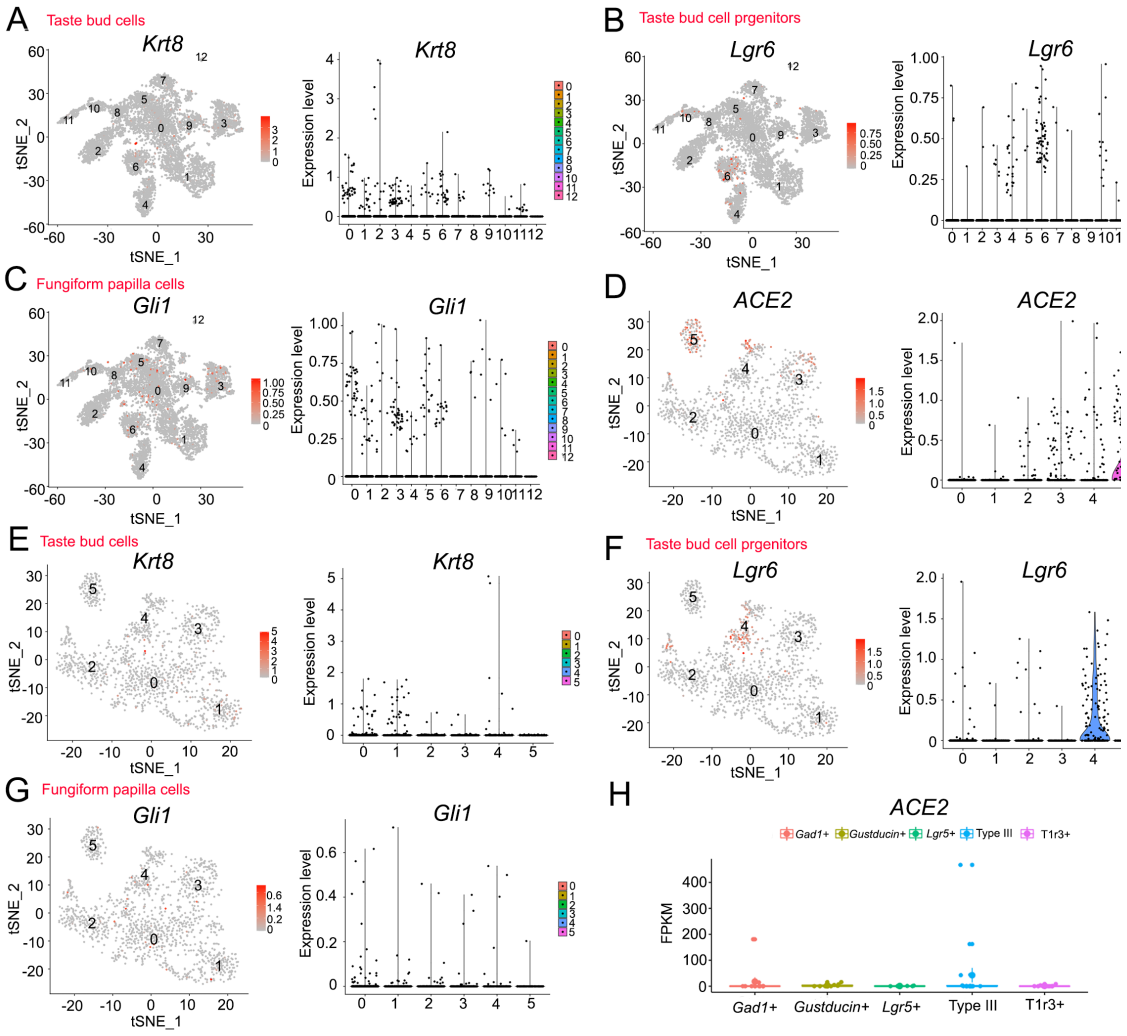
A
Taste bud cells
Krt8
tSNE_1
tSNE_2
Expression level
B
Taste bud cell prgenitors
Lgr6
C
Fungiform papilla cells
Gli1
D
ACE2
E
Taste bud cells
Krt8
F
Taste bud cell prgenitors
Lgr6
G
Fungiform papilla cells
Gli1
H
ACE2
Gad1+
Gustducin+
Lgr5+
Type III
T1r3+
FPKM

*Figure 5.4 t-SNE maps and violin plots to illustrate expression (log(UMIs count /10000+1)) of filiform papilla cell markers, Hoxc13c (A), Krt36 (B) and Krt84 (C) of distinct cell clusters in the scRNA-seq dataset (7538 cells in total) from Schaum et al. In the t-SNE maps, each dot represents an individual cell in the dataset and the color gradients of dots represent the expression levels of the gene indicated in the tittle. In the violin plots, each dot represents an individual cell that expressed the gene indicated in the title.*

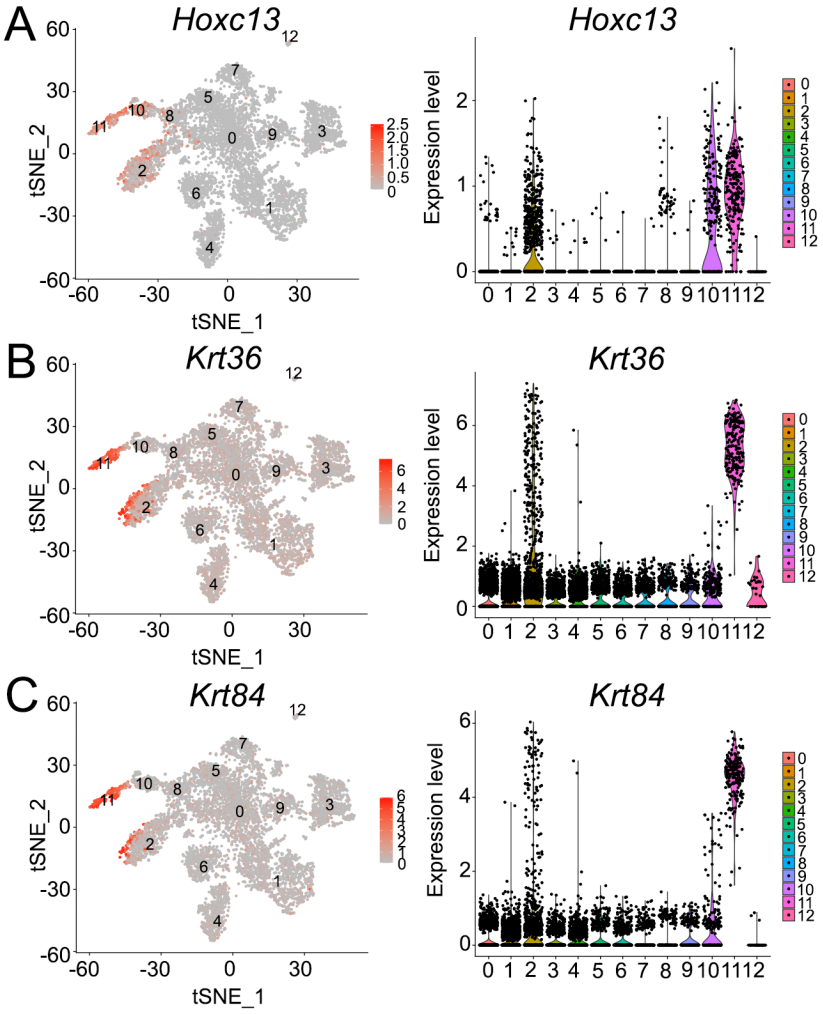
A
Hoxc13
Hoxc13
B
Krt36
Krt36
C
Krt84
Krt84
tSNE_1
tSNE_2
Expression level

*Figure 5.5 A dot-plot to illustrate gene expression (log(UMIs count /10000+1)) across the 13 cell clusters in the scRNA-seq dataset (7538 cell in total) from Schaum et al. SARS-CoV-2-, HCoV-229E-, Influenza-, MERS-CoV- and innate immune system-related genes are included . The size of dots represents the proportion of gene-expressing cells and color intensity of dots represents the average level expression of the gene expression.*

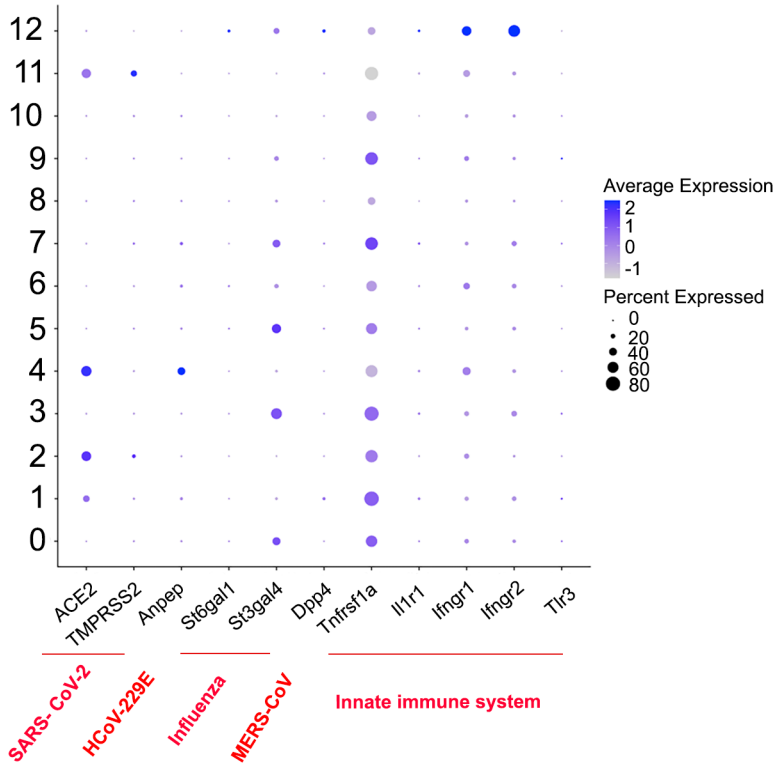
12
11
10
9
8
7
6
5
4
3
2
1
0
ACE2
TMPRSS2
Anpep
St6gal1
St3gal4
Dpp4
Tnfrsf1a
Il1r1
Ifngr1
Ifngr2
Tlr3
SARS-CoV-2
HCoV-229E
Influenza
MERS-CoV
Innate immune system
Average Expression
2
1
0
-1
Percent Expressed
0
20
40
60
80

# CHAPTER 6

## SUMMARY, CONCLUSIONS, AND FUTURE DIRECTIONS

How the development and maintenance of taste buds are regulated is one of the central questions in the field of taste biology. In present dissertation, I have tackled following three topics regarding the development of taste buds: embryonic origin of taste buds, regulation of *Evc2* gene in taste bud development and maintenance, and pathogenesis of taste loss caused by SARS-CoV-2.

Taste buds are not derived from neural crest in mouse, chicken, and zebra fish

**Rationale:** The multipotency of neural crest cells and their derived mesenchymal stromal cells make it logical to wonder whether neural crest cells are non-epithelial source of progenitors for taste bud cells. Our lineage tracing studies using multiple Cre mouse lines showed a concurrent labeling of abundant taste bud cells and the underlying connective tissue with a neural crest origin, warranting a further examination on the issue of whether there is an neural crest derivation of taste bud cells

**Findings:** In Chapter 3, we tested the contribution of neural crest lineage to taste buds in mammals, birds, and teleost fish using Sox10-iCreER$^{t2}$/tdT mouse model, GFP$^{+}$/GFP$^{-}$ chicken chimera model, and Sox10-Cre/GFP-RFP zebrafish model. We report that each of these models marks neural crest lineage specifically or/and extensively. Despite careful examination of multiple individuals in each model, we were unable to find any examples where the neural crest has contributed to cells in the taste buds.

**Future directions**: Even though neural crest does not give rise to taste bud cells, the connective tissue cells in tongue are largely derived from neural crest. Neural crest-derived mesenchymal cells interact with the overlying epithelium and play essential roles in taste bud and taste papilla development. For examples, mesenchymal FGF10 has been reported to control the size of fungiform papillae via modulating epithelial Wnt/β-catenin signals; and mesenchymal Follistatin modulates epithelial BMP7 signaling to control size and spacing of fungiform papillae and inhibits gustatory fate of intermolar eminence. Future studies using high throughput techniques will be beneficial for identifying novel factors from neural crest derivatives that are required for taste bud formation and maintenance.

Region- and stage-specific roles of EVC2 in regulating Hedgehog signaling and the development of taste organs

**Rationale**: Taste loss caused by taste bud cell degeneration is a severe heath issue. However, these is still no treatment for taste bud cell regeneration, which is largely due to that the lack of understanding of mechanisms underpin taste bud development and maintenance remains incomplete. Hedgehog signaling pathway has been reported to play essential roles in multiple events of taste organ development. Mis-regulation of Hedgehog signaling in embryos caused a number of birth defects in humans. Ellis–van Creveld syndrome, which is a rare Hedgehog signaling-related genetic disorder characterized by short limb dwarfism, polydactyly, abnormal development of fingernails as well as regional loss of taste papillae. The reason why regional taste papilla loss remain unknown.

**Findings:** In Chapter 4, to understand how taste bud development is affected in Ellis–van Creveld syndrome and to further study how EVC2 and Hedgehog signaling regulates taste papilla and taste bud development, *Evc2*$^{-/-}$ mice and Gli1-CreER/RFP mice were employed.

Through thorough examination, we found that taste papillae increased in number and size but with normal innervation in *Evc2*$^{-/-}$ tongues. Hedgehog signaling was impaired in tongue epithelial cells specifically in tongue tip region at E12.5. And RNA-seq experiment revealed that extracellular matrix (ECM) genes were dramatically up-regulated in *Evc2*$^{-/-}$ tongue epithelium. Moreover, enlarged and flatten fungiform papillae are observed in E18.5 *Evc2*$^{-/-}$ mice. BCL11B, a transcription factor essential for taste papilla morphogenesis, was missing or down-regulated in the abnormal fungiform papillae in *Evc2*$^{-/-}$ mice. Together our data revealed that EVC2 regulates Hedgehog signaling and the development of taste organs in a region- and stage-specific manner.

**Future directions**: There are three future directions which will further provide insights in region- and stage-specific roles of EVC2 in regulating Hedgehog signaling and taste organ development. First, even though number and size of fungiform papillae significantly increased in *Evc2*$^{-/-}$ mice, qRT-PCR data revealed that Hedgehog signaling activities were slightly impaired in *Evc2*$^{-/-}$ tongues and *in situ* hybridization data revealed that Hedgehog signaling activities were impaired only in epithelium of *Evc2*$^{-/-}$ tongue tips. These data suggests that there are EVC2-independent Hedgehog signaling activity or EVC2 may function irrelevantly to Hedgehog signaling. Activating Hedgehog signaling downstream EVC2, e.g. activating GLI proteins, will reveal that to which extent EVC2 relies on Hedgehog signaling to regulate taste organ development.

Second, in present study we first revealed that ECM-related genes are inhibited by EVC2 and very likely via Hedgehog signaling. Characterization of temporal and spatial expression of those ECM-related genes at both mRNA and protein levels in both *Evc2*$^{-/-}$ and control tongues will validate that ECM-regulated genes are turned up with *Evc2*, which is essential for functional studies. Label-free imaging can also be a good alternative to immunohistochemistry or mRNA *in*

*situ* hybridization for characterization of ECM. Also, functional analyses of ECM-related genes using either transgenic mouse lines or *in vitro* tissue culture will be indispensable to establish the roles of ECM in taste papilla placode specification.

Third, *Evc2*$^{-/-}$ mouse model suggests region- and stage-specific roles of Hedgehog signaling in taste organ development, especially roles in papilla morphogenesis. So, to further investigate this event, conditional and inducible deletion of *Evc2* at E15.5 and in tongue epithelium is necessary to further understand how EVC2 regulates papilla morphogenesis. After establishing conditional and inducible *Evc2* knockout mouse lines, RNA-seq analysis of E15.5 tongue epithelium will reveal more novel molecular and cellular mechanisms of papilla morphogenesis.

SARS-CoV-2 receptor ACE2 is enriched in a subpopulation of mouse tongue epithelial cells in non-gustatory lingual papillae, but not in taste buds or embryonic oral epithelium

**Rationale**: As a result of the COVID-19 pandemic, evidence revealed that SARS-CoV-2 infection caused taste loss at a higher rate than influenza. *ACE2*, the entry receptor of SARS-CoV-2, has been identified in the oral epithelium; however, it is unclear at what developmental stage *ACE2* expression emerges and whether *ACE2* is expressed in taste buds.

**Findings:** In Chapter 5, to identify the specific developmental stages when *ACE2* expression emerges, we analyzed RNA-Seq data from embryonic and newborn mouse oral tissue. We found that robust *ACE2* expression was observed in the newborn oral epithelium. In contrast, only extremely low levels, if any, of *ACE2* transcripts in the embryonic stage oral tissue were detected in the embryonic E12.5 and E14.5 oral tissue. Analyses of three public single cell RNA-seq datasets of adult mouse tongue epithelial cells showed that receptors for various viruses were enriched in distinct clusters of tongue epithelial cells. *ACE2* was enriched in a subpopulation of

epithelial cells in the basal region of non-gustatory filiform papillae, but not in the taste papillae or taste buds. Expression of *ACE2* was detected in a small proportion of type III taste cells. Our results indicate that when applied across species, non-gustatory papilla epithelial cells are the prime targets for SARS-CoV-2 infection in the tongue, and thus taste loss in COVID-19 patients is likely not caused by a direct infection of SARS-CoV-2 to taste bud cells. Additionally, fetuses at different stages of development may have distinct susceptibility to the disease.

**Future directions**: Animal models infected with SARS-CoV-2 will be indispensable to understanding the pathogenesis of taste loss caused by SARS-CoV-2. For instance, human-ACE2 transgenic mice is an ideal model for this purpose. After challenging human-ACE2 transgenic mice with SARS-CoV-2 virus, pathological and immunological analysis will reveal how tongue and taste buds are morphologically and cellularly affected. And behavioral studies will further elucidate how perception of taste is affected by SARS-CoV-2infection. Next generation sequencing-based techniques, like RNA-seq, ChIP-seq and scRNA-seq will further reveal the cellular and molecular mechanisms of taste loss. Moreover, analyzing tongue samples from human COVID-19 patients will validate mouse data and may reveal novel mechanisms which are different from those in mouse model.

Overall, investigating development and maintenance of taste buds from all three chapters facilitates understanding of pathogenesis of taste bud degeneration and is beneficial to the development of therapeutics for treatment of taste bud degeneration in a variety of diseases